University of Alberta

Delivery of siRNA using Lysine-Functionalized Rosette Nanotubes
for Cancer Therapy

by

Uyen Tra Truc Ho

A thesis submitted to the Faculty of Graduate Studies and Research
in partial fulfillment of the requirements for the degree of

Master of Science

Department of Chemistry

Fall 2013
Edmonton, Alberta

Abstract

Cancer remains to be one of the deadliest diseases world-wide due to its effect on millions of lives per year. The discovery of RNA interference and delivery of siRNA (small-interfering RNA) for protein silencing have been widely used for treatment of cancer cells. Research in our lab focuses on G∧C molecules (hybrid of guanine and cytosine bases) that can self-assemble into rosette nanotubes (RNTs) in physiological environment, proves to be biocompatible for *in vitro* and *in vivo* applications. This dissertation explores the lysine functionalized-twin RNTs (KnT RNTs, n = number of lysine residues) and lysine-functionalized mono RNTs (K1 RNTs). Gel retardation assay and fluorescence imaging showed that cationic charges on the RNTs strongly affect the binding interaction with siRNA and the intracellular delivery of the RNTs-siRNA complexes. K3T RNTs and K1 RNTs were assessed to demonstrate their low toxicity and effectiveness in siRNA delivery for protein silencing in cancer cells (A549 and HCT116).

Acknowledgements

First and foremost, I would like to express my thanks to Dr. Hicham Fenniri for giving me the opportunity to work on this project and for his continuous guidance throughout the years. He gave me the freedom to explore various experiments and entrusted to me the development of this project. The successful completion of this thesis would have been impossible without his assistance and support.

Likewise, I am truly grateful to Dr. Aws Alshamsan for his support from the start, for showing me the necessary laboratory skills and giving me the knowledge I needed to carry out this project. Special thanks is also due to Dr. Rachel Beingessner, who assisted with many very helpful explanations and discussions.

My project would not have been brought to completion without the invaluable assistance of Dr. Jae-Young Cho in the characterization of rosette nanotubes and their complexation with siRNA (SEM, TEM, AFM). Dr. Cho went out of his way to give me valuable suggestions, and he is also a great friend.

I am truly grateful to past and present colleagues: Dr. Weizheng Shen, Meijing Wang, Kumakshi Sharma, Abdullah Alshememry, Rahul Agrawal, Dr. Zhimin Yan, Dr. Mounir El-Bakkari, Liang Shuai, Zhaoyi Qin, Dr. Venkat Parthasarathy, Dr. Christophe Danumah and Dr. Takeshi Yamazaki. I feel extremely fortunate to have met these people, many of whom (S.S.A.) have become very good friends of mine. Their continuous support and useful suggestions aided me greatly throughout my work on this project.

I am very thankful to Dr. Usha Hemraz for her patience and support while reviewing the roughest drafts of my thesis and making many valuable suggestions.

I would also like to thank the support services and research facilities at the National Institute for Nanotechnology, University of Alberta and Cross Cancer Institute. Special acknowledgement goes to Geraldine Barron, Dr. Xuejun Sun, Kate Agopsowicz, Dr. Paul Concepcion, Dr. Mike Xia, Bethany Griffin, Catherine de Guzman and Daniel Solomon. The staff of the Institutes provided a great deal of assistance while I was making use of the instruments and materials.

Finally, I would like to mention my biological and extended families and my special friends: ba, mẹ, bé Vy, A. Shynkaruk, F. Zemanek, R. Hunter, B. Hunter, T. Zemanek, H. Zemanek, T. Mac, T. Tran and K. Mai, whose belief in me and loving support made it possible for me to attain my personal lifelong goals. I am truly indebted to them all.

Table of contents

List of Tables

List of figures

Page

List of Abbreviations

^{o}C	degree Celsius
Ago	Agonaute protein
AFM	Atomic Force Microscopy
ATP	Adenosine triphosphate
ATPase	Adenylpyrophosphatase
Au	Gold
Au NPs	Gold nanoparticles
BCA assay	Bicinchoninic acid assay
Bcl-2	B-cell lymphoma 2
C	Cytosine nucleotide
CD	Cytosine deaminase
CHS	Chalcone synthase
CNTs	Carbon nanotubes
Cy3	Cyanine-3
DAPI	4',6-diamidino-2-phenylindole
DCP-TEPA	Dicetylphosphate-tetraethylenepentamine
DEX	Dexamethasone
DMSO	Dimethyl sulfoxide
DNA	Deoxyribonucleic acid
DOSY	Diffusion-Ordered Spectrocopy
DOTAP	N-[1-(2,3-Dioleoyloxy)propyl]-N,N,N-trimethylammonium methyl-sulfate
DOTMA	N-[1-(2,3-dioleoyloxy) propyl]- N, N, N-trimethyl-ammonium methyl sulfate
dsRBD	Double-stranded RNA-binding domain
dsRNA	Double-stranded RNA
EDTA	Ethylenediaminetetraacetic acid
EGF	Epidermal growth factor
EGFP	Enhanced green fluorescent protein

EGFR	Epidermal growth factor receptor
ELISA	Enzyme-linked immunosorbent assay
EPR	Enhanced permeability and retention
ERK	Extracellular signal-regulated kinase
FAM	Fluorescein
FBS	Fetal Bovine Serum
FITC	Fluorescein isothiocyanate
FF-siRNA	Firefly pGL3 siRNA
G	Guanine nucleotide
GAPDH	Glyceraldehyde 3-phosphate dehydrogenase
GFPs	Green fluorescent proteins
HAADF	High-angle annular dark-field
HMDA	hexamethylenediamine
HOPG	Highly ordered pyrolytic graphite
HRP	Horse radish peroxidase
HSVtk	Herpes simplex virus thymidine kinase
K1	(one)-lysine functionalized mono base
KnT	Lysine-functionalized twin base, n = number of lysine residues
Lipidoids	Lipid-coated iron oxide nanoparticles
M	molar
MDA-7	Melanoma differentiation-associated 7
miRNA	MicroRNA
miRISC	MicroRNA-RNA induced silencing complex
mPEG-500	Poly(ethylene glycol) methyl ether
mRNA	Messenger RNA
MSNPs	Mesoporous silica nanoparticles
MTT	3-(4,5-dimethylthiazol-2-yl)-2,5-diphenyltetrazolium bromide
MW	Molecular Weight
n	mole

NMR	Nuclear Magnetic Resonance
NPs	Nanoparticles
p53	protein 53
PBS	Phosphate buffer saline
Pd	Palladium
PDDA	(poly(diallyldimethyl ammonium)chloride)
PEG	Polyethylene glycol
PEI	Polyethyleneimine
pGL3	pGL3 Luciferase Reporter Vectors
pHEMA	Poly(2-hydroxyethyl methacrylate)
PLL	Poly-L-lysine
pRL-CMV	pRL *Renilla* Luciferase Control Reporter Vectors
pri-miRNA	Primary micro RNA
pre-miRNA	Precursor micro RNA
Pt	Platinum
PVDF	Polyvinylidene fluoride
RISC	RNA-induced silencing complex
RNA	Ribonucleic acid
RNase	Ribonuclease
RNAi	RNA interference
RNTs	Rosette nanotubes
SDS-PAGE	Sodium dodecyl sulfate-polyacrylamide gel electrophoresis
SEM	Scanning Electron Microscope
SFM	Serum-free medium
siLuc2	Luciferase small-interfering RNA
siRISC	Small interfering RNA-induced silencing complex
siRNA	Small-interfering RNA
ssRNA	Single-stranded RNA
STAT	Signal transducer and activator of transcription
STAT3	Signal transducer and activator of transcription-3

SWCNTs	Single-walled carbon nanotubes
TAE	Tris-acetate-EDTA
TAM	Tamoxifen
TBL	Twin-base linker
TBST	Tris Buffer Saline-Tween
TGF- α	Transforming growth factor-α
TEM	Transmission Electron Microscopy
TFA	Trifluoroacetic acid
TfRscFv	Transferrin single chain antibody fragment
Ti	Titanium
TM-AFM	Tapping mode-Atomic Force Microscopy
TRBP	HIV-1 TAR RNA binding protein
U	Uracil nucleotide
VEGF	Vascular endothelia growth factor
WB	Western blotting

Chapter I

Introduction

1. Cancer

1.1. Overview

Cancer describes the uncontrolled growth of abnormal cells in part of the body, which then spreads out from the point of origin to other sites in the body.[1,2] Cancer is a worldwide health issue that concerns population at all ages and genders, mainly due to its wide effects on millions of lives every year.[1] In fact, not only does cancer affect human but animals, plants and nearly all the multicellular organisms on Earth.[2]

The modern cancer research started in 1860s when Johannes Müller, a German pathologist, discovered that cancers were composed of cells.[2] This was the birth of oncology, which described all the studies of mechanism, growth, causes, diagnosis and treatment of cancer, etc.[2] Although the actual mechanism of cancer remains unclear,[2] many valuable hypotheses have been proposed based on continuous studies of cancer over several centuries.[2]

Over 100 types of cancer have been reported as a result of cancer development at almost any organs in the human body.[2] About 85% of cancers are classified as carcinomas, which are derived from epithelial cells.[1] Other cancers originate from mesoderm cells (e.g. bone and muscle) called sarcomas, and glandular tissue (e.g. breast) called adenocarcinomas.[1] Due to distinguished characteristics of cells at different origins, different cancer types also possess distinct features, which bring challenges to cancer diagnosis and treatment.[1]

1.2. Cancer cells

1.2.1. Characteristics of cancer cells

Cancers are strongly believed to initiate from the alterations of the DNA sequence (mutations) in the cells, making it a genetic disease. [1,2] Cancer is the result of the accumulation of mutations over time along with the failure of cellular "machines" to repair any damaged DNA.[1,2] As a result, cancer cells grow uncontrollably and spread out to other parts of the body. [1,2]

To regulate cell numbers in the body, the three main processes include cell proliferation (cell division, cell growth), apoptosis (program of cell death) and cell differentiation (development of one cell to a more specialized cell).[1] Due to the mutations of the genetic codes that regulate these three processes, cancer cells can increase significantly in number by continuous growth, infinite division, evasion from cell death and inactive cell differentiation.[1]

By 2011, Hanahan and Weinberg summarized the ten hallmarks, recognized in most (or all) cancers (Figure 1-1)[3]

- *Growth signal autonomy* – unregulated growth of cancer cells due to the mutations of growth factor pathways
- *Evasion of growth inhibitory signals* – cancer cells do not respond to the signals from inhibitory pathways due to mutations or gene silencing of the latter
- *Unlimited replicative potential* – the genome of cancer cells can maintain length of the telomeres at the end of the chromosomal ends, leading to infinite cellular proliferation

- *Invasion and metastasis* – spreading of cancer cells to other sites in the body (major cause of cancer death)
- *Angiogenesis* – formation of new blood vessels for tumor survival and expansion
- *Evasion of cell death* – avoiding apoptotic triggering signals, leading to resistance to cell death regulation
- *Tumor-promoting inflammation* (enabling characteristics) – most cancer cells can benefit from inflammatory immune cells that provide growth factors and enzymes for angiogenesis and invasion
- *Genome instability and mutation* (enabling characteristics) – unsuccessful repair of damaged DNA leading to genomic instability in cancer cells
- *Reprogramming energy metabolism* (emerging hallmark) – increasing glycolysis to generate ATP for energy even in the presence of oxygen.
- *Evading immune destruction* (emerging hallmark) – ability of cancer cells to not stimulate or interfere with immune response to avoid cellular destruction

These hallmarks have described crucial characteristics of cancer cells, namely, how they maintain their growth and survival, thereby serving as guide for diagnosis and treatment of cancer cells.[3] To date, many therapeutic treatments have been targeting specific molecules that associate these hallmarks to kill the cancer cells by one pathway or another.[3]

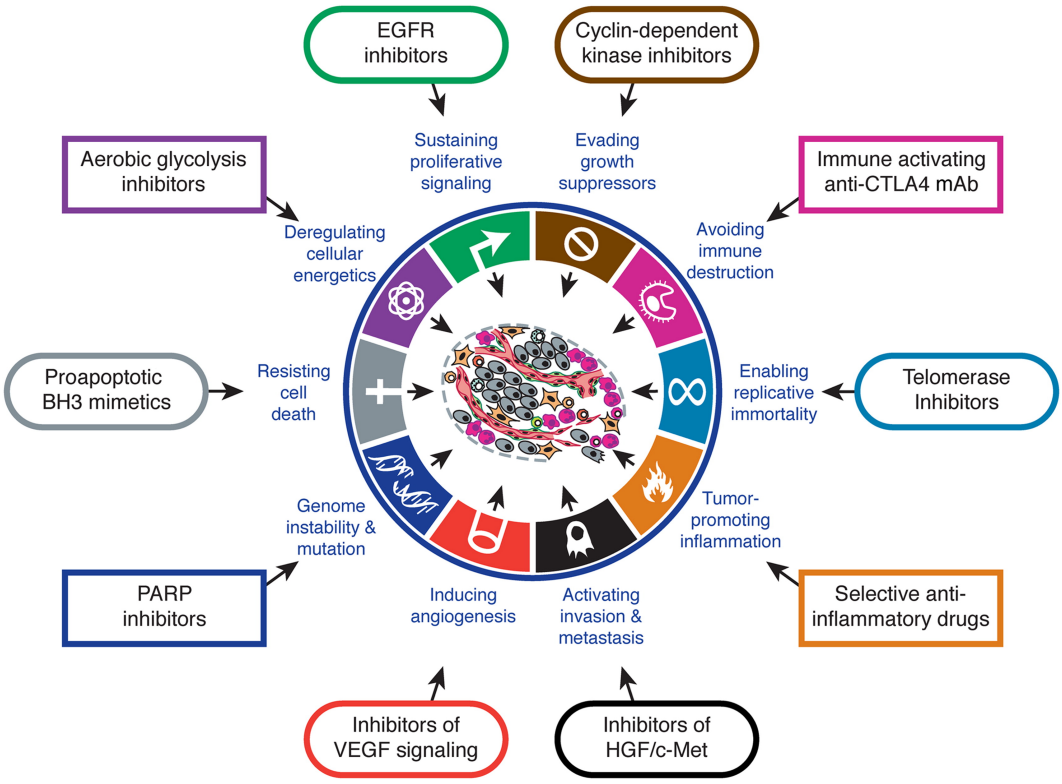

Figure 1-1: The ten hallmarks of cancer cells and the therapeutic targeting of these hallmarks.[3] (Reprinted from Cell, Vol 144, Hanahan, D. and Weinberg, R.A. Hallmarks of Cancer: The Next Generation, 646, Copyright (2011), with permission from Elsevier).

1.2.2. Proteins in cancer cells

In order to maintain their survival, cancer cells overexpress various proteins and antigens in order to maintain their growth and inhibit any apoptotic signal. The first anti-death gene discovered was Bcl-2 family, which is overexpressed in various cancer cell types (pancreatic, prostate, lung and breast, etc.).[4] The Bcl-2 family proteins regulate (by inducing or reducing) all the cell death programs,[5] including apoptosis[5] (programmed cell death: nuclear condensation and chromosomal DNA fragments are packaged inside apoptotic bodies),[6] necrosis[5]

(result from ATP depletion leading to breakdown of plasma membrane and induction of inflammation)[6] and autophagy[5] (self-digest: double membrane vesicles within the cytosol encapsulates the whole organelles and bulk cytoplasm).[6] Research has found that reducing Bcl-2 level can lower tumor growth and its resistance to chemotherapy, hence promoting cell death.[5] Similar to Bcl-2, survivin protein is found to be a member of apoptosis-inhibitor family.[7] Therefore, the overexpression of survivin in many cancer cells leads to resistance of the cells to apoptosis.[7] Preclinical studies also found that inhibition of survivin expression significantly decreases cell proliferation and induce apoptosis of cancer cells.[7]

Another protein type called epidermal growth factor receptor (EGFR), which belongs to erbB family of cell membrane receptors, is highly expressed in malignant cells compared to non-malignant cells.[8] EGFR is responsible for cell proliferation, angiogenesis and metastasis of cancer cells and is activated upon binding with amphiregulin, EGF (epidermal growth factor) or TGF-α (transforming growth factor-α) at the extracellular domain of the receptor (EGFR).[8] Inhibition of EGFR demonstrated anti-angiogenic activity and increase in cellular apoptosis.[8]

Lastly, signal transducer and activator of transcription (STAT) family, especially STAT3, are commonly overexpressed in breast, ovary, pancreas, prostate tumors and melanoma.[9] STAT3 functions as nuclear transcription factor, which can induce large number of cancer-promoting inflammation genes, and regulate genes associated with tumor proliferation, survival, angiogenesis and

invasion.[10] The promoted inflammation can affect from the initiation point to metastasis of tumorigenesis and thus, making it a promising protein for targeted cancer therapy.[10]

1.3. Types of cancer treatments

Many methods have been developed in effort to treat cancer.[11] Surgical removal of tumor was the first approach for cancer treatment thousand of years ago and is still used to date.[11] This conventional method is most successful at early stage, where the cancer cells have not been spread to other sites via metastasis.[11] Nowadays, other less invasive ways have been developed, such as cryosurgery (freezing to kill abnormal cells), use of lasers (cut of tissue or to vaporize cancer cells), or radiofrequency ablation (heat to kill cancer cells).[12]

Advance in modern technology at the late 1900s showed the use of radiation (X-ray) to destroy cancerous tumors with precision, limiting the damage to surrounding normal tissues.[12] The discovery of chemotherapy successfully treated many people with cancer, however, reducing the harmful side effects of chemotherapy remains challenging.[12] Continuous development of biotechnology in the 20th century gave more insight about cancer and their mechanism of operation.[12] Consequently, targeted therapy was developed to target cancer cells based on their distinct characteristics from normal cells, hence reduced severe side effects compared to chemotherapy.[12] This treatment directs on inhibiting the growth factors, cell-cycle proteins, angiogenesis-induced molecules, signaling molecules and apoptosis suppressor.[13]

The fast growing field of nanotechnology, which works with materials at nanoscale (10^{-9} meter), has opened new era for medical diagnosis and treatments of various diseases including cancer.[13] Substantially, the nanomaterial can be used as a carrier to deliver specific drugs, nucleic acid, proteins and peptides to cancer cells in a more direct way.[13] Section 1.4 of this dissertation discusses recent advances in cancer treatment using nanocarriers, including applications of materials such as nanoparticles, lipid-like materials, polymer nanocomposite, nanotubes and other emerging nanomaterials.

1.4. Advances in nanotechnology for cancer treatment

1.4.1. Targeting pathways

Even though surgery operations, radiation and chemotherapy are still widely used for treatments of cancer, they also tend to affect negatively to the normal cells and cause toxicity to the patients.[14] Development of nanotechnology has exploited characteristics of cancer cells for molecular-targeted treatment. [14]

The first being passive targeting, which bases on the leaky properties of the tumor vascular, called EPR (enhanced permeability and retention) effect, which allows the accumulation of drug nanocarriers at the tumor sites.[15] However, to promote the passive targeting therapy, the nanocarriers need to demonstrate long blood circulation half-life, so that the nanocarriers can have sufficient time to reach the target sites.[15] Thus, coating the nanoparticles (NPs) or liposome with hydrophilic polymers, such as polyethylene glycol (PEG) is commonly done to increase the hydrophilicity of the carriers and thus, increase their solubility and circulation in the bloodstream.[15] Although used widely for targeted cancer

therapies, some limitations arise for the passive targeted therapy, such as the lack of EPR effect in certain types of cancer and also, the multiple-drug resistance induced in the cancer cells.[14] This can be overcome by the introduction of targeting agents, such as antibodies, ligand molecules, peptides or aptamers (small pieces of DNA/RNA) on the nanocarriers, which then interact at high affinity with the cell surface markers via ligand-receptor interaction.[14,15] This active targeting method allows selective delivery of nanocarriers to cancer cells, which usually overexpress certain surface markers (antigens or receptors) that can be recognized by the targeting agents on the nanocarriers surface.[14,15,16]

1.4.2. Anti-cancer agents

Advanced knowledge of cancer cells and development of various nanocarriers have allowed the delivery of anti-cancer drugs to target tumors. Many drugs have been discovered to target different traits of the cancer cells, such as using alkylating agents to damage DNA (covalent linkage to the N-7 position on guanine bases), antimetabolites to interfere with DNA synthesis (substituting normal building blocks of DNA and RNA), plant alkaloids to block mitosis (interfere with formation of mitotic spindles) and anthracycline (hinder activities of enzymes involved in DNA replication).[17] For instance, the plant alkaloid drug, paclitaxel (Taxol®, Figure 1-2A), stabilizes the cellular microtubules via polymerization and inhibit with the cell division.[18] Various nanodelivery systems such as micelles, liposomes, nanoparticles, dendrimers and nanohydrogels are successfully used to promote targeted delivery that can reduce the side effects but increase its therapeutic efficiency of paclitaxel.[18] Doxorubicin (Adriamycin®,

Rubex®, Doxil®, Figure 1-2B), an anthracycline antibiotic drug, is liposomal-delivered and can interfere with the synthesis of nucleic acids (DNA and RNA), resulting in apoptosis of cancer cells.[19] Additionally, application of 5-fluorouracil (an anti-metabolite) works by incorporation into RNA in place of uracil (U) base thereby, inhibit the nucleotide synthetic enzyme thymidylate synthase [20] and has been successfully delivered by dendrimers of poly(amidoamine) modified with mPEG-500 (Poly(ethylene glycol) methyl ether, average MW ~500 g/mol).[21]

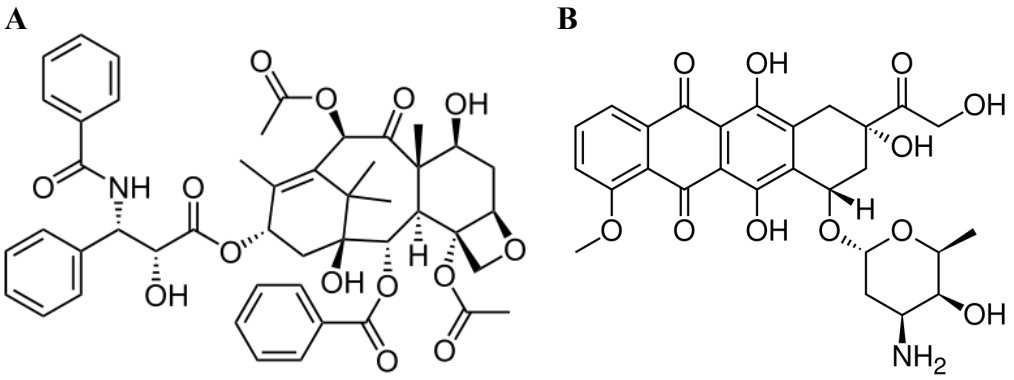

Figure 1-2: Chemical structures of (A) Paclitaxel and (B) Doxorubicin molecules

Along with using drug molecules for cancer therapy, an exciting field of nucleic acids (DNA and RNA) delivery is also rapidly emerging as a promising cancer therapy due to its high specificity and low toxicity.[22] The delivered genes can induce specific protein expression, which can lead to cancer cell apoptosis[23] (e.g. delivery of suicide genes encoding herpes simplex virus thymidine kinase, HSVtk or cytosine deaminase, CD, etc.), inhibit angiogenesis[24] (e.g. genes encoding interferon, IFN or interleukin-12, IL-12 proteins) or inhibit cell proliferation[25] (e.g. genes encoding p53[26] or MDA-7[27] proteins). Finally, a rapidly growing cancer treatment, via RNA interference pathway, involves the delivery of

small RNA that can down-regulate any targeted proteins to suppress the growth, angiogenesis, metastasis and induce apoptosis of the cancer cells.

2. RNA interference

2.1. History

RNA interference (RNAi) is a post-transcriptional gene expression where a short double-stranded RNA binds with RNA-induced silencing complex (RISC) to cleave the targeted mRNA, which then leads to the suppression of the corresponding protein. The discovery of RNA interference (RNAi) more than two decades ago has been a remarkable revolution that opened new pathways for biological and medical researches worldwide.

Napoli and Jorgensen were the first to discover about RNAi effect in 1990.[28] The accidental finding was an attempt to overexpress the synthesis of chalcone synthase (CHS) in petunias by introducing the chimeric petunia CHS gene. Instead, the introduction of the exogenous gene reduced the CHS mRNA level by 50-fold compared to the wild type levels.[28] Romano and Macino also reported the same phenomenon in 1992 when they introduced homologous RNA sequences to *Neurospora crassa*, which caused the suppression of the endogenous carotenogenic albino-3 and albino-1 gene.[29]

In 1998, Fire and Mello published a break-through article demonstrating the effectiveness of gene interference by introducing dsRNA to *Caenorhabditis elegans*.[30] They also emphasized that the dsRNA could be 10- to 100-fold more efficient than the single-stranded RNA (ssRNA) in gene silencing.[30] This

discovery and the works followed had earned them a Nobel Prize in Physiology or Medicine in 2006.

However, the understanding of the silencing mechanism of RNAi was not clear until Tuschl and coworkers observed small piece of RNAs (21-23 nt) in the extracted RNAi samples.[31] This later suggested that these fragments of dsRNA, called micro-RNA (miRNA) or small-interfering RNA (siRNA), were responsible for guiding of the mRNA cleavage at a discrete position.[31]

2.2. Mechanism of RNA interference

There were many efforts to isolate and identify the proteins that are involved in the RNA interference system. The triggering phase of the RNAi process is the introduction of dsRNAs to the cytoplasm, where the dsRNAs are cleaved into short functionalized RNAs. To further investigate, Hannon and colleagues looked into RNase III family members, since they were known to be responsible for cleaving of dsRNAs (double-stranded RNAs).[32] They found a type III endonuclease enzyme encoded by gene number CG4792, known as Drosha or Dicer that was responsible for producing the small RNA with 21-23 nucleotides.[32]

Dicer generally includes DEXD/H ATPase domain, a PAZ domain, and two tandem RNase III domains and a dsRNA-binding domain (dsRBD).[33] Firstly, the dsRBDs is responsible for binding of dsRNA.[33] Then, the Dicer PAZ domain specifically binds to RNA ends, especially RNA duplex with short 3' overhangs.[33] The dsRNA (either precursor stem-loop microRNA or long dsRNA) is centered within the dimer of the RNase II domains, where the two strands are cleaved to yield short RNA with ends of ~2 nt at 3' overhangs.[33] Lastly, the ATPase domain

is found to promote the processing of dsRNA.[33] The role of ATPase domain is not mandatory in human Dicer but it showed to have an autoinhibitory effect on dsRNA processing.[33]

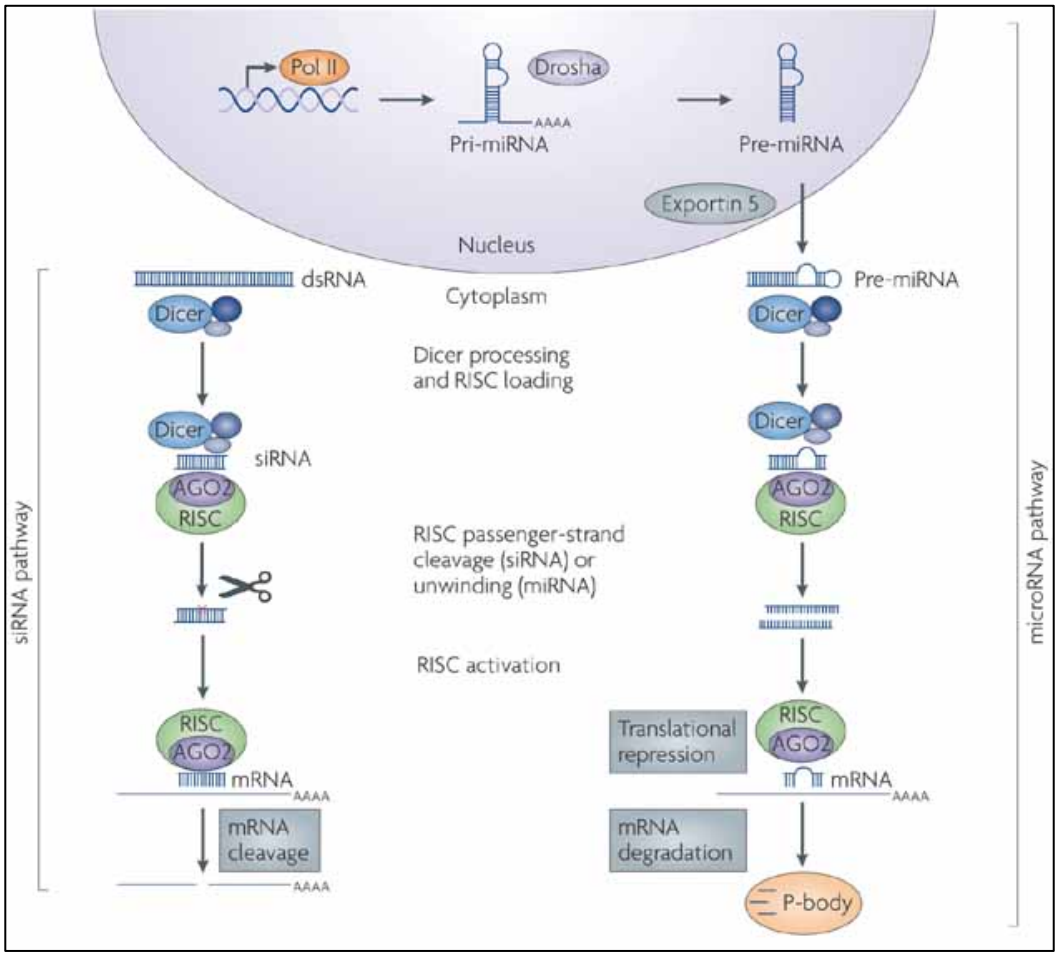

Figure 1-3: Mechanism of RNAi in mammalian cells showing siRNA and miRNA pathways [34] (Reprinted by permission from Macmillan Publishers Ltd: Nature. (Fougerolles, A.; Vornlocher, H-P.; Maraganore, J.; Lieberman, J. Interfering with disease: a progress report on siRNA-based therapeutics. *Nat. Rev. Drug Discov*. **2007**, 6, 443-453), copyright (2007))

The short dsRNA product from Dicer is then introduced to the RISC assembly pathway, where it is unfolded.[33] Here, one of the strands in the duplex is

discarded, whereas the other one is stably bound to Ago effector protein.[32] This Ago protein is responsible for the cleavage of mRNA, resulting in suppression of the target gene expression (Figure 1-3).[32]

2.3. Biogenesis of small functional RNAs

The two small functional pieces are microRNA (miRNA), which occur naturally in plants, animals and can regulate endogenous genes and siRNAs, which respond to foreign nucleic acids from viruses, transgene and transposons. [35] The miRNA was found to originate from stem-loop (hairpin) precursors, whereas siRNA was processed from long and perfectly complementary dsRNAs.[36] These small RNA duplexes go through different pathways called miRISC and siRISC for miRNA and siRNA respectively.[36]

2.3.1. Micro RNA (miRNA)

The miRNAs are single-stranded (folded into hairpin-like structure), expressed naturally in plants, animals and are inhibitors of genes (mRNAs).[35] Most miRNAs are transcripted by RNA polymerase II, capped and polyadenylated and are called primary miRNAs (pri-miRNA) (Figure 1-3).[37] The pri-miRNA displays a terminal loop, an imperfectly paired stem (~33 bp) with flanking segment, which are then processed by RNase III (Dicer) to obtain the stem-loop segment called precursor miRNA (pre-miRNA).[38] Once exported out to the cytoplasm (in animals but inside nucleus in plants), the loop on pre-miRNA is excised to form a mature miRNA duplex (~22 bp) ready for complexation with RISC.[38] During the RISC assembly, miRNA duplexes incorporate into Ago

proteins via an ATP-dependent process.[38] The duplex is unfolded and the unfavorable miRNA strand is discarded from the Ago protein.[38] The functions that RISC performs depends upon the characteristics of Ago protein and complementarity between the target mRNA and miRNA.[38] For instance, low complementarity between mRNA and miRNA leads to translation repression, whereas perfect complementarity between mRNA and miRNA acts similar to siRNA, such that the target mRNA will be cleaved by Ago protein.[38] As such, the mismatching property of miRNA can therefore target up to hundreds of mRNAs.[38]

2.3.2. Small interfering RNA (siRNA)

The double-stranded siRNAs occur naturally in plants and some animals, and mainly known as exogenous gene regulator.[35] In human, siRNAs go through siRISC assembly, which involves three main components: Dicer to cleave the bound dsRNAs into siRNA duplex, TRBP is a dsRNA-binding protein and Ago-2 is responsible for cleaving of the passenger strand (or sense strand) to obtain functional RISC and cleavage of target mRNA (Figure 1-3).[39] The guide strand (or anti-sense strand) selected for continuous function with RISC is the one with the less stable base-paired at the 5' terminus.[39] Cleavage of the targeted mRNA is done precisely between siRNA residues positions 10 and 11 (from the 5' terminus) by the PIWI domain of the Ago protein to yield 5'-monophosphate and 3'-hydoxyl termini.[36] Once completed, the cleaved pieces of mRNA dissociate from the siRNA and the RISC can continue to cleave additional targets.[36] The perfect complementarity between siRNA and target mRNA making the former a

regulator for specific gene knockdown and are the most common RNA to be used for therapeutic purposes.[35]

3. Delivery systems

3.1. Nanoparticles

Gold nanoparticles (Au NPs) are widely used as intracellular nanocarriers for nucleic acids (DNA, miRNA and siRNA) due to their ease of synthesis and functionalization with relatively low toxicity.[40] For instance, Au NPs was used to carry thiolated luciferase-siRNA on the surface via Au-thiol interaction to target luciferase-transfected cells (Figure 1-4).[41] The obtained result showed effective delivery of siRNA to the cytoplasm of the cells within 6 hours and silencing result of ~70% compared to the free siRNA (~33%).[41] In addition, layer-by-layer deposition of polyethyleneimine (PEI)/siRNA/PEI-Au NPs also showed promising EGFP (enhanced green fluorescent protein) silencing of delivered siRNA, which was due to the homogenous property of the synthesized NPs.[42]

Aside from Au NPs, mesoporous silica NPs (MSNPs) were also used to deliver siRNA by modifying the surface with PEI, which promoted cellular uptake and siRNA adhesion on the surface (via electrostatic interaction).[43] The resulting MSNPs/siRNA complexes were able to transfect the cells to knock down green fluorescent proteins (GFPs) expression in HEPA-1 cells.[43] Recently, cationic lipid-coated iron oxide nanoparticles (lipidoids), which possess magnetic property was shown to guide targeting delivery of siRNA to the cells, so that target genes were silenced even at low concentration of siRNA.[44]

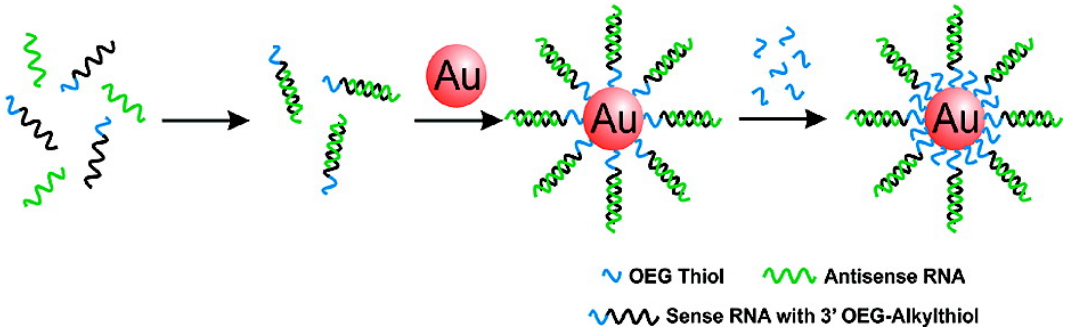

Figure 1-4: Design of Au NPs-thiolated siRNA complexes used for delivery of siRNA.[41] (Reprinted (adapted) with permission from Giljohann, D.; Seferos, D.; Prigodich, A.; Patel, P.; Mirkin, C. Gene Regulation with Polyvalent siRNA-Nanoparticle conjugates. *J. Am. Chem. Soc.* **2009**, 131, 2072-2073. Copyright (2009) American Chemical Society).

3.2. Liposome and lipid-like materials

Liposomes are vesicles made of phospholipid bilayer that can encapsulate drug molecules or nucleic acids within the vesicles.[45] They are low in cytotoxicity and have extensively been used as nanocarriers for more than two decades, especially for siRNA for cancer therapy.[45] Neutral liposome was firstly used due to the low toxicity, low immunogenicity and easy production, but had low transfection efficiency due to the low surface charges.[46] Hence, cationic liposomes were developed to significant improve cellular transfection and release siRNA upon interaction with intracellular serum proteins, lipoproteins leading to effective protein silencing.[46]

For instance, a cationic liposome composed of DOTAP (N-[1-(2,3-Dioleoyloxy)propyl]-N,N,N-trimethylammonium methyl-sulfate) and DOTMA (N-[1-(2,3-dioleoyloxy) propyl]- N, N, N-trimethyl-ammonium methyl sulfate) was functionalized with TfRscFv (transferrin single chain antibody fragment) to

target the receptors commonly over-expressed in cancer cells.[47] The delivered HER-2 siHybrid (human epidermal growth factor receptor 2, sense-DNA/antisense-RNA) successfully inhibited HER-2 expression, reduced the growth and induced apoptosis of pancreatic cells (PANC-1).[47] More recently, a polycation liposomes composed of DCP-TEPA (dicetylphosphate-tetraethylenepentamine) and modified with cyclic RGD-linked DSPE-PEG (distearoylphosphatidylethanolamine-polyethylene glycol) demonstrated effective delivery of luciferase siRNA (siLuc2) to B16F10 murine melanoma cells *in vitro*, and also to B16F10 tumors in the lungs of mice.[48] To date, numerous lipid-based reagents have been commercialized, such as lipofectamine, oligofectamine, TransGene and RNAifect for siRNA transfection.[49]

3.3. Polymers

Cationic polymers such as polyethyleneimine (PEI), poly-L-lysine (PLL), chitosan, polyethylene glycol (PEG) have long been used as delivery system for siRNA, mainly due to the electrostatic interaction with the negatively charged siRNA.[50] PEIs can form compact complexes with siRNA due to it high cationic charges and offer low cytotoxicity to the transfected cells.[50] Recently, a bio-reducible PEI (800 Da), which possesses disulfide bond that can degrade in reducing environment of the cellular cytoplasm was used to deliver VEGF (vascular endothelia growth factor) siRNA.[51] *In vitro* (HepG2 cells) and *in vivo* (mouse model) result was promising as it showed inhibition of reduction in VEGF protein level and tumor growth respectively.[51]

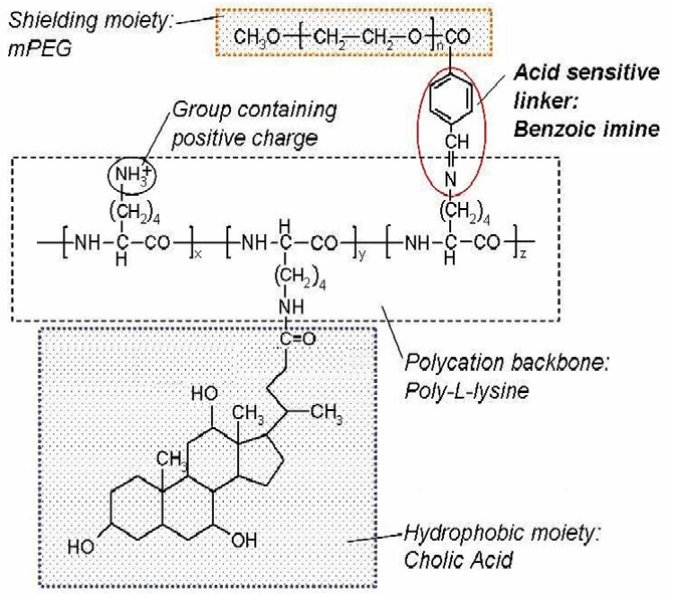

Figure 1-5: Chemical structures of PEGylated PLL-cholic acid.[52] (Reprinted from European Journal of Pharmaceutical Sciences, Vol 45, J. Guo, W. Cheng, J. Gu, C. Ding, X. Qu, Z. Yang, C. O'Driscoll, Systemic delivery of therapeutic small interfering RNA using a pH-triggered amphiphilic poly-L-lysine nanocarrier to suppress prostate cancer growth in mice, 521, Copyright (2011), with permission from Elsevier).

Micelles modified with cholic acid, and PEG-grafted PLL were able to capture the siRNA to target various prostate cancer cell lines (PC-3, TRAMP C1) (Figure 1-5).[52] Result showed effective endolysosomal escape (due to hydrolysis of PEG at low pH), which led to significant gene knockdown (luciferase gene) in the transfected cells.[52] Lastly, PEG is known for its hydrophilicity that promotes longer blood circulation. Complexes of folic acid/PEG/siRNA was delivered to human KB and murine Neuro2A cells to silence EGFP luciferase expressed in the cells, which showed promising silencing of approximately 70-80%.[53]

3.4. Carbon Nanotubes

Carbon nanotubes (CNTs) are highly elongated cylindrical nanostructures that are low in toxicity and immunogenicity.[54] CNTs as nanocarriers have been explored over the last decade for their ability to deliver drugs, proteins and nucleic acids such as DNAs and RNAs to cells.[54] They can interact with the cargos (siRNA) covalently or non-covalently due to the ability to functionalize the surface of CNTs.

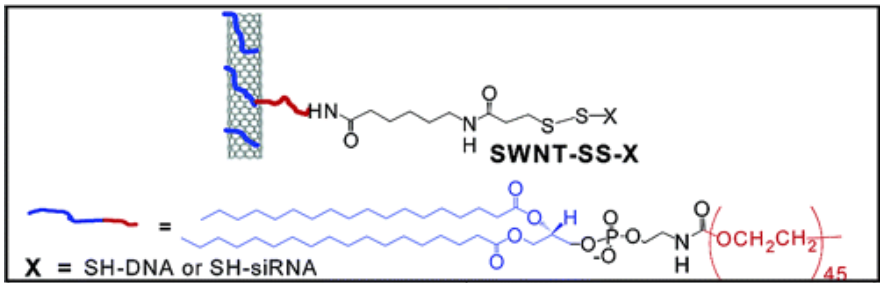

Figure 1-6: SWNT functionalization by thiolated biological molecule X (SH-DNA or SH-siRNA).[55] (Reprinted (adapted) with permission from (Kam, N. W. S.; Liu, Z.; Dai, H. Functionalization of carbon nanotubes via cleavable disulfide bonds for efficient intracellular delivery of siRNA and potent gene silencing. *J. Am. Chem. Soc*. **2005**, 127, 12492-12493. Copyright (2005) American Chemical Society).

Firstly, the functionalized single-walled CNTs (SWCNTs) and thiolated siRNA formed covalent disulfide bond that can be cleaved in reducing environment and has demonstrated effective intracellular delivery of siRNA to mammalian cells (Figure 1-6).[55] In addition, the covalent linkage between PDDA (poly(diallyldimethyl ammonium)chloride) and HMDA (hexamethylenediamine) functionalized SWCNTs and ERK (extracellular signal-regulated kinase) siRNA

was able to transfect primary cardiomyocytes leading to 75% silencing of the target protein.[56]

On the other hand, InsP3Rs (inositol trisphosphate receptor–membrane glycoprotein complex) siRNA interacting non-covalently with carboxyl (COOH)-functionalized SWCNTs could enter hard-to-transfect cell types (neuronal and cardiomyocytes) for efficient protein silencing.[57] More recently, the complexes of siRNA/PEG/SWCNT was studied *in vitro* (lung, NSCLC and pancreatic, MiaCaPa-2 cancer cells) and *in vivo* (mouse model). Results demonstrated protection of siRNA towards serum degradation, with good and uniform cellular uptake and silencing of target proteins.[54] It was also noticed that PEG-modified SWCNTs-siRNA complex has increased the half-life of SWCNTs in the plasma and increased tumor uptake.[54] Significant efforts were made to determine that short SWCNTs (~ 150 nm) are uptaken by cells via endocytotic pathway.[58] Even though there was interaction between the membrane and SWCNTs, the insertion energy was not enough for the penetration of the CNTs through the membrane.[58] This is an important finding that can also help us understand the nature of cellular uptake in our nanotubes system.

4. Rosette nanotubes

4.1. Design

Following the on-going discovery and wide application of nanomaterials (Section 3), a novel class of self-assembly nanotubes, called rosette nanotubes (RNTs) was reported in 2001 by Fenniri *et al.*[59] The building block of the RNTs is called the G∧C base, a hybrid between Watson-Crick's guanine and cytosine

nucleobases (Figure 1-7A).[59] The guanine side of G∧C base possesses donor-donor-acceptor hydrogen bonds (H-bonds) and the cytosine side expresses acceptor-acceptor-donor H-bonds (Figure 1-7 B).[59] The complementary nature of the H-bond arrays between G∧C bases guide six of these molecules to assemble into a supermacrocycle (also known as a rosette, Figure 1-8 A).[59] Due to the spatial arrangement, π-π stacking and hydrophobic property of the bicyclic base, the rosettes stack and self-assemble into RNTs in water or organic solvents (Figure 1-8 B).[59] It is believed that the growth of the RNTs is entropically driven, thus increasing length of RNTs is observed as the temperature of the RNTs solution increases.[60] This temperature-dependent property of the RNTs will be further emphasized in this dissertation (Chapter III and IV), where it plays an important role in the complex formation with siRNA.

One of the advantages of using the RNTs is the ability to covalently attach the G∧C motif with diverse functional linkers, such as, amino acid,[61,62] organic molecules,[60] or peptide sequences.[63, 64, 65, 66] However, these mono-RNTs (with a single G∧C base per molecule) can face stability challenges, especially when the peptide chains on the G∧C motif contain high number of amino acids, or have certain set of amino acids that can be electrostatically or sterically unfavorable for the growth (self-assembly) of the RNTs.[67, 68, 66]

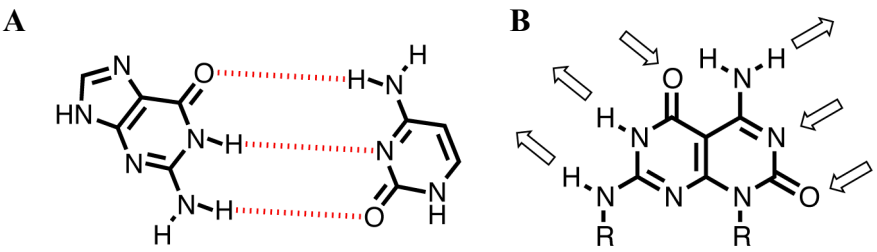

Figure 1-7: (A) Watson-Crick guanine and cytosine bases and their H-bonding and (B) design of a G∧C molecule with arrows showing donor and acceptor sites

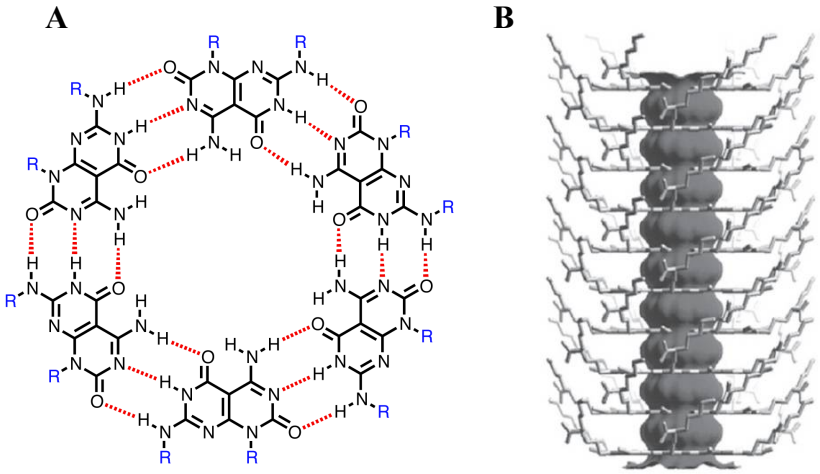

Figure 1-8: (A) H-bond array of six G∧C molecules forming a rosette and (B) a lysine functionalized RNT

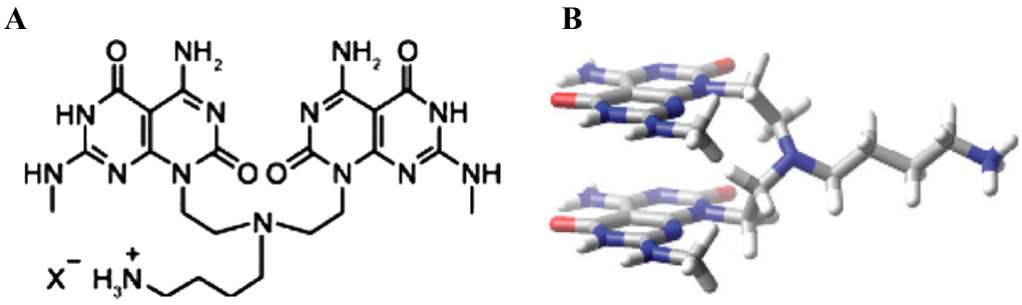

Figure 1-9: (A) Design of twin-G∧C base motif with a linker (TBL) and (B) molecular model of a TBL unit (a twin G∧C derivative).[65,68]

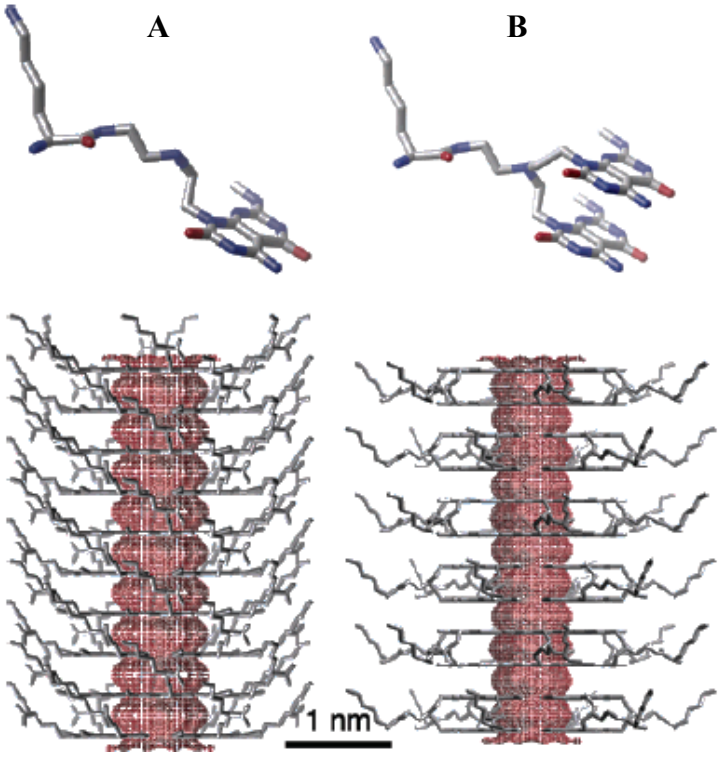

Figure 1-10: Molecular models of G∧C derivatives in (A) mono-RNT and (B) twin-RNT showing the reduction in number of side chains in the twin-base model compared to the mono-base model.[67] (Reprinted (adapted) with permission from (Moralez, J.; Raez, J.; Yamazaki, T.; Motkuri, K.; Kovalenko, A.; Fenniri, H. Helical Rosette Nanotubes with Tunable Stability and Hierarchy. J. *Am. Chem. Soc*. **2005**, 127, 8307-8309.). Copyright (2005) American Chemical Society).

Therefore, the twin-G∧C base model was designed,[67] where two G∧C units are covalently linked at the amino position attaching to one side chain (Figure 1-9).[67] Subsequently, the stability of the twin-RNTs is enhanced by the reduction of side chains number by half (compared to the mono-RNTs) (Figure 1-10).[67, 68] This results in the reduction of steric and electrostatic effects expressed on the surface of RNTs. Since then, numerous twin-RNTs modified with peptides have been

reported such as KRSR-twin RNTs,[65] lysine functionalized twin-RNTs (KnT, n = 1 to 15),[66,69] KSNVILKKYRN-twin RNTs[70] and KKPCCAPTQLN-twin RNTs.[70]

4.2. Applications

This dissertation will focus on the applications of RNTs functionalized with single amino acid or peptides, and their applications in nanoparticles (NPs) synthesis, bone tissue engineering and drug delivery. Firstly, the lysine twin-RNTs (twin RNTs-K) has been explored in NP synthesis.[71,72] Specifically, the nucleation pockets on twin RNTs-K are composed of adjacent lysine side chains. Due to the protonation of lysine molecules at neutral pH, they can attract negatively charged metal entities ($[MCl_4]^{n-}$, M = Au, n = 1, Pd, Pt, n = 2) to create nearly mono-dispersed Au,[71] Pd and Pt[72] nanoparticles. During the process, RNTs demonstrates high stability, showing great potential to act as substrate for metal NPs in catalysis and nano-electronics applications.[72]

In addition, the nature-inspired design of G∧C motif suggested the high biocompatibility of the RNTs *in vitro* and *in vivo*.[61, 62, 73] Moreover, the helical structure of the RNTs[59] reminisces natural bone components such as collagen fibers and hydroxyapatite crystals chemically and structurally.[61] These advantageous properties of RNTs were thus considered for tissue engineering application, where they could help enhancing the osteoblasts (bone-forming cells) adhesion on titanium (Ti) surface to improve the compatibility of Ti for clinical orthopaedic implant.[61] Indeed, significant increase in osteoblast adhesion to a Ti surface was observed from coating Ti with arginine-mono RNTs,[61] lysine-mono RNTs [62] (K1 RNTs), KRSR-twin RNTs [65] or RGD-mono RNTs.[65] In addition,

RNTs-hydrogel nanocomposites, which were created by incorporating poly(2-hydroxyethyl methacrylate) (pHEMA) either with K1 RNTs.[63,73,74,75] or RGDSK-RNTs,[63] also significantly promote the adhesion of the osteoblast and chondrocytes for implantation. Moreover, endothelial cells also showed increasing binding affinity to Ti surface coated with K1 RNTs.[65,76] K95/RGD5–RNTs (co-assembly of K1 RNTs and RGD-mono RNTs)[65] or aminobutane-twin RNTs.[65]

Furthermore, the hydrophobic property of the inner channel of RNTs suggested the ability to capture hydrophobic molecules (specifically drugs and steroids, etc.).[77] For example, tamoxifen (TAM), an anticancer drug for estrogen receptor-positive breast cancer[78] and dexamethasone (DEX),[79] an inflammatory and bone-growth promoting steroid are hydrophobic in nature. These water-insoluble drugs have limited delivery and diffusion to targeted cells in physiological environment.[77] RNTs such as TBL (Figure 1-9) or K1 RNTs possess hydrophilic surface due to the lysine side chains and thus favor blood-stream diffusion. In contrast, the hydrophobic core can encapsulate TAM[77] and DEX[79] drugs. In both cases, studying of the drug diffusion coefficient (by DOSY Nuclear Magnetic Resonance, NMR) and height profiles (by Atomic Force Microscopy, AFM) showed significant decrease in diffusion coefficient of the drug molecules, and dramatic increase in height profile of the cross section of K1 RNTs. Even though the mechanism was unclear, the data strongly supported the incorporation of TAM and DEX with the RNTs. Furthermore, studying the delivery of DEX by K1 RNTs to osteoblast cells showed slow release of DEX

over an extended period of time. This suggested the effective encapsulation, delivering, and release of DEX by RNTs in biological system. These results suggest RNTs material offers an innovative *in vitro* and *in vivo* delivery system to transport hydrophobic drugs.[77, 79]

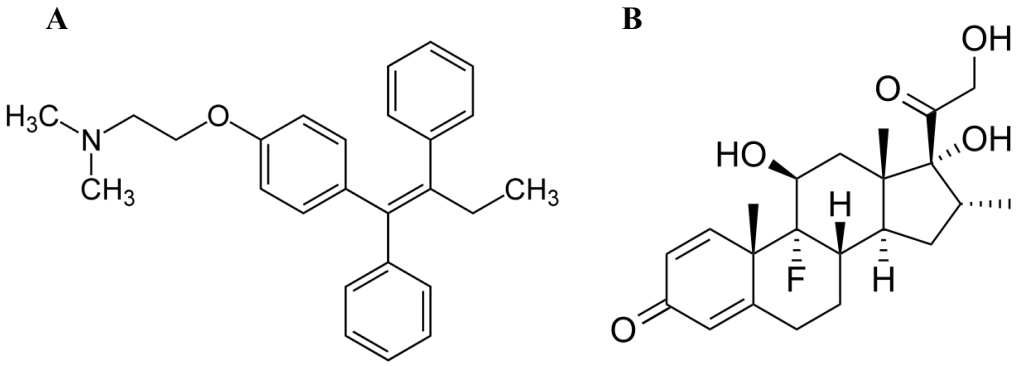

Figure 1-11: Chemical structures of (A) Tamoxifen and (B) Dexamethasone

5. Objectives of the thesis

Keeping in mind the biocompatibility of RNTs and its success in drug delivery (Section 4.2), preliminary experiments also investigated the ability for a library of lysine-functionalized twin-RNTs (KnT, n is number of lysine residues, ranging from 1 to 15) to serve as siRNA carrier[69] lysine functionalized twin-RNTs (KnT, n = 1 to 15).[66,80] A series of fifteen KnT RNTs allowed study of the charge effect of the carrier (RNTs) on the intracellular delivery of siRNA, such as uptake and silencing efficacy of the siRNA.

The second chapter will evaluate the fifteen KnT RNTs on their binding affinity with siRNA at different molar ratios as well as the delivery ability of siRNA by these KnT RNTs. Next, the third chapter will be focused on the low charged twin-RNTs, K1T to K5T RNTs, to improve their intracellular transfection

of siRNA. Here, K3T RNTs-siRNA complexes were the main focus for morphology study and ability of protein silencing. Finally, chapter four will explore the K1 RNTs-siRNA complexes with respect to their binding affinity, cellular transfection and the ability for the delivered siRNA to inhibit the production of targeted proteins.

References

1. Pecorino, L. *Molecular Biology of Cancer,* 3rd ed.; Oxford University Press, 2012.

2. Knowles, M.A.; Selby, P. *Introduction to the Cellular and Molecular Biology of Cancer*. New York: Oxford University Press. 2012

3. Hanahan, D.; Weinberg, R.A. Hallmarks of Cancer: The next generation. *Cell*, **2011**, 144, 646-674.

4. Fahy, B.N.; Schlieman, M.G.; Mortenson, M. M.; Virudachalam, S.; Bold,R. J. Targeting BCL-2 overexpression in various human malignancies through NF-kappaB inhibition by the proteasome inhibitor bortezomib. *Cancer Chemother Pharmacol*. **2005**, 56, 1, 46-54.

5. Yip, K.W.; Reed, J.C. Bcl-2 family proteins and cancer. *Oncogene*. **2008**, 27, 6398-6404.

6. Edinger, A.; Thompson, C. Death by design: apoptosis, necrosis and autophagy *Curr. Opin. Cell Biol.* **2004**, 16, 663-669.

7. Fukuda, S.; Pelus, L. Survivin, a cancer target with an emerging role in normal adult tissues. *Mol. Cancer Ther.* **2006**, 5, 1087-1098.

8. Baselga, J. Why the Epidermal Growth Factor Receptor? The Rationale for Cancer Therapy. *The Oncologist*. **2002**, 7, 4, 2-8.

9. Siddiquee, K.; Turkson, J. STAT3 as a target for inducing apoptosis in solid and hematological tumors. *Cell Res.* **2008**, 18, 2, 354-267.

10. Yu, H.; Pardoll, D.; Jove, R. STATs in cancer inflammation and immunity: a leading role for STAT3. *Nature Rev.* **2009**, 9, 798-809.

11. American Cancer Society. Treatment Types. http://www.cancer.org/treatment/treatmentsandsideeffects/treatmenttypes (accessed July 10, 2013).

12. American Cancer Society. The History of Cancer. http://www.cancer.org/acs/groups/cid/documents/webcontent/002048-pdf. (accessed July 10, 2013).

13. Urruticiechea, A.; Alemany, R.; Balart, J.; Villanueva, A.; Vinal, F.; Capella, G. Recent Advances in Cancer Therapy: An Overview. *Curr. Pharm. Des.*; **2010**, 16, 3-10.

14. Peer, D.; Karp, J. M.; Hong, S.; Farokhzad, O.; Margalit, R.; Langer, R. Nanocarriers as an emerging platform for cancer therapy. *Nature Nanotech.* **2007**, 2, 751-760.

15. Koo, O.M.; Rubinstein, I.; Onyuksel, H. Role of nanotechnology in targeted drug delivery and imaging: a concise review. *Nanomedicine: NBM*. **2005**, 193-212.

16. Grobmyer, S.R.; Moudgil, B.M. *Cancer Nanotechnology: Methods and Protocols*; Methods in Molecular Biology 624; Humana Press. 2010. pp 3-5.

17. American Cancer Society: Different types of chemotherapy drugs. http://www.cancer.org/treatment/treatmentsandsideeffects/treatmenttypes/chemotherapy/chemotherapyprinciplesanin-depthdiscussionoftheechniquesanditsrolein treatment/chemotherapy-principles-types-of-chemo-drugs. (accessed August 1, 2013)

18. Zhang, Z.; Mei, L.; Feng, S. Paclitaxel drug delivery systems. *Expert Opin on Drug Deliv*. **2013**, 10, 3, 325-340.

19. Mitra, S.; Gaur, U.; Ghosh, P.C.; Maitra, A.N. Tumour targeted delivery of encapsulated dextran–doxorubicin conjugate using chitosan nanoparticles as carrier. *J. Control. Release*. **2001**, 74, 317-323.

20. Longley, D.B.; Harkin, P.; Johnston, P. 5-Fluorouracil: Mechanism of action and clinical strategies. *Nat. Rev. Cancer.* **2003**, 3,5, 330-338.

21. Bhadra, D.; Bhadra, S.; Jain, S.; Jain, N.K. A PEGylated dendritic nanoparticulate carrier of fluorouracil. *Int. J. Pharm.* 2003, 257, 111-124.

22. Patil, S.; Rhodes, D.; Burgess, D. DNA-based Therapeutics and DNA Delivery System: A Comprehensive Review. *AAPS J*. **2005**, 7, 1, E61-77.

23. Duarte, S.; Carle, G.; Faneca, H.; Pedroso de Lima, M.; Pierrefit-Carle, V. Suicide gene therapy in cancer: Where do we stand now? *Cancer Lett*. **2012**, 324, 2, 160-170.

24. Tandle, A.; Blazer, D.G.; Libutti, S.K. Antiangiogenic gene therapy of cancer: recent developments. *J. Trans. Med.* **2004**, 2, 22, doi:10.1186/1479-5876-2-22.

25. Cross, D.; Burmester, J.K. Gene Therapy for Cancer Treatment: Past, Present and Future. *Clin. Med. Res.* **2006**, 4, 3, 218-227.

26. Prabha, S.; Sharma, B.; Labhasetwar, V. Inhibition of tumor angiogenesis and growth by nanoparticle-mediated p53 gene therapy in mice. *Can. Gene Ther.* **2012**, 19, 530-537.

27. Inoue, S.; Shanker, M.; Miyahara, R.; Gopalan, B.; Patel, S.; Oida, Y.; Branch, C.; Munshi, A.; Meyn, R.; Andreeff, M.; Tanaka, F.; Mhashilkar, A.; Chada, S.; Ramesh, R. MDA-7/IL-24-Based Cancer Gene Therapy: Translation from the Laboratory to the Clinic. *Curr. Gene Ther.* **2006**, 6, 73-91.

28. Napoli, C.; Lemieux, C.; Jorgensen, R. Introduction of a Chimeric Chalcone Synthase Gene into Petunia Results in Reversible Co-Suppression of Homologous Genes in trans. *Plant Cell.* **1990**, 2, 279-289.

29. Romano, N.; Macino, G. Quelling: transient inactivation of gene expression in Neurospora crassa by transformation with homologous sequences. *Mol. Microbiol.* **1992**, 6, 22, 3343-3353.

30. Fire, A.; Xu, S.; Montgomery, M.; Kostas, S.; Driver, S.; Mello, C. Potent and specific genetic interference by double-strnaded RNA in Caenorhabditis elegans. *Nature*, **1998**, 391, 806-811.

31. Zamore, P.; Tuschl, T.; Sharp, P.; Bartel, D. RNAi: Double-stranded RNA directs the ATP-dependent cleavage of mRNA at 21 to 23 nucleotide intervals. *Cell*. **2000**, 101, 25-33.

32. Liu, J.; Carmell, M.; Rivas, F.; Marsden, C.; Thomson, M.; Song, J.; Hammond, S.; Joshua-Tor, L.; Hannon, G. Argonaute2 is the Catalytic engine of mammalian RNAi. *Science*. **2004**, 305, 1437-1441.

33. Carthew, R.; Sontheimer, E. Origins and Mechanisms of miRNAs and siRNAs. *Cell*. **2009**, 136, 4, 642-655.

34. Fougerolles, A.; Vornlocher, H.-P.; Maraganore, J.; Lieberman, J. Interfering with disease: a progress report on siRNA-based therapeutics. *Nat. Rev. Drug Discov*. **2007**, 6, 443-453.

35. Mack, G. MicroRNA gets down to business. *Nature Biotechnology*. **2007**, 25, 631-638.

36. Tomari, Y.; Zamore, P.D. Perspective: machines for RNAi. *Genes Dev*. **2005**, 19, 517-529.

37. Kim, V.N. MicroRNA biogenesis: coordinated cropping and dicing. *Nat. Rev. Mol. Cell Biol.* **2005**, 6, 376-385.

38. Kwakk, P.B., Iwasaki, S.; Tomari, Y. The microRNA pathway and cancer. *Cancer Sci.* **2010**, 101, 11, 2309-2315.

39. Macrae, I.J.; Ma, E.; Zhou, M.; Robinson, C.V.; Doudna, J.A. In vitro reconstitution of the human RISC-loading complex. *Proc. Natl. Acad. Sci. USA*, **2008**, 105, 512-517.

40. Ghosh, P.; Han, G.; De, M.; Kim, C.; Rotello, V. Gold nanoparticles in delivery applications. *Adv. Drug. Deliv. Rev.* **2008**, 60, 11, 1307-1315.

41. Giljohann, D.; Seferos, D.; Prigodich, A.; Patel, P.; Mirkin, C. Gene Regulation with Polyvalent siRNA-Nanoparticle conjugates. *J. Am. Chem. Soc.* **2009**, 131, 2072-2073.

42. Elbakry, A.; Zaky, A.; Liebl, R.; Rachel, R.; Goepferich, A.; Breunig, M. Layer-by-Layer Assembled Gold Nanoparticles for siRNA delivery. *Nano Lett.* **2009**, 9, 5, 2059-2064.

43. Xia, T.; Kovochich, M.; Liong, M.; Meng, H.; Kabehie, S.; George, S.; Zink, J.; Nel, A. Polyethyleneimine Coating Enhances the Cellular Uptake of Mesoporous Silica Nanoparticles and Allows Safe Delivery of siRNA and DNA Constructs. *ACS Nano*. **2009**, 3, 10, 3273-3286.

44. Kiang, S.; Eltoukhy, A.; Love, K.; Langer, R.; Anderson, D. Lipidoid-Coated Iron Oxide Nanoparticles for Efficient DNA and siRNA delivery. *Nano Lett*. **2013**, 13,3, 1059-1064.

45. Navarro, G.; Essex, S.; Torchilin, V.P. The "Non-viral" Approach for siRNA Delivery in Cancer Treatment: A Special Focus on Micelles and Liposomes. In *DNA and RNA Nanobiotechnologies in Medicine: Diagnosis and Treatment of Diseases*; Erdmann, V.A. & Barciszewski, J.; Springer: Berlin, 2013; pp 241-262.

46. Gao, Y.; Liu, X.L.; Li, X.R. Research progress on siRNA delivery with nonviral carriers. *Int. J. Nanomed.* **2011**, 6, 1017-1025.

47. Hogrefe, R.; Lebedev, A.; Zon, G.; Pirollo, K.; Rait, A.; Zhou, Q.; Yu, W.; Chang, E. Chemically Modified Short Interfering Hybrids (siHYBRIDS): Nanoimmunoliposome Delivery *In Vitro* and *In Vivo* for RNAi of HER-2. *Nucleosides, Nucleotides and Nucleic Acids*. **2006**, 25, 889-907.

48. Yonenaga, N.; Kenjo, E.; Asai, T.; Tsuruta, A.; Shimizu, K.; Dewa, T.; Nango, M.; Oku, N. RGD-based active targeting of novel polycation liposomes bearing siRNA for cancer treatment. *J. Control. Release.* **2012**, 160, 2, 177-181.

49. Lu, Y.; Mahato, R. *Pharmaceutical Perspectives of Cancer Therapeutics*, Springer, 2009.

50. Zhang, S.; Zhao, B.; Jiang, H.; Wang, B.; Ma, B. Cationic lipids and polymers mediated vectors for delivery of siRNA. *J. Control. Release.* **2007**, 123, 1-10.

51. Xia, W.; Li, Y.; Lou, B.; Wang, P.; Gao, X.; Lin, C. Bioreducible PEI-siRNA Nanocomplex for Liver Cancer Therapy: Transfection, Biodistribution, and Tumor Growth Inhibition In Vivo. *J. Nanomat.* **2013**, 384717.

52. Guo, J.; Chen, W.; Gu, J.; Ding, C.; Qu, X.; Yang, Z.; O'Driscoll, C. Systemic delivery of therapeutic small interfering RNA using a pH-triggered amphiphilic poly-L-lysine nanocarrier to suppress prostate cancer growth in mice. *Eur. J. Pharm. Sci.* **2012**, 45, 521-532.

53. Dohmen, C.; Frohlich, T.; Lachelt, U.; Rohl, I.; Vornlocher, H.P.; Hadwiger, P.; Wagner, E. Defined Folate-PEG-siRNA conjugates for receptor-specific gene silencing. *Mole. Ther. Nucleic Acids*. **2012**, 1, e7, doi: 10.1038/mtna.2011.10

54. Kirkpatrick, L.; Weiss, M.; Naumov, A.; Bartholomeusz, G.; Weisman, R.B.; Gliko, O. Carbon Nanotubes: Solution for the Therapeutc Delivery of siRNA? *Materials*. **2012**, 5, 278, 301.

55. Kam, N.W.S.; Liu, Z.; Dai, H. Functionalization of carbon nanotubes via cleavable disulfide bonds for efficient intracellular delivery of siRNA and potent gene silencing. *J. Am. Chem. Soc*. **2005**, 127, 12492-12493.

56. Krajcik, R.; Jung, A.; Hirsch, A.; Neuhuber, W.; Zolk, O. Functionalization of carbon nanotubes enables non-covalent binding and intracellular delivery of small interfering RNTA for efficient knock-down of genes. *Biochem. Biophys. Res. Comm.* **2008**, 369, 595-602.

57. Ladeira, M. S; et al. Highly efficient siRNA delivery system into human and murine cells using single-wall carbon nanotubes. *Nanotechnology*. **2010**, 21, 385101-385112.

58. Yaron, P.; Holt, B.; Short, P.; Losche, M.; Islam, M.; Dahl, K. Single wall carbon nanotubes enter cells by endocytosis and not membrane penetration. *J. Nanobiotech.* **2011**, 9, 45.

59. Fenniri, H.; Mathivanan, P.; Vidale, K.L.; Sherman, D.M.; Hallenga, K.; Wood, K.V.; Stowell, J.G. Helical Rosette Nanotubes: Design, Self-Assembly, and Characterization. *J. Am. Chem. Soc.* **2001**, 123, 3854-3855.

60. Fenniri, H.; Deng, B.L.; Ribbe, A.; Hallenga, K.; Jacob, J.; Thiyagarajan, P. Entropically driven self-assembly of multichannel rosette nanotubes. *Proc. Natl. Acad. Sci.* **2002**, 99, 2, 6587-6492.

61. Chun, A.L.; Moralex, J.G.; Fenniri, H.; Webster, T. J. Helical rosette nanotubes: a more effective orthopedic implant material. *Nanotechnology*, **2004**, 15, S234-S239.

62. Chun, A.L.; Moralex, J.G; Webster, T.J.; Fenniri, H. Helical rosette nanotubes: A biomimetic coating for orthopedics? *Biomaterials*, **2005**, 26, 35, 7304-7309.

63. Zhang, L.; Rakotondradany, F.; Myles, A. J.; Fenniri, H.; Webster, T. J. Arginine-glycine-aspartic acid modified rosette nanotube–hydrogel composites for bone tissue engineering. *Biomaterials*, **2009**, 30, 1309-1320.

64. Suri, S.; Rakotondradany, F.; Myles, A.; Fenniri, H.; Singh, B. The role of RGD-tagged helical rosette nanotubes in the induction of inflammation and apoptosis in human lung adenocarcinoma cells through the P38 MAPK pathway. *Biomaterials***, 2009**, 30, 3084-3090.

65. Zhang, L.; Hemraz, U.D.; Fenniri, H.; Webster, T. J. Tuning cell adhesion on titanium with osteogenic rosette nanotubes. *J. Biomed. Mater. Res. A.* **2010**, 95, 2, 550-563.

66. El-Bakkari, M.; Beingessner, R.L.; Alshamsan, A.; Cho, J.-Y.; Fenniri, H. Electrostatic and Steric Effect of Peptides Functionalized on Self-Assembled Rosette Nanotubes. *Mater. Res. Soc. Symp. Proc.* **2011**, 1316, mrs10.1557/ opl.2011.436

67. Moralez, J.; Raez, J.; Yamazaki, T.; Motkuri, K.; Kovalenko, A.; Fenniri, H. Helical Rosette Nanotubes with Tunable Stability and Hierarchy. *J. Am. Chem. Soc.* **2005**, 127, 8307-8309.

68. Hemraz, U.; Fenniri, H. Rosette Nanotubes: Factors affecting the self-assembly of the monobases versus the twin base system. *Mater. Res. Soc. Symp. Proc.* **2008**, 1057.

69. Alshamsan, A.; El-Bakkari, M.; Fenniri, H. Efficiency of Cationic Rosette Nanotubes for siRNA Delivery *Mater. Res. Soc. Symp. Proc.* **2011**, 1316, mrs10.1557/opl.2011.435

70. Alsbaiee, A.; El-Bakkari, M.; Fenniri, H. The Synthesis and Self-Assembly of Two Bioactive BMP-7 Short Peptides Modified Rosette Nanotubes for Bone Tissue Engineering. *Mater. Res. Soc. Symp. Proc.* **2011**, 1316.

71. Chhabra, R.; Moralez, J.; Raez, J.; Yamazaki, T.; Cho, J-Y.; Myles, A. J., Kovalenko, A.; Fenniri, H. One-Pot Nucleation, Growth, Morphogenesis, and Passivation of 1.4 nm Au Nanoparticles on Self-Assembled Rosette Nanotubes. *J. Am. Chem. Soc*. **2010**, 132, 32-33.

72. Chhabra, R.; Fenniri, H. Electroless Synthesis of 1.4 nm Pd and Pt Nanoparticles on Self-Assembled Rosette Nanotubes. *Mater. Res. Soc. Symp. Proc.* **2011**, 1301, 45-50.

73. Zhang, L.; Ramsaywack, S.; Fenniri, H.; Webster, T. J. Helical Rosette Nanotubes as a Biomimetic Tissue Engineering Scaffold Material. *Proc. of AIChE*, *Annual Meeting*, **2006.**

74. Zhang, L.; Chen, Y.; Rodriguez, J.; Fenniri, H.; Webster, T. Biomimetic helical rosette nanotubes on nanocrystalline hydroxyapatite coatings on titanium for improving orthopedic implants. *Int. J. Nanomed.* **2008**, 3, 3, 323-333.

75. Chen, Y.; Bilgen, B.; Pareta, R.; Myles, A.; Fenniri, H.; Ciombor, D.; Aaron, R.; Webster, T. J. Self-assembled rosette nanotube/hydrogel composites for cartilage tissue engineering. *Tissue Engineering: Part C*. **2010**, 16, 6, 1233-1244.

76. Fine, E.; Zhang, L.; Fenniri, H.; Webster, T. J. Enhanced endothelial cell functions on rosette nanotube-coated titanium vascular stents. **2009**, 4, 91-97

77. Song, S.; Chen, Y.; Yan, Z.; Fenniri, H.; Webster, T. J. Self-assembled rosette nanotubes for incorporating hydrophobic drugs in physiological environments. *Int. J. Nanomed.* **2011**, 6, 101-107.

78. Macgregor, J.; Jordan, V. C. Basic guide to the mechanisms of antiestrogen action. *Pharmacol Rev.* **1998**, 50, 2, 151-196.

79. Chen, Y.; Song, S.; Zhimin, Y.; Fenniri, H.; Webster, T. J. Self-assembled rosette nanotubes for incorporating hydrophobic drugs in physiological environments. *Int. J. Nanomed.* **2011**, 6, 1035-1044.

80. Alshamsan, A.; El-Bakkari, M.; Fenniri, H. Efficiency of Cationic Rosette Nanotubes for siRNA Delivery *Mater. Res. Soc. Symp. Proc.* **2011**, 1316, mrs10.1557/opl.2011.435

Chapter II

Screening of K1T to K15T Rosette Nanotubes as siRNA carrier

1. Introduction

Current research in siRNA delivery demonstrates increasing use of synthetic cationic polymer systems due to their low toxicity and the ability to form high complexation with siRNA.[1,2] In most of these systems, non-covalent electrostatic interaction is the key for binding of negatively charged siRNA and positively charged polymers.

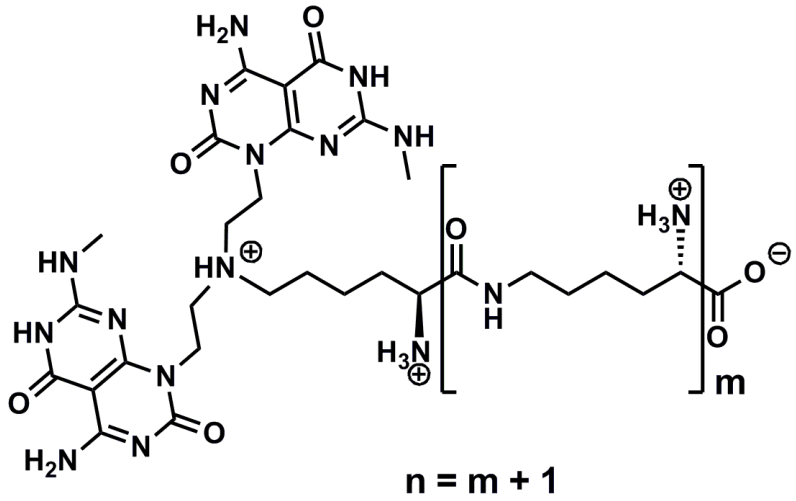

Figure 2-1: Design of lysine functionalized twin-G∧C with n = 1 to 15 for K1T to K15T molecules.

Rosette nanotubes (RNTs) compose of G∧C bases organizing to form stable nanostructure that can be functionalized with (single) amino acid or peptides. The RNTs system can act in similar way as cationic polymers with positively charged side chains, such as lysine peptides, expressing on the surface of the RNTs. A library of fifteen lysine-functionalized twin-RNTs (KnT RNTs, n = 1 to 15, Figure 2-1) was synthesized[3] with one to fifteen lysine molecules attached on the twin-G∧C motif. An example of K1T molecule is shown (Figure 2-2, Figure 2-3A), where six of these molecules arrange into a rosette (Figure 2-3B), many of which then stack via π- π bonding to form K1T RNT

(Figure 2-3C). The cationic lysine residues on the surface of the RNTs (Figure 2-3C) enable electrostatic interaction with siRNA[4] and moreover, with the anionic cellular membrane. As such, RNTs can be used to enhance intracellular delivery of siRNA to cancer cells for therapeutic purposes.[4]

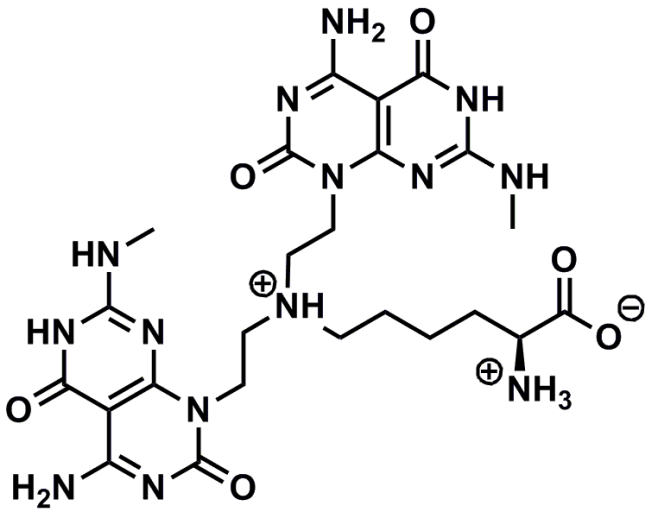

Figure 2-2: Design of K1T molecules.

This chapter aims to examine the siRNA delivery ability of these fifteen KnT RNTs (Figure 2-1) *in vitro*. Firstly, we assessed the binding efficiency of the KnT RNTs with siRNA, along with the protecting ability of the former against serum degradation of siRNA. In addition, the effect of lysine side chains in fifteen KnT compounds was observed using Scanning Electron Microscope (SEM), regarding to the formation of the KnT RNTs. Most importantly, the chapter studied the cellular uptake efficiency and uptake mechanism of the KnT RNTs-siRNA complexes in HCT116 cell line. Lastly, *in vitro* cytotoxicity of KnT RNTs was evaluated dose and time-dependently to evaluate the biocompatibility of these RNTs to the cells.

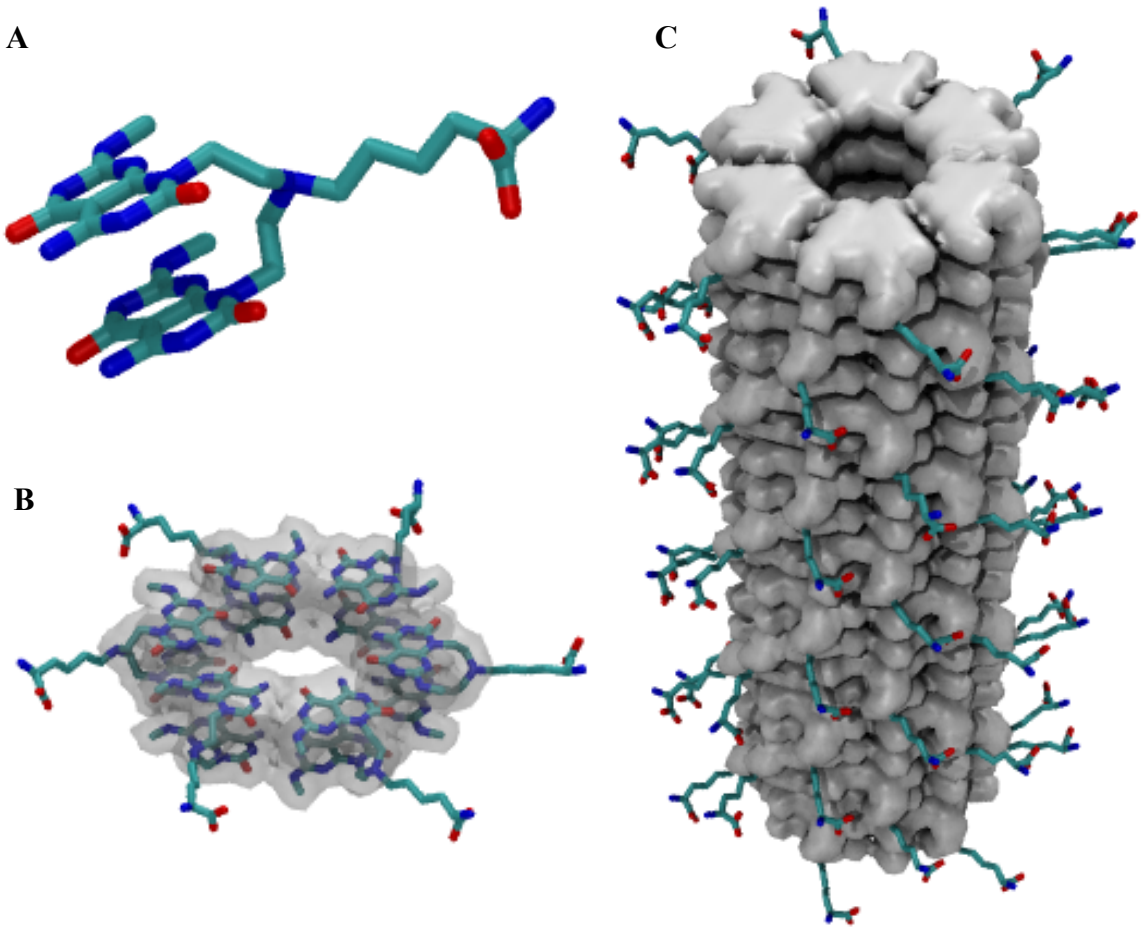

Figure 2-3: Molecular model of (A) K1T molecule, (B) K1T rosette and (C) K1T RNTs.

2. Materials and Methods

2.1. Materials

Compounds of lysine functionalized twin-G∧C motif (K1T to K15T) were synthesized previously in Fenniri lab by Dr. El-Bakkari.[3] Buffers used were Tris-acetate-EDTA (TAE, 4.84 g of Tris-base, 1.142 mL of acetate, 20 mL of 0.5 M sodium EDTA in 1L), phosphate buffer saline (PBS, NaCl 137 mmol/L, 0.02% KCl, 0.144% Na_2HPO_4, 0.024% KH_2PO_4, pH 7.4) and 10x DNA loading buffer (0.25% Bromophenol Blue, 0.25% Xylene Cyanol, 0.2 M EDTA, 50% v/v glycerol).

Silencer Negative Control siRNA, Silencer FAM Labeled Negative Control siRNA #1 were purchased from Ambion. HCT116 cells, McCoy5A medium were purchased from ATCC. Reagents for cell culture, Fetal Bovine Serum (FBS), 0.25% Trypsin-EDTA, penicillin and streptomycin were purchased from GIBCO. Cell labeling reagents, LysoTracker Red DND-99, Prolong Gold Antifade Reagent with DAPI were obtained from Invitrogen. INTERFERin was purchased Polyplus transfection. Thiazolyl blue tetrazolium bromide, paraformaldehyde was obtained from Sigma-Aldrich. Circular coverslip was obtained from VWR. TEM carbon-coated 400-mesh copper grids were purchased from Electron Microscopy Sciences.

2.2. General Methods

Stock solutions of K1T to K15T RNTs (1 mg/mL) were dissolved in deionized water, followed by sonication and heating in the oil bath at 90 ^{o}C for 15 minutes. The molecular weight obtained from elemental analysis, molar concentration of each KnT RNTs solutions and net charges for the KnT compounds were summarized in Table 2-1. Net charge of each KnT compound is calculated based on the summation of all positive and negative charges per KnT molecule. For instance, K1T has a net charge of +1 (Figure 2-2). Stock solutions of negative control siRNA and FAM-negative control siRNA (average MW ~14000 g/mol) were dissolved in nuclease-free water (1 mg/mL, 0.07 M).

HCT116 (human colorectal carcinoma) cells were cultured in McCoy5A medium (10% FBS, 100 units/mL penicillin, 100 μg/mL streptomycin) in a 37 ^{o}C incubator at 5% CO_2 atmosphere. Cells were detached for sub-culturing by trypsin solution.

Compounds	MW (g/mol)	Concentration (mM)	Net charge
K1T	972.83	1.03	+1
K2T	1194.45	0.84	+2
K3T	1493.53	0.67	+3
K4T	1696.63	0.59	+4
K5T	1968.70	0.51	+5
K6T	2294.80	0.44	+6
K7T	2536.89	0.39	+7
K8T	2844.98	0.35	+8
K9T	3039.08	0.33	+9
K10T	3395.16	0.29	+10
K11T	3673.26	0.27	+11
K12T	3633.34	0.28	+12
K13T	4037.41	0.25	+13
K14T	4231.50	0.24	+14
K15T	4037.41	0.25	+15

Table 2-1: MW of K1T to K15T compounds and molar concentration (mM) of the RNTs solutions (1 mg/mL) prepared.

2.3. Agarose Gel Electrophoresis

2.3.1. Complexation of siRNA with RNTs

All the agarose gel electrophoresis experiments used 2% gel (2.4 g of agarose in 120 mL of hot TAE buffer). RNTs were mixed with siRNA (0.1 nmol, 1.4 μL) at various molar ratios (0.5, 1, 2.5, 5, 10 and 20:1, RNTs to siRNA respectively) in 10 μL of (A) PBS and (B) serum-free McCoy5A medium (SFM). The RNTs-siRNA complexes were incubated for 30 minutes at rt, followed by the addition of 10x gel-loading buffer (1 μL) prior to loading the samples on the gel. The gel was set up using Bio-Rad apparatus, running at 150 V for 20 minutes, followed by ethidium bromide (0.5 μg/ml) staining for 20 minutes. Gel visualization was done using UVP BioDocIt BioImaging System. The signal of unbound siRNA on the gel image was measured by ImageJ software.

2.3.2. Protection of siRNA by RNTs from serum degradation

The degree of siRNA degradation dose and time-dependency was first tested. Solutions of negative control siRNA (0.1 nmol) in 10 μL PBS (0, 10, 25, and 50% FBS) were incubated in a 37 ^{o}C shaker (200 rpm) for 0, 1, 6, 12 and 24 hours. Agarose gel experiment was then performed (description in Section 2.3.1).

Next, complexes of K1T to K15T RNTs with siRNA (molar ratio of 20:1) were prepared in PBS buffer (Section 2.3.1). FBS was added to each solution to obtain final concentrations of 10% FBS. The RNTs-siRNA mixture was incubated in a 37 ^{o}C shaker for 24 hours. After the incubation, heparin (5 μL, 20 μg/μL) was added to the RNTs-siRNA mixture for 1 hour at rt to displace siRNA from the RNTs. Agarose gel experiment was performed (description in Section 2.3.1) to detect the intact siRNA protected by RNTs from serum degradation.

2.4. Characterization by Scanning Electron Microscopy

RNTs samples were diluted with deionized water (0.012 μg/μL). K5T, K10T and K15T RNTs-siRNA complexes (molar ratio of 20:1, 0.1 nmol siRNA) were prepared in 50 μL SFM, followed by 30 minutes incubation and dilution in deionized water (0.012 μg/μL RNTs).

SEM samples were prepared by depositing the diluted solutions on carbon-coated 400-mesh copper grids and blotting after 20 seconds. All samples were air-dried and heated on a hotplate for 5 minutes prior to imaging. SEM images were obtained at 30 kV accelerating voltage, 20 μA and a working distance of 5 to 8 mm on a high-resolution Hitachi S-4800 cold field emission SEM and ultra high-resolution Hitachi S-5500 cold field emission SEM.

2.5. Confocal and Fluorescence Imaging

2.5.1. General Methods

The cells were seeded onto circular cover slips in a 12-well plate (1 mL per well, 50-60% cell confluence) and incubated for 24 hours. The medium was then discarded and SFM was added to the wells. The KnT RNTs-FAM siRNA complexes (molar ratio of 20:1) were prepared in SFM (50 μL) as described in Section 2.4. Positive control INTERFERin-FAM siRNA complex was used (mixture of 4 μL INTERFERin solution and 1.4 μL FAM siRNA, 20 minutes incubation), whereas the negative control sample was FAM-siRNA only (1.4 μL). The KnT RNTs-siRNA complexes and the two controls were added to the wells. After the required incubation time, the cells were washed with PBS (3 x 30 seconds) and incubated with 1mL of LysoTracker Red DND-99 in SFM (1 μM) for 20 minutes at 37 ^{o}C. The cells were washed with PBS (3 x 30 seconds) before fixation with 4% paraformaldehyde for 10 minutes. One drop of DAPI mounting medium was deposited on the microscope slide and the coverslip was mounted on the slide.

The cells were imaged using fluorescence (Olympus IX81) and confocal laser scanning (Zeiss LSM 710) microscopes. Image processing was done using Metamorph software for fluorescence imaging, Zeiss LSM software (ZEN) for confocal imaging. FITC (green), DAPI (blue), Cy3 (red) channels were used to observe FAM-labeled siRNA, DAPI-labeled nucleus and DND99-labeled acidic compartments respectively. Sliced images of cells (in z-direction) were taken in selected area using z-stack experiment on ZEN software and processed by Imaris software to form 3D visualization of the imaged area.

2.5.2. Temperature-dependent endocytosis test

HCT116 cells seeded in two petri dishes were transfected with K15T RNTs-FAM siRNA for two hours at two temperature settings: (A) 4 ^{o}C refrigerator and (B) 37 ^{o}C incubator. The cells were fixed, stained with DAPI and imaged using fluorescence microscope (Section 2.5.1).

2.5.3. Cell uptake of KnT RNTs and siRNA complexes

The cells were treated with K1T to K15T RNTs-FAM siRNA for 24 hours. The cells were fixed, stained with DAPI and imaged using fluorescence microscope (Section 2.5.1).

2.5.4. Time-point study

HCT116 cells in 12 well-plates were treated with K5T, K10T and K15T RNTs-FAM siRNA for 3, 6, 12, 24, 36, 48, 72 and 96 hours. Cells were labeled with DND99, fixed, stained with DAPI and imaged using confocal microscope (Section 2.5.1).

2.6. Cell viability study

HCT116 cells were seeded in 96-well plate (100 μL/well) for 24 hours prior to transfection with RNTs. Cells were transfected with (A) K10T RNTs (0.25, 0.5, 1, 2 and 4 μM) for 24, 48, 72, 96 hours and (B) K15T RNTs (0.002, 0.004, 0.008, 0.016, 0.031, 0.063, 0.125, 0.25, 0.5, 1 and 2 μM) for 48, 72 and 96 hours. At the end of the treatment, the medium from each well was discarded and cells were rinsed with PBS (2 x 30 seconds). Then, thiazolyl blue tetrazolium bromide in SFM (100 μL, 5 μg/μL) was added to each well followed by 4 hours of incubation at 37 ^{o}C. Medium from the wells was then removed and DMSO (100μL) was added to each well to dissolve the insoluble MTT

formazan. Cell viability was determined by measuring the absorbance of each sample of the formazan product read at 570 nm using a microplate reader (AD-LD).

3. Results and Discussions

3.1. Complexation of siRNA and KnT RNTs

For the RNTs to serve as a successful carrier for the cargo (siRNA), it has to demonstrate good binding ability with siRNA. Ideally, we want the maximum number of siRNA to be captured and delivered to the cytosol of the cells. Since RNTs do not bind covalently to the siRNA, electrostatic interaction plays a major role in the binding of siRNA (anionic phosphate backbones) and the RNTs (cationic lysine side chains).

Here, agarose gel shift assay was used to measure the amount of unbound siRNA in solutions of KnT RNTs. A common trend was observed in both solvents of PBS (Figure 2-4) and SFM (Figure 2-5). As the number of lysine residues increased on the RNTs (from 1 to 15), lower molar ratio of RNTs : siRNA was required to fully capture the siRNA. This is expected due to the increasing net charge per mole of G∧C motif from K1T to K15T (Table 2-1).

Percentage of unbound siRNA showed a more subtle reduction when exposing to K1T to K15T RNTs in PBS (Figure 2-4). Interestingly, a sudden change was observed for siRNA interaction with K1T-K6T RNTs compared with K7T-K15T RNTs in SFM (Figure 2-5). In both PBS and SFM solvents, the increase in siRNA binding relative to the increase in positive charges on the RNTs is a strong indication of electrostatic interaction in the system.

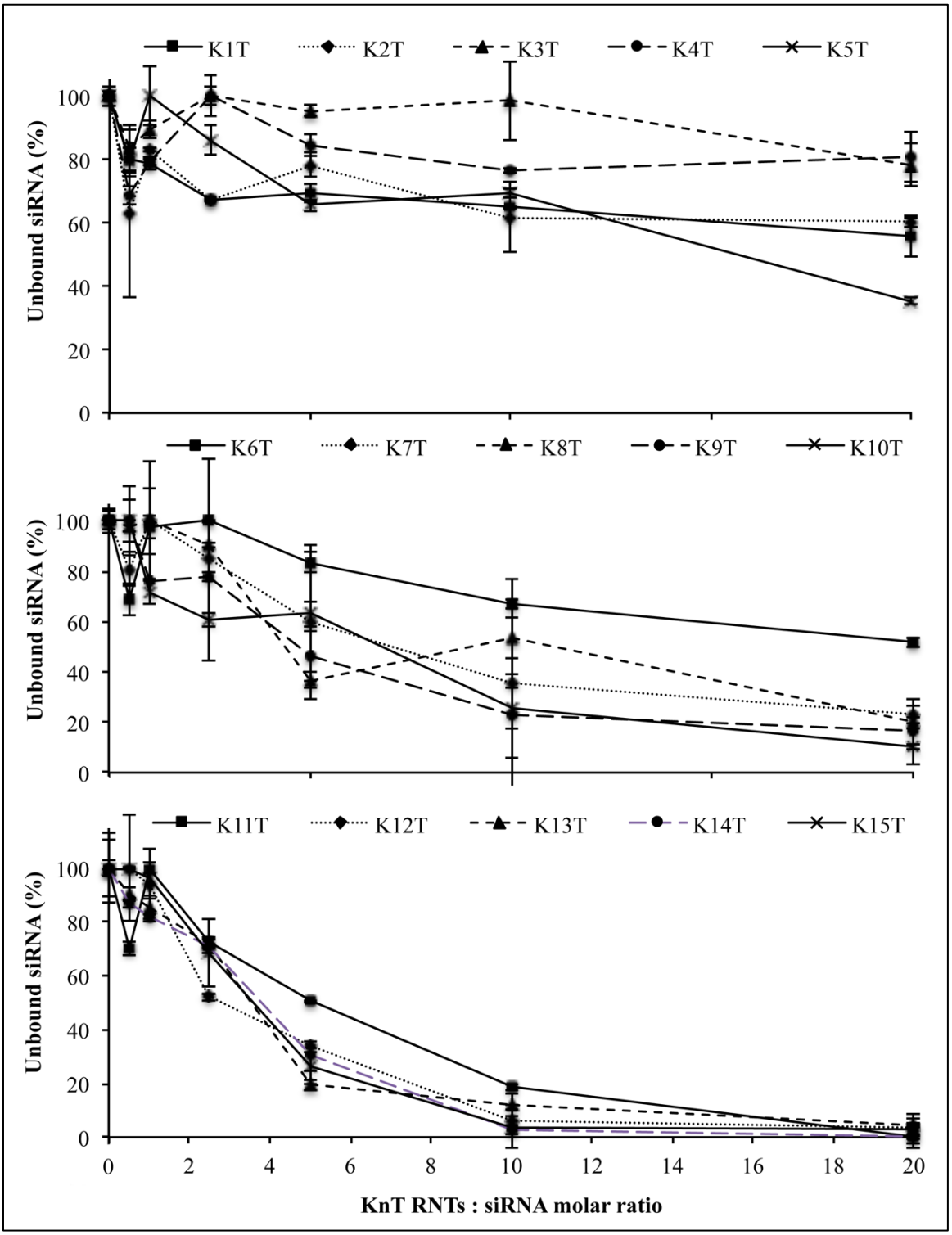

Figure 2-4: Binding study of KnT RNTs (n = 1 – 15) and siRNA in PBS (molar ratio of 0.5, 1, 2.5, 5, 10 and 20:1) using agarose gel shift assay.

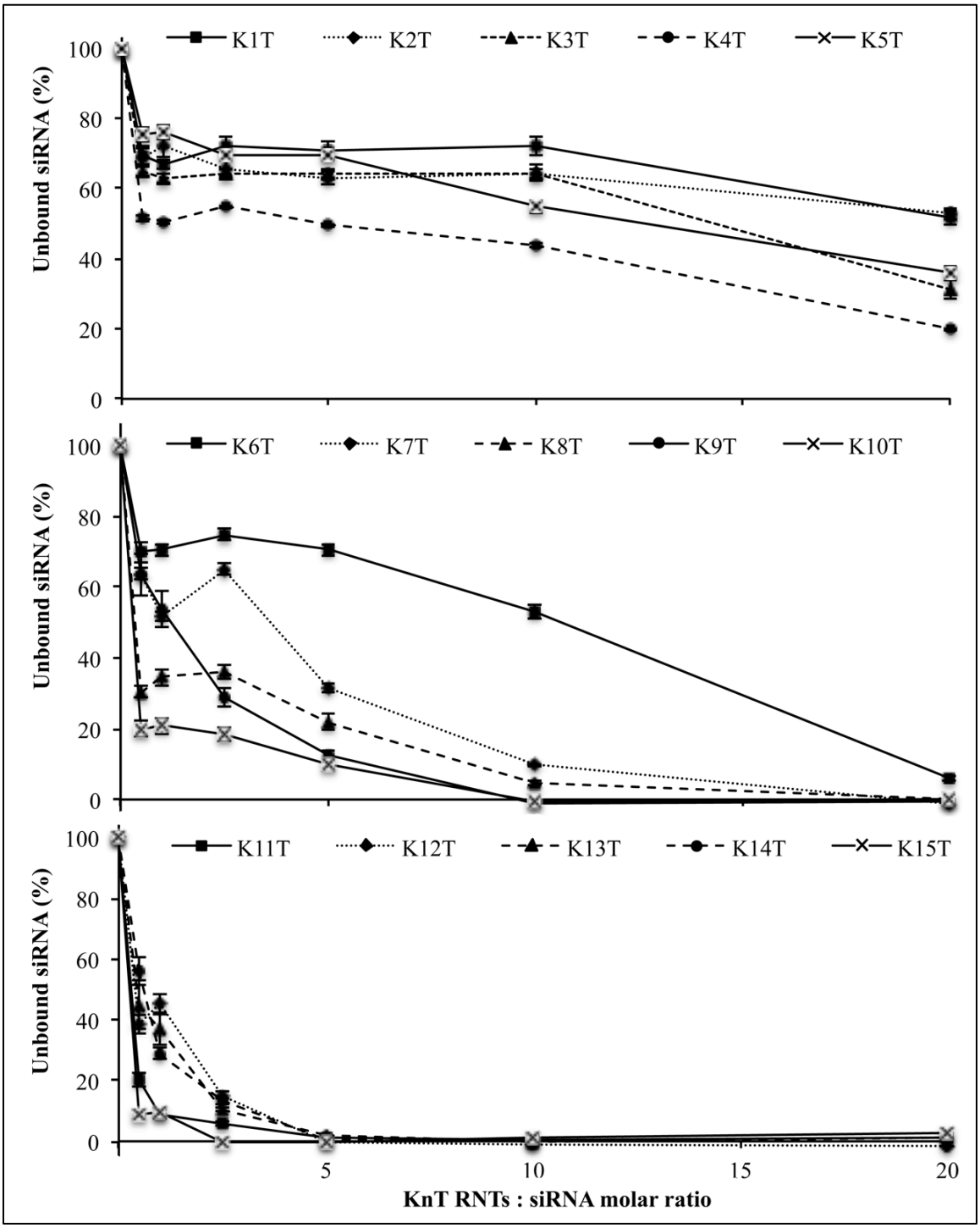

Figure 2-5: Binding study of KnT RNTs (n = 1 – 15) and siRNA in SFM (molar ratio of 0.5, 1, 2.5, 5, 10, 20:1) using agarose gel shift assay.

3.2. Protection of siRNA by KnT RNTs from serum degradation

In the physiological environment, unprotected siRNA undergoes serum degradation due to the presence of RNase. As such, a carrier system for siRNA is required so that the former protects the siRNA from degradation. Here, we examine the stability of the RNTs and siRNA complexes in serum environment (nuclease-containing FBS). More specifically, the RNTs are required to bind strongly to the siRNA, preventing them from being displaced by the polyanion competitor and digested by RNase in the serum.

Firstly, the degree of siRNA degradation dose and time-dependency was tested by incubating siRNA in various FBS concentrations (0, 10, 25 and 50% FBS in medium) at different incubation times (0, 1, 6, 12 and 24 hours) (Figure 2-6). Incubation of naked siRNA at 10% FBS medium for 24 hours showed almost complete degradation of siRNA and thus, this condition was selected to test for the protection of siRNA by KnT RNTs.

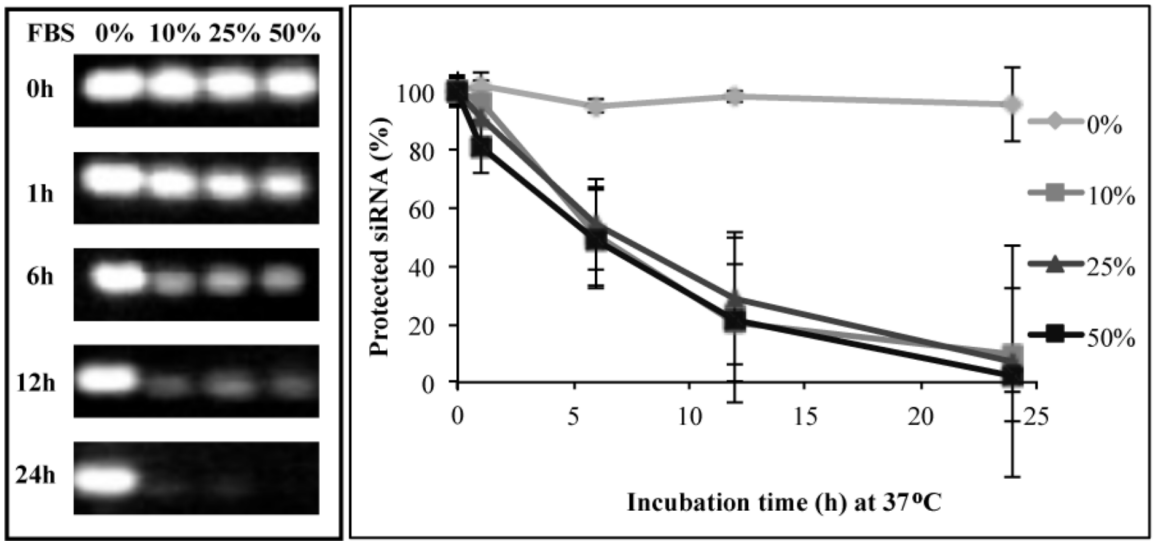

Figure 2-6: Study of siRNA degradation in 0%, 10%, 25%, 50% of FBS for 0, 1, 6, 12 and 24 hours at 37 ^{o}C.

The experiment to test the protection ability of KnT RNTs against siRNA degradation was performed by incubating fifteen RNTs-siRNA complexes (molar ratio of 20:1) in 10% FBS for 24 hours. The result (Figure 2-7) showed that K1T to K4T RNTs were able to protect less than 40% of siRNA during the serum incubation. This is due to the low siRNA loading ability (Section 3.1) and ease in siRNA displacement (by the polyanion competitors) of K1T to K4T RNTs leading to serum degradation of naked siRNA. On the other hand, K5T to K15T RNTs demonstrated good protection ability of siRNA against serum degradation with greater than 55% of siRNA recovered. Especially in the case of K9T to K15T RNTs, where they were able to protect more than 80% of siRNA during the 24 hours of serum incubation.

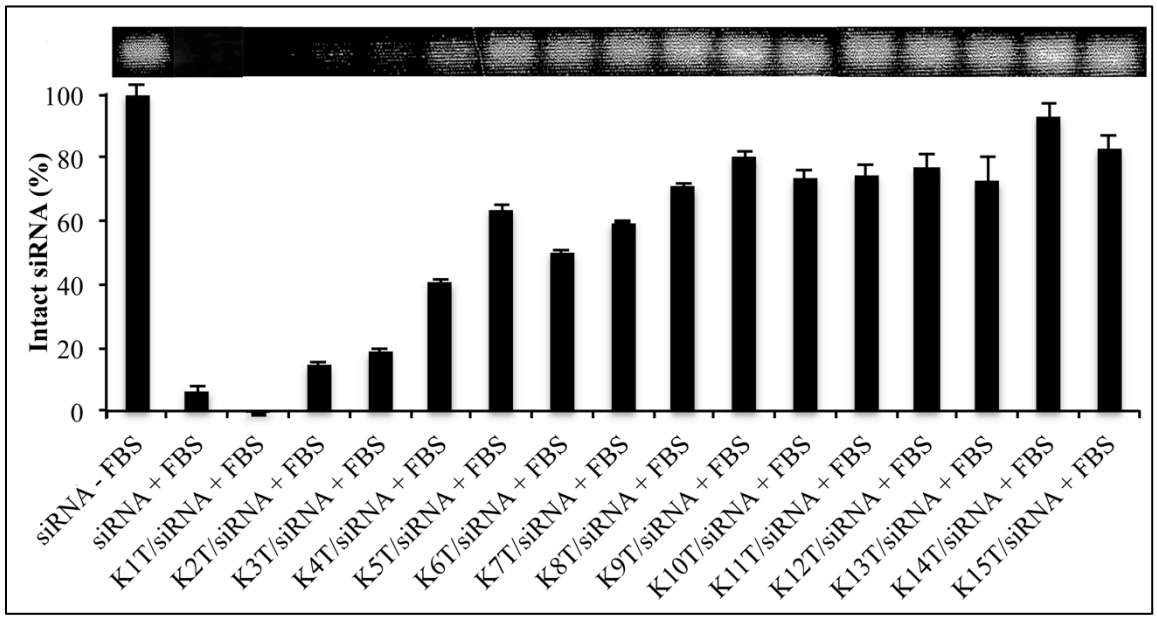

Figure 2-7: Study of intact siRNA protected by KnT RNTs (n = 1 - 15) in presence of FBS (+ FBS) compared to the control of siRNA without FBS (- FBS).

Improvement in protective ability from K1T to K15T RNTs against serum degradation of siRNA implies the significance of electrostatic interaction in the RNTs-

siRNA system. Specifically, higher cationic charges on the RNTs can bind and create stable complexation with the siRNA hence, blocking the nuclease access to the siRNA. Stable RNTs-siRNA complexes can also prevent the displacement of siRNA by the negatively charged competitors in the serum, so that most of siRNA can be delivered to the cells. Thus far, encouraging binding and protective ability of siRNA by the KnT RNTs indicate that these RNTs can act as siRNA carrier, protecting them during the treatment for protein silencing purposes.

3.3. Characterization of KnT RNTs and their complexes with siRNA

The morphology of KnT RNTs (formed in water) and the complexes of KnT RNTs-siRNA (formed in SFM) were determined by SEM. Generally, SEM images (Figure 2-8, 2-9, 2-10) showed obvious decrease in length of the KnT RNTs as the number of lysine increased on the twin-G∧C molecules (1 to 15). Formation of RNTs for K1T to K7T compounds was observed, whereas K8T to K15T compounds in solution showed little to no obvious RNTs. This accounts for the steric hindrance and electrostatic repulsion from the bulky and higher net charged lysine peptides on the twin-G∧C base.[3] Hence, stacking of the hexameric G∧C rosettes (supramacrocycle) or possibly the formation of the rosette itself is restricted.[3] However, short K10T and K15T RNTs were observed in SFM (Figure 2-11 B, C). This is resulted from the neutralization of the cationic lysine side chains by the salt content in SFM, which further suggests the stacking limitation caused by electrostatic repulsion of the long lysine peptide chains.

Complexes of K5T, K10T and K15T RNTs-siRNA (molar ratio of 20:1) forming in SFM were also examined by SEM (Figure 2-11). Observation showed presence of bundles indicated the attracted interaction between KnT RNTs and siRNA, which

supported earlier result from Section 3.1. The complexation may initiate from the electrostatic attraction between the lysine side chains on the RNTs and phosphate backbone of siRNA, leading to neutralization of the RNTs. These neutral RNTs could then attract to each other, free RNTs or siRNA to form bigger aggregates.

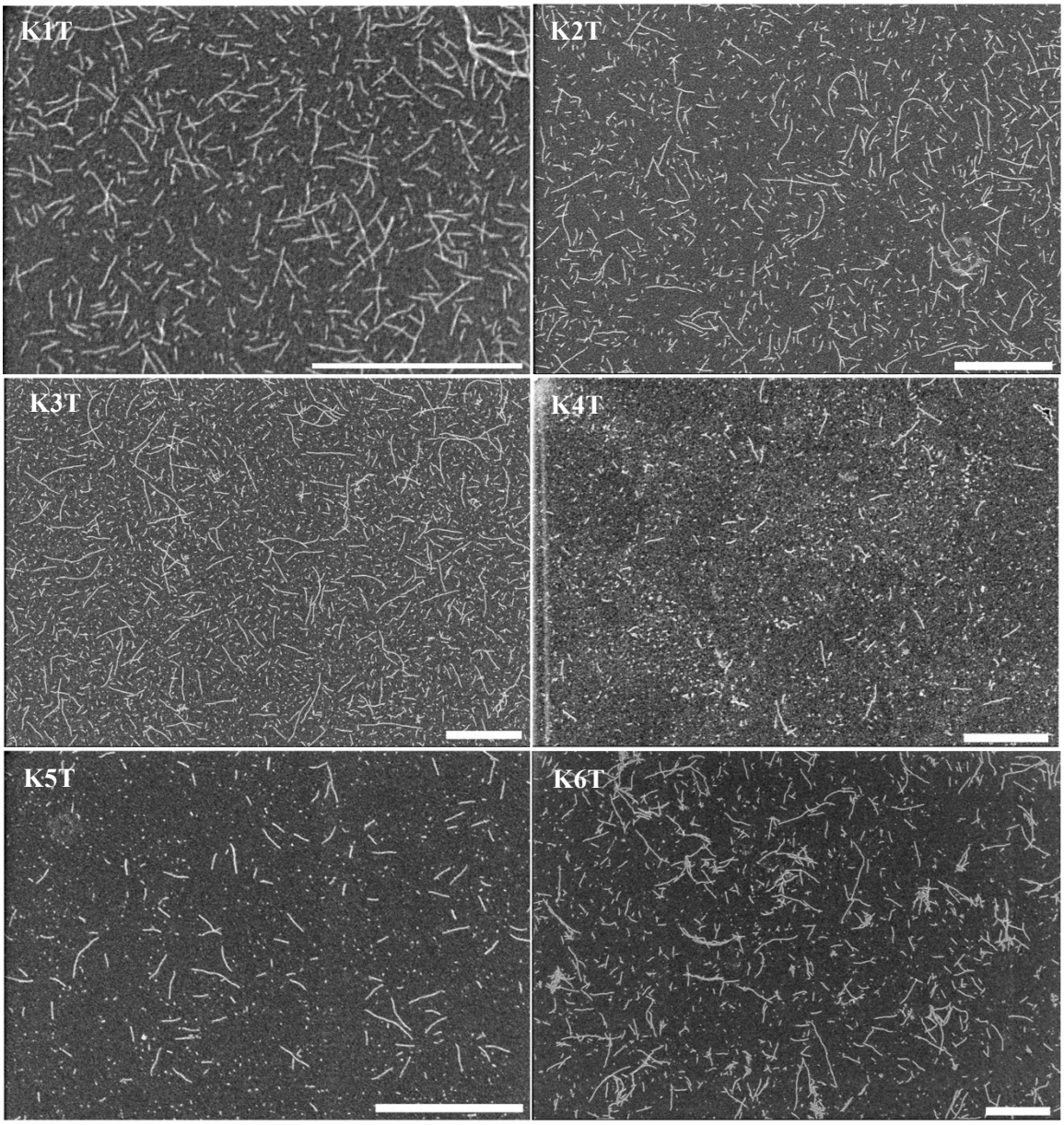

Figure 2-8: SEM images of RNTs series, K1T to K6T RNTs, sample concentration of 0.0125 mg/mL. Scale bar = 500 nm.

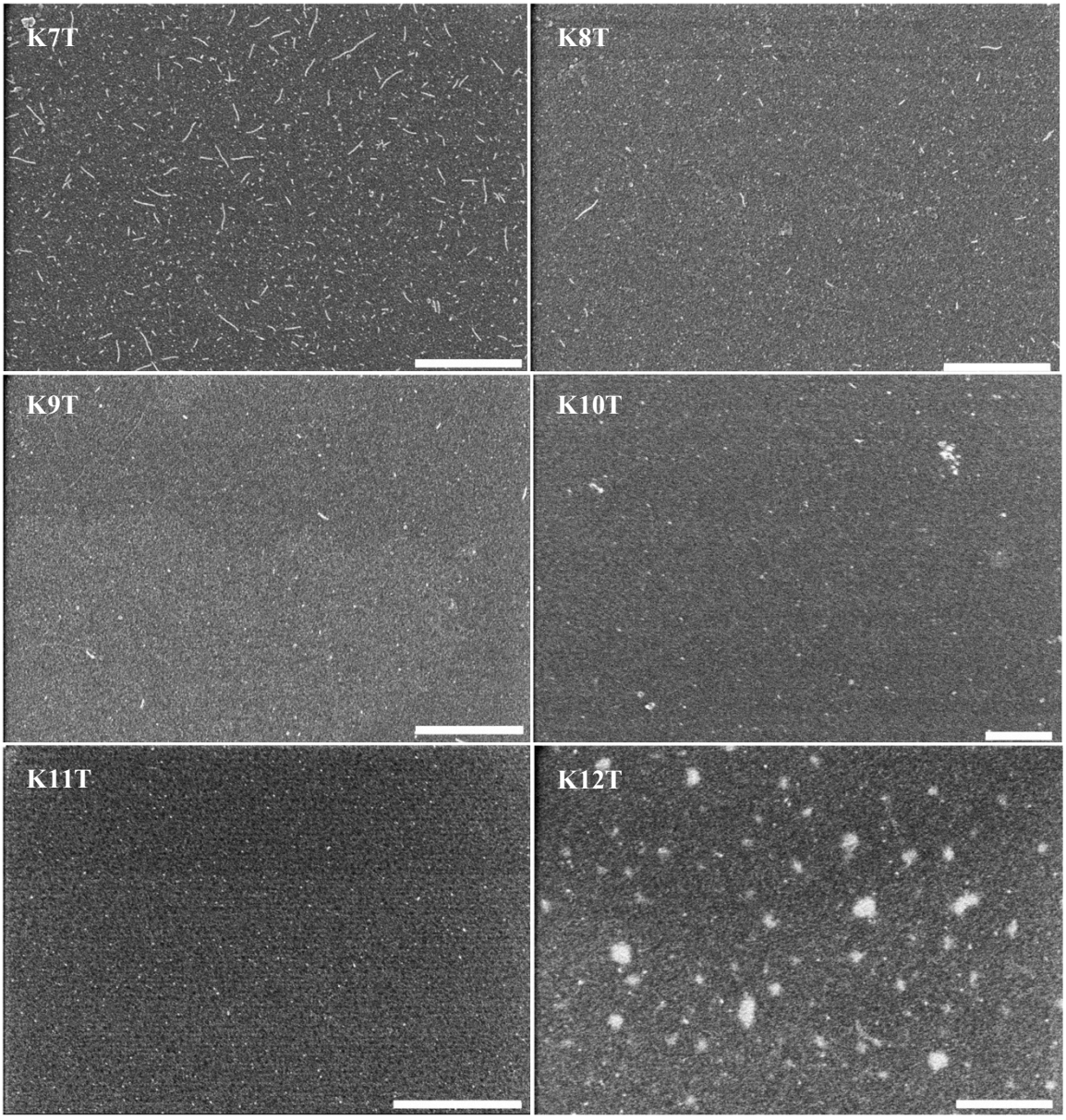

Figure 2-9: SEM images of RNTs series, K7T to K12T RNTs, sample concentration of 0.0125 mg/mL. Scale bar = 500 nm.

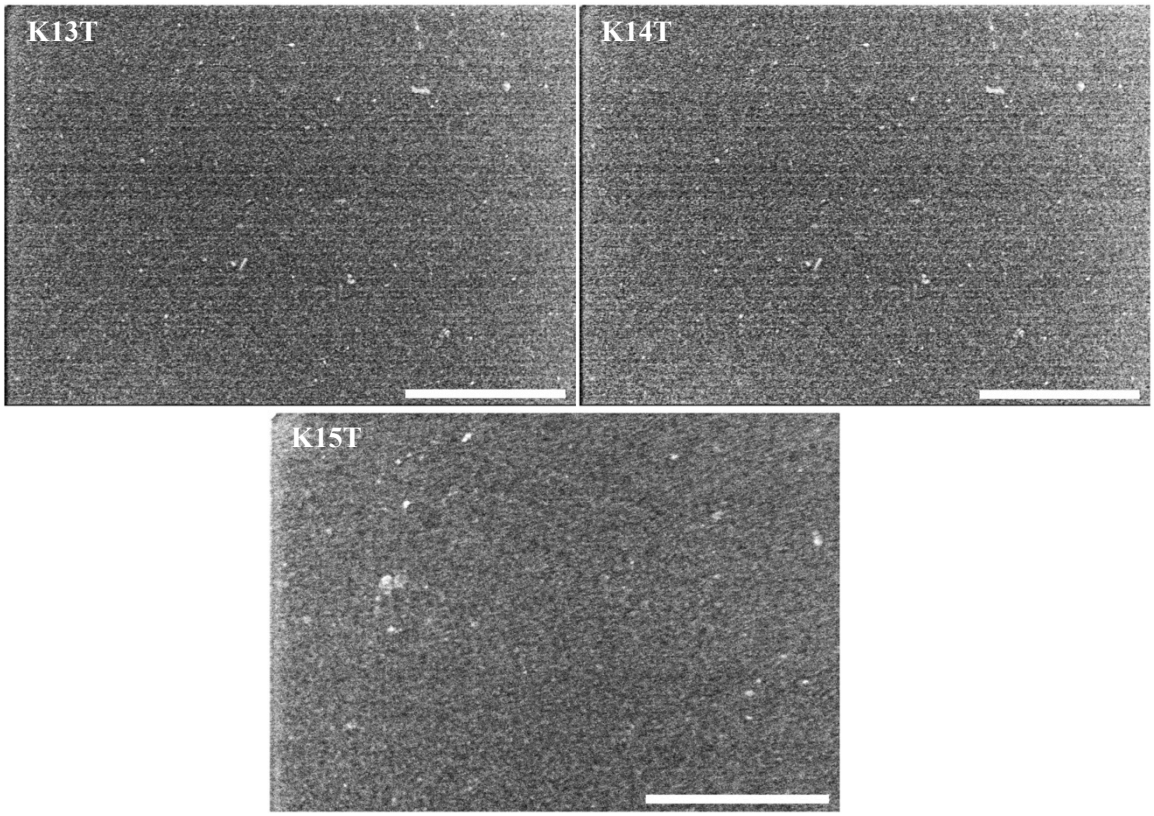

Figure 2-10: SEM images of RNTs library, K13T to K15T RNTs, sample concentration of 0.0125 mg/mL. Scale bar = 500 nm.

Due to electrostatic aggregation nature of the RNTs-siRNA system, long RNTs can result in big complexes (> 500 nm) when interact with siRNA, which may lower their uptake efficiency by the cells. Thus, for more effective cell transfection, the RNTs should be relatively short prior to mixing with siRNA so that smaller RNTs-siRNA complexes are formed.

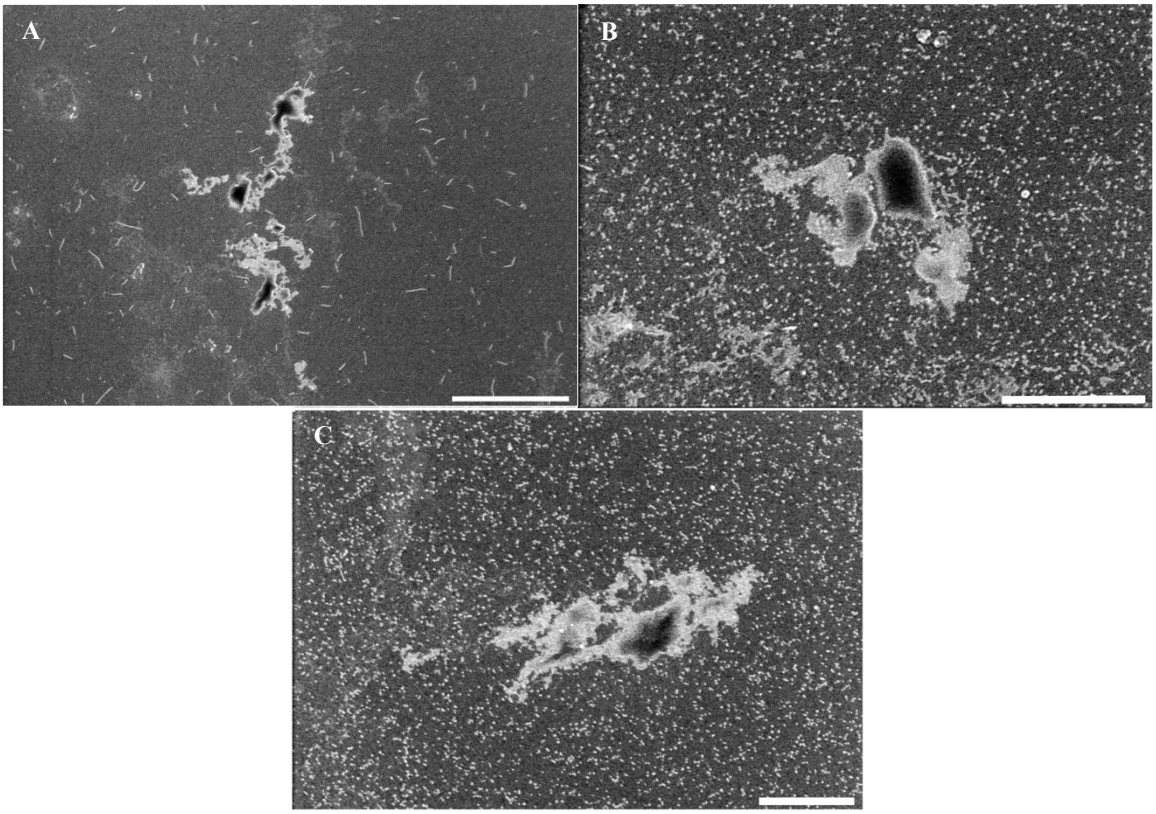

Figure 2-11: SEM images of K5T (A), K10T (B), K15T (C) and siRNA (20:1 mole ratio). Sample concentration is 0.0125 mg/mL. Scale bar = 500 nm.

3.4. Cell transfection efficiency of siRNA delivered by KnT RNTs

Fluorescence imaging of HCT116 cells (blue fluorescence of DAPI-labeled nuclei) by labeling the siRNA with FAM dye (green fluorescence) helps visualize the effectiveness of siRNA delivery by KnT RNTs. Here, HCT116 cells were transfected with fifteen KnT RNTs-siRNA complexes (molar ratio of 20:1) for 24 hours. The result showed more siRNA was delivered from K1T to K15T RNTs respectively (Figure 2-12), which was due to the increase in siRNA loading from K1T to K15T RNTs (as observed in Section 3.1). It is evident here that increasing cationic charges on RNTs was important to the enhancement of siRNA being delivered to the cells.

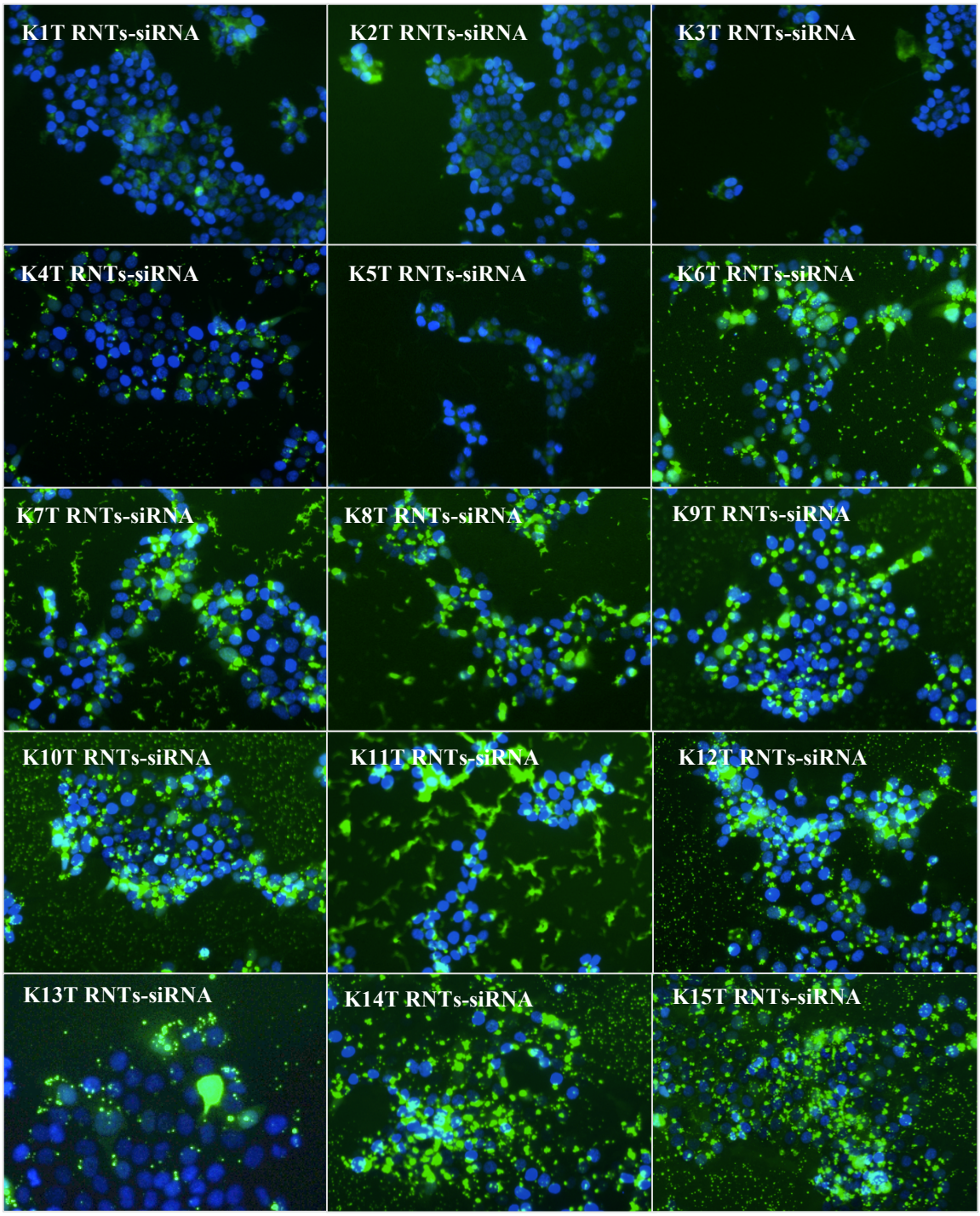

Figure 2-12: Fluorescence imaging of uptake study for K1T to K15T complexes with siRNA (molar ratio 20:1). Blue: nuclei (DAPI), green: FAM-siRNA.

The obtained images showed green dots in the backgrounds (where no nucleus located) of KnT RNTs-FAM siRNA complexes, especially in samples of K6T to K15T

RNTs, which could be accounted for the adsorption of the highly charged KnT RNTs to the coverslip. This gave us an opportunity to visualize the complexes of KnT RNTs-siRNA during the cell transfection, supporting earlier discussion about the binding attraction between RNTs and siRNA.

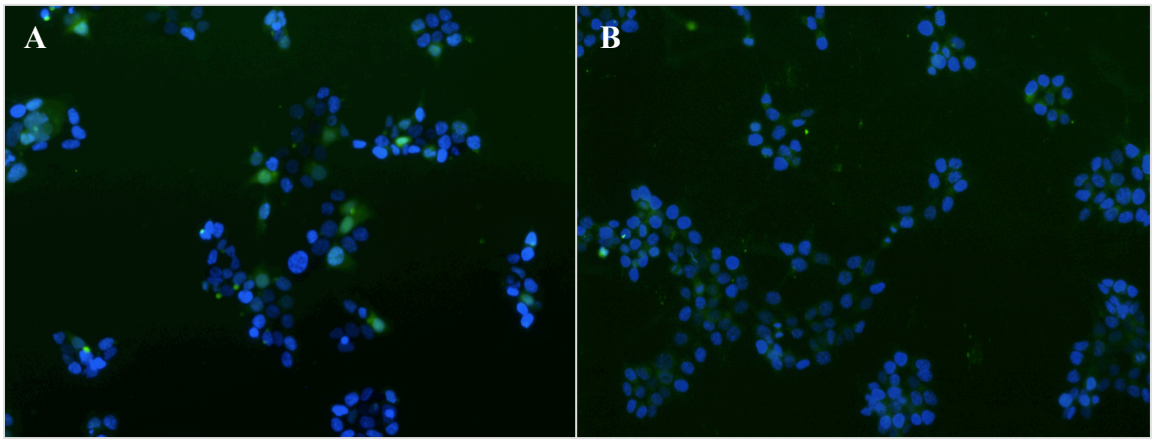

Figure 2-13: Fluorescence imaging of uptake study of HCT116 cells transfected with (A) positive control of INTERFERin-siRNA complexes and (B) negative control of siRNA alone.

Interestingly, the delivery of siRNA by KnT RNTs was shown to be more efficient than the positive control of INTERFERin, a commercial transfection reagent, and much more than the negative control of naked siRNA without carrier (Figure 2-13). Thus, the experiment has shown exciting new result implying the ability of KnT RNTs to deliver siRNA effectively to the cells. The significant influence of cationic charges on the RNTs in the transfection of siRNA was also observed, such that higher net charges resulted in enhanced siRNA loading and delivery efficiency.

3.5. Temperature-dependent endocytosis assay

Endocytosis is an energy dependent process that can be manipulated by changing the incubating temperature of the cells (blue fluorescence of DAPI-labeled nuclei) during the transfection with the K15T RNTs-FAM siRNA (green fluorescence). In this experiment, transfection with K15T RNTs-siRNA complexes (molar ratio of 20:1) was carried out, since their uptake was the most efficient due to their higher cationic charges compared to the other RNTs (Section 3.4). Therefore, more obvious difference in FAM-siRNA signal could be observed in the two samples incubated at different temperatures even for short duration.

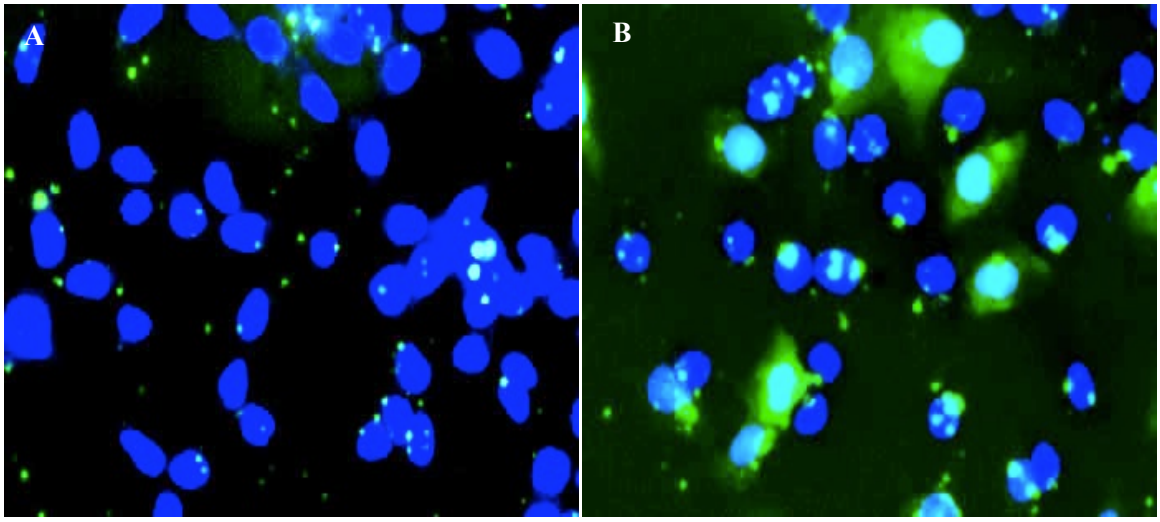

Figure 2-14: Fluorescence images of HCT116 cells when treated with K15T-siRNA complexes at (A) 4 ^{o}C and (B) 37 ^{o}C for 2 hours. Blue: nucleus (DAPI), green: FAM-siRNA.

At 4 ^{o}C, the active endocytotic processes were inhibited,[5] resulting in negligible siRNA uptake (Figure 2-14A). The green dots on the cells incubated at 4 ^{o}C could be accounted for the adsorption of the K15T RNTs-siRNA complexes during the incubation period, or the initial uptake of the complexes during the 30 minutes incubation of DND-

99 at rt. On the contrary, when cells were incubated at 37 ^{o}C (Figure 2-14B), a significant increase in cellular uptake was seen, including the distribution of siRNA inside the cells (green region around the nucleus). The temperature-dependent endocytosis assay strongly suggests that endocytosis pathway is the main mechanism for the uptake of KnT RNTs-siRNA complexes by the cells.

3.6. Time-course experiment

In order to examine the uptake rate of RNTs-siRNA by HCT116 cells (blue fluorescence of DAPI-labeled nucleus), K5T, K10T and K15T RNTs-siRNA complexes were delivered to the cells at various time periods (3, 6, 12, 24, 36, 48, 72 and 96 hours) (Figure 2-15, 2-16, 2-17). Result showed strongest green fluorescent signal of siRNA in the cells when delivered by K10T RNTs (Figure 2-16) and K15T RNTs (Figure 2-17), lowest by K5T RNTs (Figure 2-15). This shows that the cationic charges on KnT RNTs have significant impact on their siRNA loading ability as K10T and K15T RNTs captured 100% of siRNA, compared to 60% of siRNA by K5T RNTs at molar ratio of 20:1 (Section 3.1). Moreover, increasing net charges from K5T to K15T RNTs demonstrated enhanced interaction with the negatively charged cellular membrane thus, fastest cellular uptake was seen for K15T RNTs-siRNA complexes. For instance, within 3 hours of cell transfection, highest siRNA fluorescent signal was seen in sample of K15T RNTs-siRNA (Figure 2-17A), followed by K10T RNTs (Figure 2-16A) and K5T RNTs (Figure 2-15A) respectively. Complete cell transfection (no further obvious increase in FAM-siRNA signal) by the K5T RNTs-siRNA complexes was seen within 36 to 48 hours of the treatment (Figure 2-15 E, F), compared to 24 to 36 hours for K10T (Figure 2-16 D, E) and K15T RNTs (Figure 2-17 D, E).

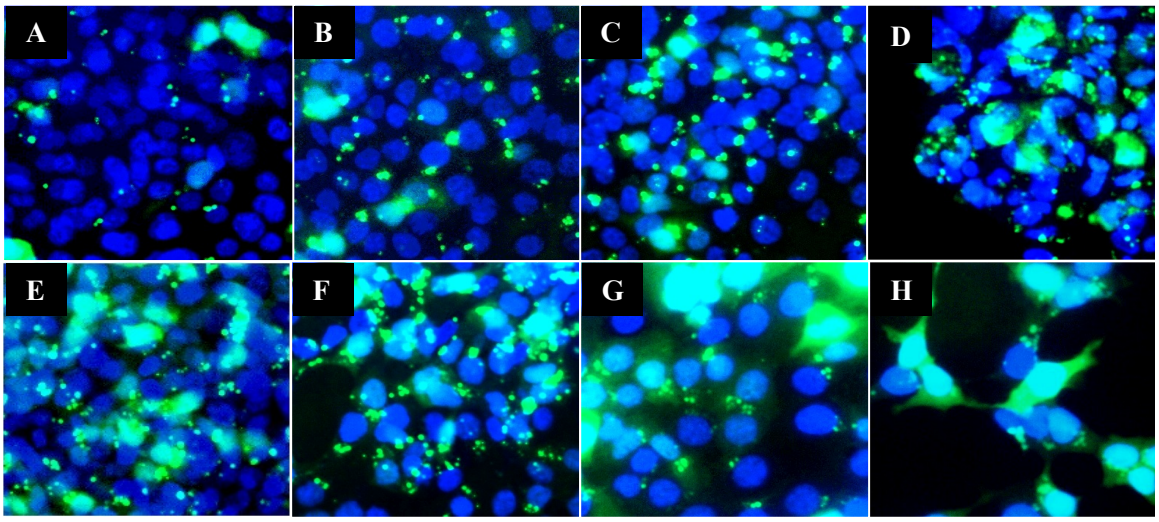

Figure 2-15: Fluorescence imaging for K5T complexes with siRNA (20:1 molar ratio) at (A) 3, (B) 6, (C) 12, (D) 24, (E) 36, (F) 48, (G) 72 and (H) 96 hours.

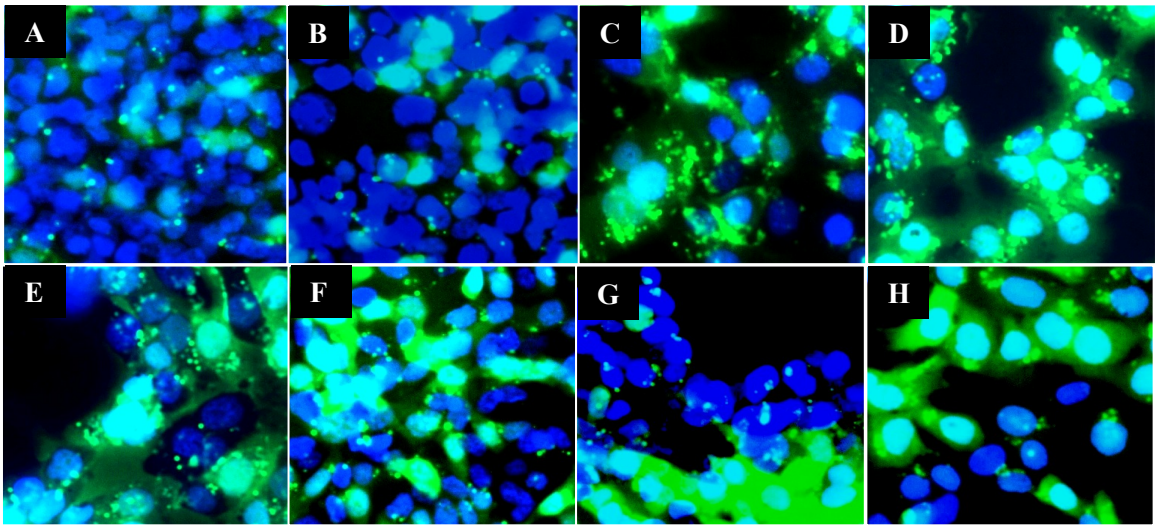

Figure 2-16: Fluorescence imaging for K10T complexes with siRNA (20:1 molar ratio) at (A) 3, (B) 6, (C) 12, (D) 24, (E) 36, (F) 48, (G) 72 and (H) 96 hours.

In the confocal experiment, the nuclei were stained with DAPI (blue), siRNA was labeled with FAM dye (green) and the acidic compartments of the cells were labeled with DND-99 (red). Confocal images of HCT116 cells transfected with K5T (Figure 2-18), K10T (Figure 2-19) and K15T (Figure 2-20) RNTs-siRNA complexes (0.5, 2 and 6

hours) were also in agreement with the results shown in fluorescence imaging. Indeed, K15T RNTs-siRNA complexes showed greater delivery to the cells after 6 hours, including the siRNA distribution (green regions), compared to K10T and K5T RNTs. Image of the cells transfected with K10T and K15T RNTs-siRNA showed stronger green fluorescent signal compared to the negative control of naked siRNA (Figure 2-21A), and slightly more than the siRNA delivery by commercial transfection reagent of INTERFERin (Figure 2-21B).

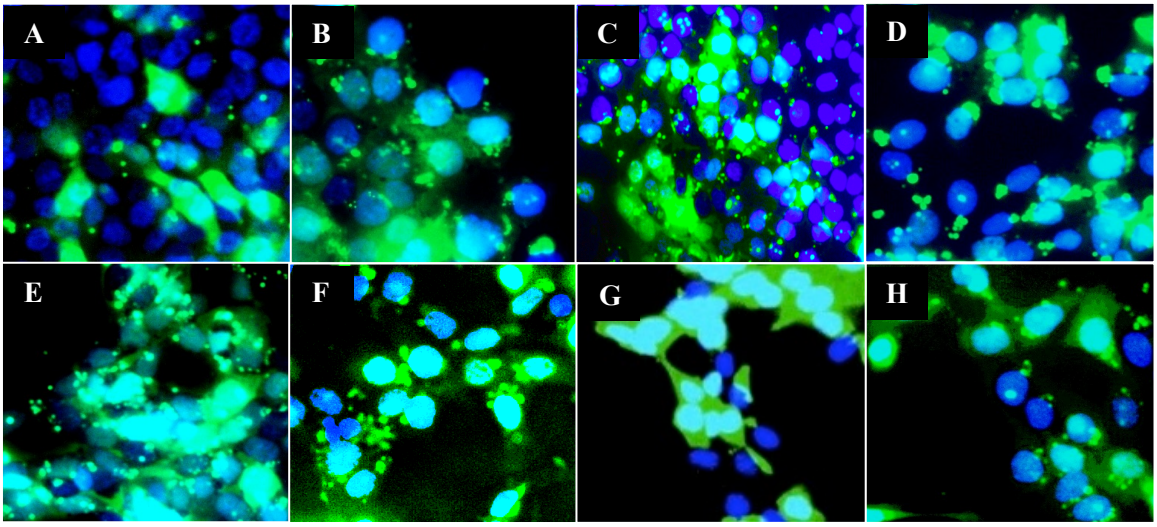

Figure 2-17: Fluorescence imaging for K15T complexes with siRNA (20:1 molar ratio) at (A) 3, (B) 6, (C) 12, (D) 24, (E) 36, (F) 48, (G) 72 and (H) 96 hours.

Observation of confocal images also enabled us to monitor the uptake mechanism of the RNTs-siRNA complexes. The yellow fluorescent dots in the confocal images represented the co-localization of FAM-siRNA (green) and endosomes (red), which supported earlier result (Section 3.5) that the RNTs-siRNA complexes were being internalized to the cells via endocytosis pathway. Furthermore, green fluorescence of FAM siRNA was observed mainly inside the cytoplasm of the cells (Figure 2-18, 2-19, 2-20 and 2-22), which indicated initial endosomal escape of siRNA to the cytosol.

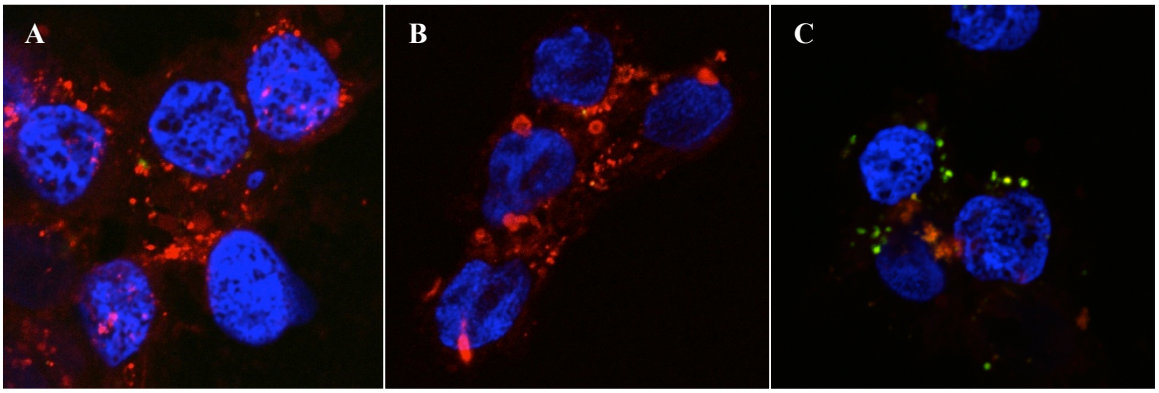

Figure 2-18: Confocal imaging of HCT116 transfected with K5T RNTs-siRNA complexes (20:1 molar ratio) for (A) 0.5, (B) 2 and (C) 6 hours. Blue: nucleus (DAPI), green: FAM-siRNA, red: acidic component (LysotrackerRed DND-99).

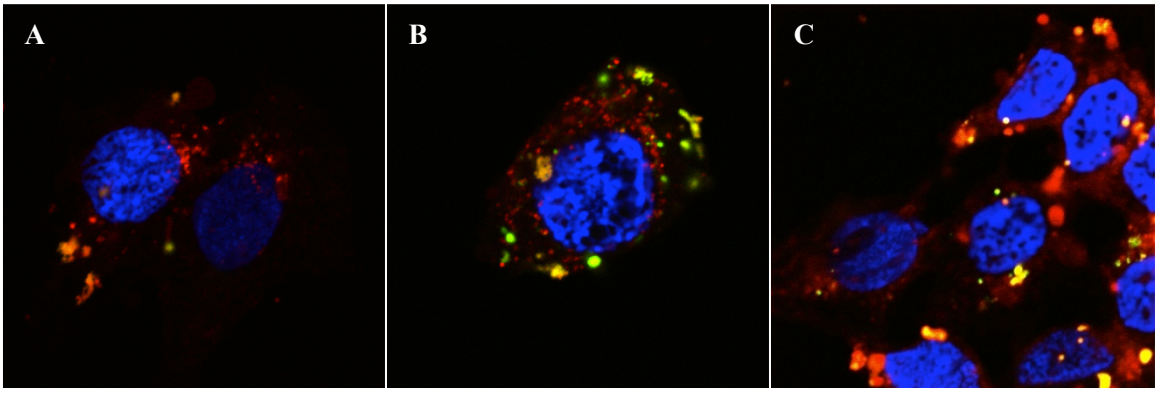

Figure 2-19: Confocal imaging of HCT116 transfected with K10T RNTs-siRNA complexes (20:1 molar ratio) for (A) 0.5, (B) 2 and (C) 6 hours.

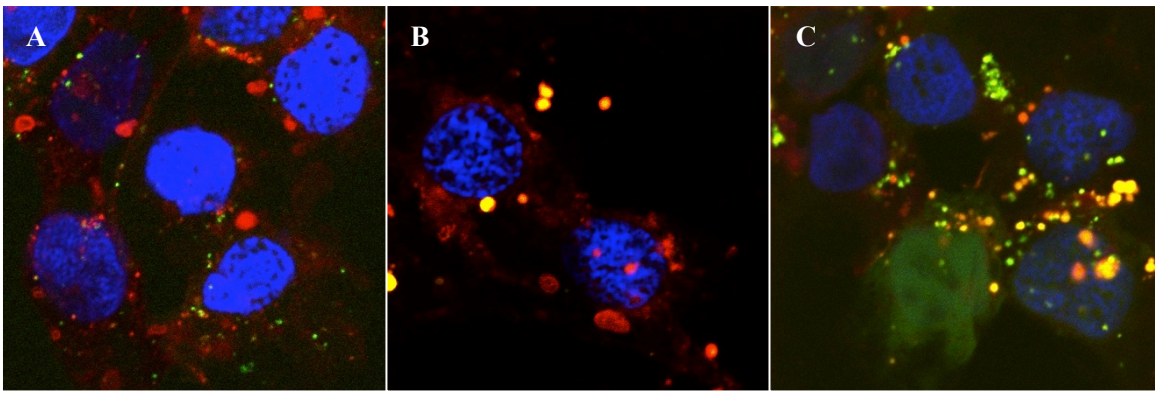

Figure 2-20: Confocal imaging of HCT116 transfected with K15T RNTs - siRNA complexes (20:1 molar ratio) for (A) 0.5, (B) 2 and (C) 6 hours.

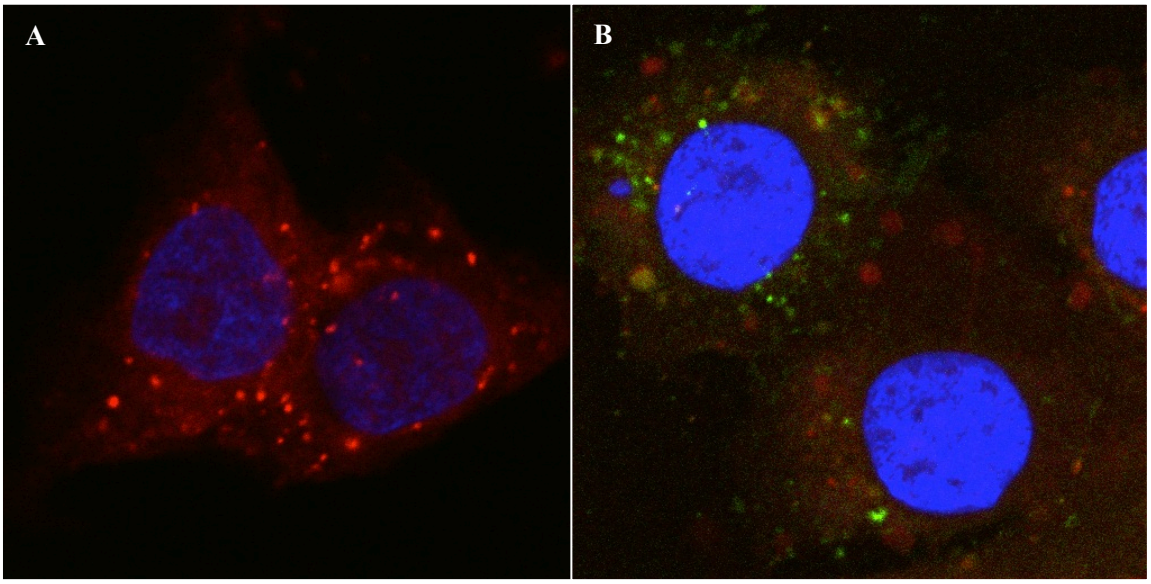

Figure 2-21: Confocal imaging of HCT116 transfected with (A) negative control sample of siRNA alone and (B) positive control sample of INTERFERin-siRNA, both treated for 6 hours.

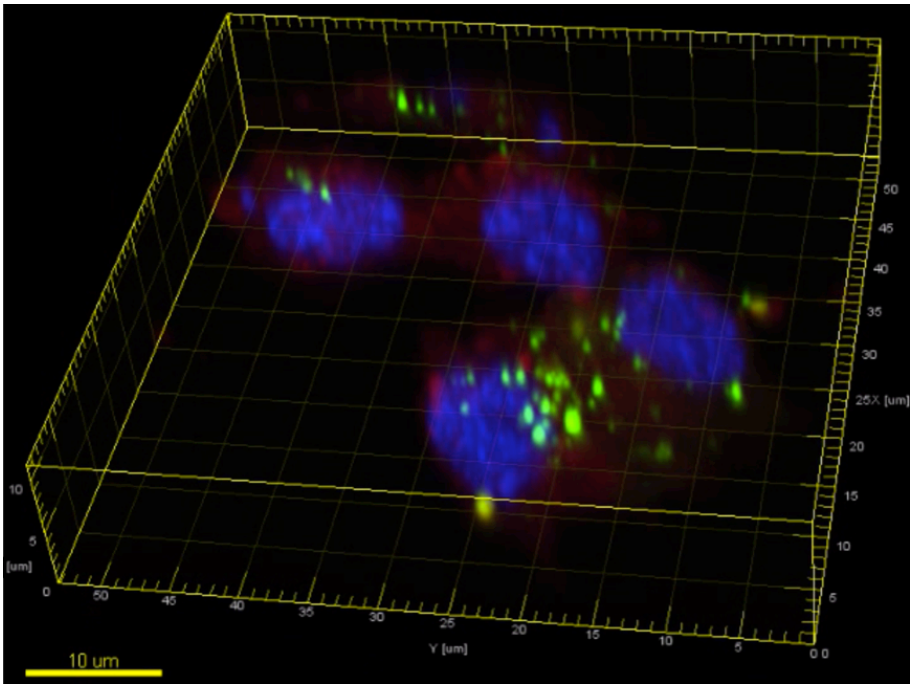

Figure 2-22: 3D confocal image of HCT116 cells transfected with K10T RNTs-siRNA for 2 hours. Scale bar = 10 μm.

Fluorescence imaging techniques (fluorescent and confocal microscopies) have allowed us to visually observe the delivery efficiency of siRNA by the library of KnT RNTs (molar ratio of 20:1) over time, and also confirmed siRNA location in the cytoplasm of the cells. Similar to Section 3.5, the cationic charges on RNTs demonstrated significant impact in the delivery of siRNA, with higher positive charges resulted in increasing loading ability and delivery efficiency, as well as increased in cell transfection rate of the RNTs-siRNA complexes.

3.7. Cytotoxicity test of KnT RNTs

In order for KnT RNTs to be applied for therapeutic purposes, they must demonstrate low toxicity effect towards the cells. Here, K10T and K15T RNTs were tested for potential harmful effects to the cells by incubating them at various concentrations for up to 96 hours.

Cells were first transfected with K10T RNTs (0.25, 0.5, 1, 2, 4 μM) over various time periods (24, 48, 72 and 96 hours) (Figure 2-23). At time points of 24 and 48 hours, little to no harmful effect was seen in the cells that could be caused by K10T RNTs. However, at 72 and 96 hour time-points, the cell viability percentage decreased. This could be due to the high accumulation of the RNTs inside the cells over long period of time.

Next, cells were tested with K15T RNTs solutions at various concentrations (highest concentration of 2 μM, with ten two-fold serial dilutions) for 48, 72 and 96 hours (Figure 2-24). Even though K15T RNTs possessed higher positively charged side chains than K10T RNTs, the toxicity was low leading to more than 80% cell viability over 96 hours of cell transfection. This may be explained by the property of KnT compounds

obtained from the synthesis. This was because K10T RNTs solution used was older compared to K15T RNTs solution and thus, resulted in higher contamination in the sample.

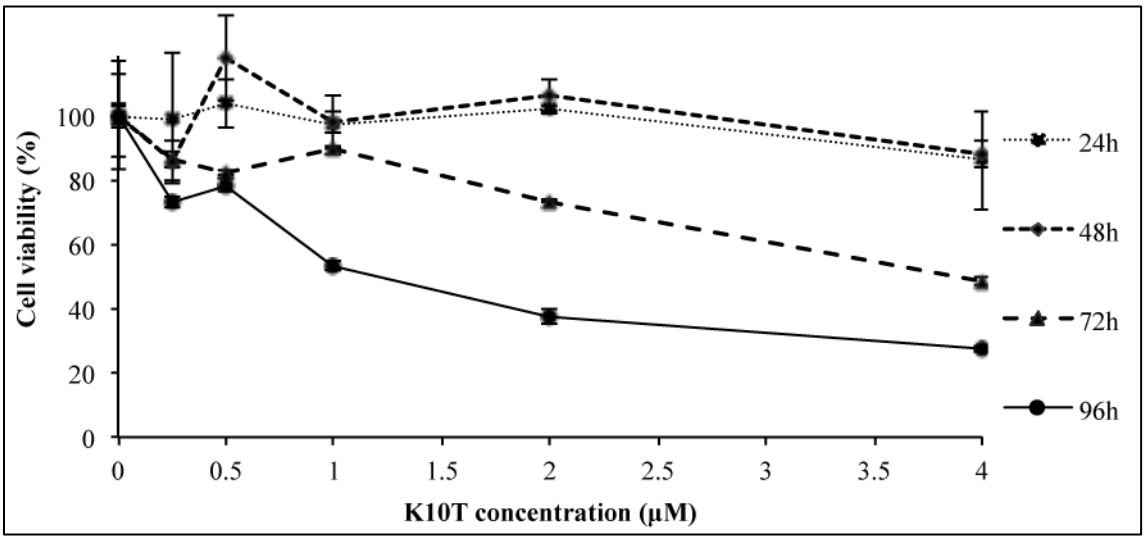

Figure 2-23: MTT assay determines the cell viability of HCT116 cells transfected with K10T RNTs at concentrations of 0.25, 0.5, 1, 2, 4 μM for 24, 48, 72, 96 hours

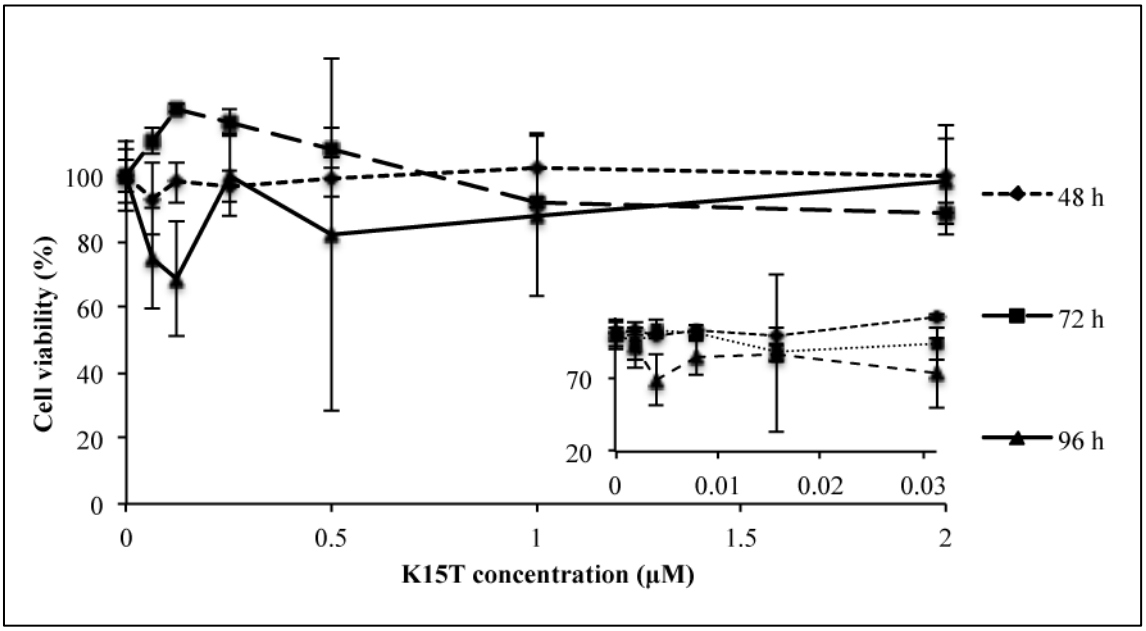

Figure 2-24: MTT assay determines the cell viability of HCT116 cells transfected with K15T RNTs at concentrations of 0.0625, 0.125, 0.25, 0.5, 1 and 2 μM for 48, 72 and 96 hours and 0.002, 0.004, 0.008, 0.016, 0.031, 0.0625 μM (inlet)

In our experiments, maximum concentration of 2 μM of K10T and K15T RNTs is used thus, was safe for *in vitro* experiment. In addition, since these highly charged RNTs could fully bind to siRNA at molar ratio of 10:1 (1 μM of KnT), higher concentration of RNTs might not be required for the cell transfection. The relatively low toxicity of RNTs showed encouraging results for the KnT-RNTs to be used for *in vitro* and *in vivo* therapeutic application.

4. Conclusion

The library of KnT RNTs (n = 1 to 15) was assessed to evaluate their ability to serve as siRNA carrier. Gel shift assay showed that increasing cationic charges on the KnT RNTs demonstrated increasing siRNA binding and protecting ability against serum degradation. SEM visualization showed shorter RNTs formed when the lysine peptide chains were longer due to the steric hindrance and electrostatic repulsion. The morphology of RNTs-siRNA complexes was affected by the size of the RNTs, such that shorter RNTs resulted in smaller aggregates with siRNA, which may benefit the intracellular uptake. Moreover, when cells were imaged using fluorescence and confocal techniques, highly charged K15T RNTs showed the most efficient and fastest siRNA delivery to the cells, followed by K10T and K5T RNTs (all via endocytosis). K10T and K15T RNTs also showed relatively low toxicity, which is important for future use in cancer therapy applications.

References

1. Ornelas-Megiatto, C.; Wich, P. R.; Frechet, M.J., Polyphosphonium Polymers for siRNA Delivery: An Efficient and Nontoxic Alternative to Polyammonium Carriers. *J. Am. Chem. Soc.*, **2012**, 134, 1902-1905.

2. Boyer, C.; Teo, J.; Phillips, P.; Erlich, R. B.; Sagnella, S.; Sharbeen, G.; Dwarte, T.; Duong, H.; Goldstein, D.; Davis, T.; Kavallaris, M.; McCarroll, J. Effective Delivery of siRNA into Cancer Cells and Tumors Using Well- Defined Biodegradable Cationic Star Polymers. *Mol. Pharm.* **2013**, 10, 2435-2444

3. El-Bakkari, M.; Beingessner, R.L.; Alshamsan, A.; Cho, J.-Y.; Fenniri, H. Electrostatic and Steric Effect of Peptides Functionalized on Self-Assembled Rosette Nanotubes. *Mater. Res. Soc. Symp. Proc.* **2011**, 1316, mrs10.1557/opl.2011.436

4. Alshamsan, A.; El-Bakkari, M.; Fenniri, H. Efficiency of Cationic Rosette Nanotubes for siRNA Delivery. *Mater. Res. Soc. Symp. Proc*. **2011**, 1316, mrs10.1557/opl.2011.435

5. Jiao, C.-Y.; Delaroche, D.; Burlina, F.; Alves, I.D.; Chassaing, G.; Sagan, S. Translocation and Endocytosis for Cell-penetrating Peptide Internalization. *J. Biol. Chem.* **2009**, 284, 33957-33965.

Chapter III

Delivery of siRNA using K3T

Rosette Nanotubes for Protein Silencing

1. Introduction

Lysine twin-base (KnT) RNTs have demonstrated increasing siRNA binding ability and effective delivery as the net charges of the KnT compounds increase (Chapter II). However, some of our initial experiments showed low silencing effect by highly charged K10T RNTs-siRNA (molar ratio of 20:1) (Chapter II). Although fluorescence microscopy results showed great delivery of siRNA to the cells, strong binding between RNTs and siRNA could lead to inability for siRNA to enter RNAi pathway, which could in turn lead to low silencing effect of the targeted proteins. Therefore, the five lowest net charged KnT RNTs, from K1T to K5T RNTs[1], were being considered for further experiments. Molecular models of K2T and K3T molecules along with their associated rosettes and RNTs structures are shown (Figure 3-1, 3-2).

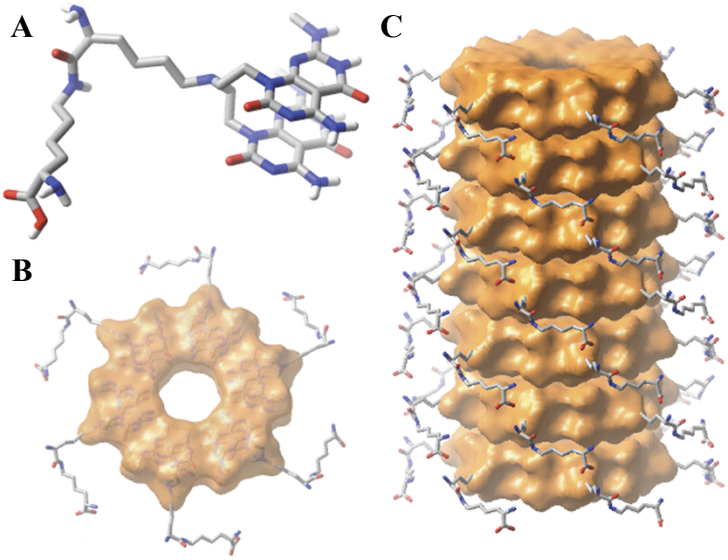

Figure 3-1: Molecular models of (A) structure, (B) a rosette and (C) a RNT of K2T compound. Atoms shown: oxygen (red), nitrogen (blue), carbon (grey), hydrogen (white).

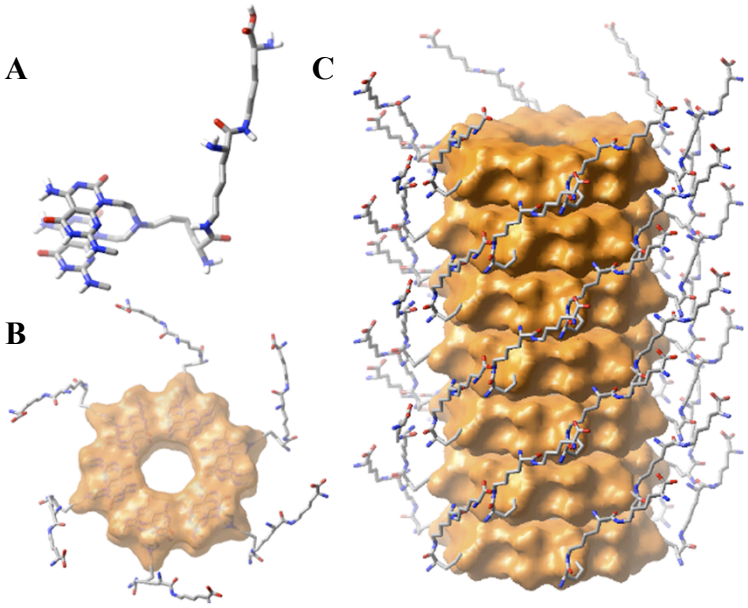

Figure 3-2: Molecular models of (A) structure, (B) a rosette and (C) a RNT of K3T compound.

The objective of chapter II is to explore the five KnT RNTs (K1T to K5T RNTs) on their ability to deliver siRNA effectively to the cells, with most attention on K3T RNTs (Figure 3-2) used to deliver siRNA for protein silencing. Firstly, gel agarose assay was used to calculate the binding efficiency of KnT RNTs-siRNA complexes at higher molar ratio (up to 50:1 of KnT RNTs to siRNA respectively). In addition, SEM was performed to visualize the complexes of KnT RNTs-siRNA at molar ratio of 30:1 and assess the effect of sonication to the complexes of K3T RNTs-siRNA. Confocal microscopy was performed to further examine the delivery efficiency of siRNA by these KnT RNTs over time. Cytotoxicity of the five KnT RNTs was also evaluated using MTT assay. Finally, K3T RNTs-siRNA complexes were used to study the protein silencing effect of

STAT3 (signal transducer and activator of transcription 3) and firefly luciferase proteins triggered by the delivered siRNA in the cells.

2. Materials and Methods

2.1. Materials

pGL3 siRNA sequence 5'-rCrUUACGCUGAGUACUUCG-3', 5'-AArUCGAAGUACUCAGGU (MW = 13318.2 g/mol) was synthesized, pGL3 (encoding firefly luciferase) and pRL-CMV (encoding Renilla luciferase) were purified by Dr. Mohamed (Department of Pharmacy and Pharmaceutical Sciences, University of Alberta) using DNA synthesizer and Plasmid Mini Kit (Qiagen) respectively. FlexiTube siRNA Hs STAT3 7 was purchased from Qiagen. A549 cell line and F-12K medium were obtained from ATCC.

Buffers used were SDS-PAGE (sodium dodecyl sulfate-polyacrylamide gel electrophoresis) loading buffer (5x, 0.25% bromophenol blue, 0.5 M dithiothreitol, 50% glycerol, 10% SDS), SDS-PAGE running buffer (25 mM Tris base, 19 mM glycine, 0.1% SDS), Western blotting transfer buffer (25 mM Tris, 192 mM glycine, 10% methanol) and Tris Buffer Saline-Tween (TBST, 50 mM Tris, 50 mM NaCl, 0.05% Tween 20, pH 7.4).

HOPG (highly ordered pyrolytic graphite) used for Atomic Force Microscopy (AFM) was obtained from MikroMasch Inc. Lipofectamine® 2000 Transfection Reagent, PVDF membranes (0.2 μm pore size) were purchased from Invitrogen. Cell lysis buffer, composed of Instant One ELISA Cell Lysis buffer and Instant One ELISA Enhancer Solution (10:1 v/v), both buffers were obtained from eBioscience. ECL Prime Western blotting detection was purchased from GE

Healthcare. Micro BCA Protein Assay Kit and CL-XPosure Film were purchased from Thermo Scientific. Primary antibodies STAT3 (F-2) mouse monoclonal IgG_1, GAPDH mouse monoclonal IgG1 and secondary antibody goat anti-mouse IgG HRP conjugated were all purchased from SCBT. Dual Luciferase Reporter Assay System (containing Passive Lysis Buffer, LAR II, Stop & Glow substrate solutions) was purchased from Promega.

2.2. General Methods

K1T to K5T RNTs stock solutions (1 mg/mL) in deionized water were prepared (Chapter II, Section 2.2). Formation of K1T to K5T RNTs and siRNA complexes at various molar ratios were prepared in 50 μL of SFM (Chapter II, Section 2.2). K3T-siRNA complexes (molar ratio of 50:1) used in silencing study were prepared with 30 minutes incubation, and where indicated, was followed by 30 seconds of sonication. All the experiments were carried out with constant concentration of siRNA (100 nM).

A549 (lung carcinoma) cells were cultured in F-12K medium (10% FBS, 100 units/mL penicillin, 100 μg/mL streptomycin) in a 37 ^oC incubator at 5% CO_2 atmosphere. Cells were detached for sub-culturing by trypsin solution.

2.3. Complexation of K1T-K5T RNTs and siRNA by gel shift assay

K1T to K5T RNTs-siRNA complexes (molar ratios of 10:1, 20:1, 30:1, 40:1 and 50:1) were prepared according to the procedure described in Section 2.2. Gel shift assay was then performed (Chapter II, Section 2.3.1).

2.4. Characterization by Microscopy

SEM samples of K1T to K5T RNTs-siRNA complexes (molar ratio 30:1), and K3T RNTs-siRNA complexes (molar ratio of 50:1, with and without 30 seconds sonication) were prepared (Chapter II, Section 2.4).

AFM sampling was done by depositing the prepared solutions by spin-coating at 2500 rpm for 30 seconds on clean HOPG substrates (1 x 1 cm^2). Sample surface was observed using a Digital Instruments/Veeco Instruments MultiMode Nanoscope IV AFM equipped with an E scanner. For getting optimized height profile in this investigation, silicon cantilevers (MikroMasch USA, Inc.) with low spring constants of 4.5 N/m were used in tapping mode (TM-AFM). To obtain a clear image from surface, low scan rate (0.5-1 Hz) and amplitude setpoint (1 V) were chosen during measurement.

TEM samples were prepared by depositing a droplet of prepared solution on a carbon-coated 400-mesh copper grid, then, blotted after 10 seconds. Staining of the sample was performed by depositing one droplet of uranyl acetate (2% aqueous solution) for 120 seconds. The grid was then blotted, air-dried and heated on the hotplate prior to imaging. TEM imaging was carried out on JEOL 2200 FS TEM – 200kV Schottky field emission instrument equipped with an in-column omega filter. Bright field and high-angle annular dark-field (HAADF) TEM images are acquired using energy filtered zero loss beams (slit width 10 eV).

2.5. Confocal microscopy

HCT116 and A549 cells were treated with K1T to K5T RNTs-siRNA complexes (molar ratio of 30:1) for 5 and 10 hours. Confocal microscopy samples were prepared and visualized (Chapter II, Section 2.5.1)

2.6. Cell Viability Study

The cytotoxicity of K1T to K5T RNTs (0.75, 1.5, 3, 6, 12 μM) was evaluated using MTT assay (Chapter II, Section 2.6).

2.7. Proteins silencing by K3T RNTs

2.7.1. Luciferase experiment

A549 and HCT116 cells were seeded in 6 or 12-well plate to 80-90% confluence for 24 hours. Next, the cells were transfected for another 24 hours with K3T RNTs-siRNA complexes (molar ratio of 50:1) along with the negative control (no siRNA treatment). The medium was then discarded and all the cells were transfected with Lipofectamine-plasmids DNA complexes (1.6 μg of plasmids containing firefly pGL3 and Renilla-CMV in 10:1 ratio w/w per well in 12-well plate) in SFM for another 24 hours. Cells were washed with PBS (2 x 30 seconds) and lysed to collect proteins using Passive Lysis Buffer. Firefly, Renilla luminescent signals produced when exposing the lysed proteins to LAR II and Stop & Glow substrates respectively, were measured using FLUOstar Omega (BMG Labtech). Results were calculated as the ratio of signal produced by the targeted firefly luciferase to the control Renilla luciferase (FF/Renilla ratio).

2.7.2. STAT3 silencing

Cells after 24 hours of seeding (50-60% confluence) were transfected with K3T RNTs-STAT3 siRNA (molar ratio of 50:1). Lysis buffer (200 μL) was added to each well, followed by shaking of the plates on ice for 15 minutes. The lysed solutions were collected in the eppendorf tubes and centrifuged (4 ^{o}C) for 15 minutes at 12,000 rpm. BCA Protein Assay was performed to measure the concentration of collected proteins.

The same amount of total protein for all lysed samples (20 to 25 μg) was resolved on SDS-PAGE (4% stacking gel, 12% running gel) at 150 V for 1 hour. The gels were electro-blotted onto PVDF membranes. Membranes were blocked with 5% milk in TBST overnight at 4 ^{o}C, followed by washing with TBST (3 x 10 minutes). Then, they were incubated with primary antibody (STAT3 or GAPDH) at dilution of 1:1000 in 5% milk in TBST for 2 hours at rt or overnight at 4 ^{o}C. Membranes were washed with TBST (3 x 10 minutes) and incubated with goat anti-mouse IgG HRP conjugated at dilution of 1:2000 for 1 hour at rt or 2 hours at 4 ^{o}C. Signals detected from the exposure to ECL Prime were collected onto CL-XPosure Film, and measured with ImageJ software.

3. Results and Discussions

3.1. Complexation of K1T to K5T RNTs and siRNA

Earlier in chapter II, K1T to K5T RNTs-siRNA complexes formed at molar ratio of 20:1 showed low binding ability compared to RNTs with higher lysine residues on the side chains. However, increasing the molar ratio of KnT RNTs:siRNA also improved siRNA loading by the RNTs. Here, gel shift assay

(Figure 3-3) was used to measure the binding affinity of the RNTs and siRNA at various molar ratios (10, 20, 30, 40 and 50:1, RNTs to siRNA respectively).

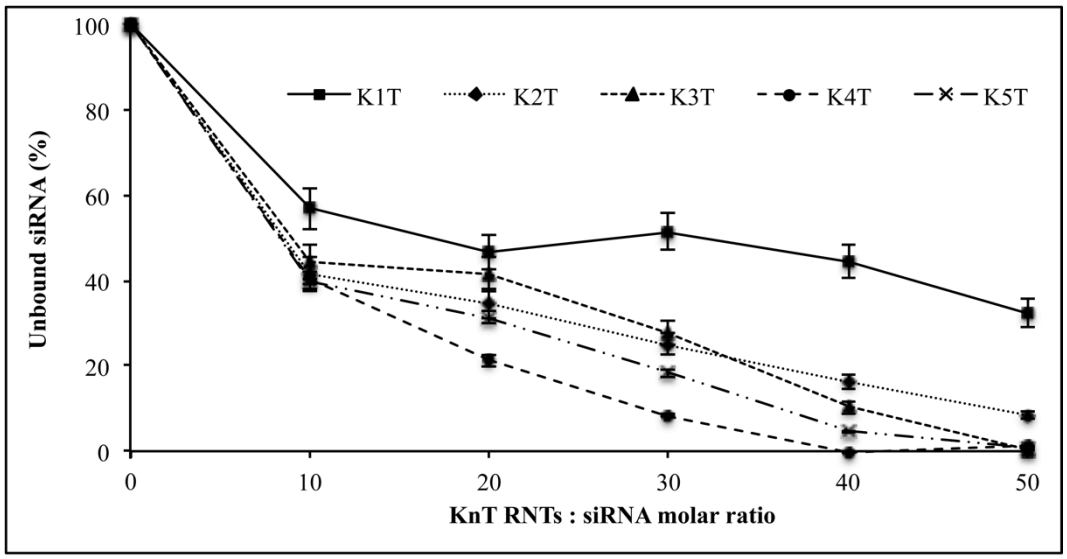

Figure 3-3: Gel shift assay measuring percentage of unbound siRNA when incorporated with K1T to K5T RNTs at various molar ratios.

The gel retardation results (Figure 3-3) showed a reduction in unbound siRNA with increasing molar ratio of KnT RNTs : siRNA and from K1T to K5T RNTs (increasing net charge). At molar ratio of 50:1, K3T, K4T and K5T RNTs showed complete binding with siRNA. Ultimately, the gel retardation experiment has showed that the RNTs with low net charges were able to fully capture siRNA at increasing molar ratio of RNTs:siRNA. Study of siRNA binding ability of K1T to K5T RNTs helped understanding the possibility for these RNTs with lower cationic charges to act as siRNA carrier for protein silencing.

3.2. Characterization of K1T to K5T RNTs-siRNA complexes

3.2.1. Scanning Electron Microscopy of K1T to K5T RNTs-siRNA

The morphology of K1T to K5T RNTs-siRNA complexes at 30:1 molar ratio (Figure 3-4) could be visualized using SEM imaging. The images showed coating of the RNTs by siRNA, indicating the favorable interaction between siRNA and the lysine side chains on the surface of the RNTs.

Large aggregates in the micrometer scale were observed for KnT RNTs-siRNA (n = 1 – 5). However, large complexes are known to have lower cellular uptake.[2] Essentially, earlier results from Chapter II showed that the size of the complexes depends on three main factors: the amount of KnT RNTs used (which is related to molar ratio of RNTs:siRNA), the size (length) of the RNTs prior to complexation and the net charges of KnT compounds.

Here, increase in KnT RNTs amount enhanced the complexation by capturing more siRNA, and also more RNTs were available in solution to contribute to the complexes. Due to the low number of lysine residues (n = 1 to 5) on K1T to K5T compounds, the latter was able to form long RNTs leading to formation of big complexes. The length of the RNTs could essentially be controlled by using different KnT RNTs in the library (more lysine residues yield shorter nanotubes), but this would attribute to a change in net charges, which affects the interaction with siRNA. Another approach is based on the self-assembly property of RNTs which is entropically driven[3] hence, adjusting the preparation procedure of the stock samples, such as shortening the heating time at low temperature setting, would produce short RNTs. Future study should optimize

the conditions for RNTs formation to yield uniformly short and stable (slow growth) RNTs.

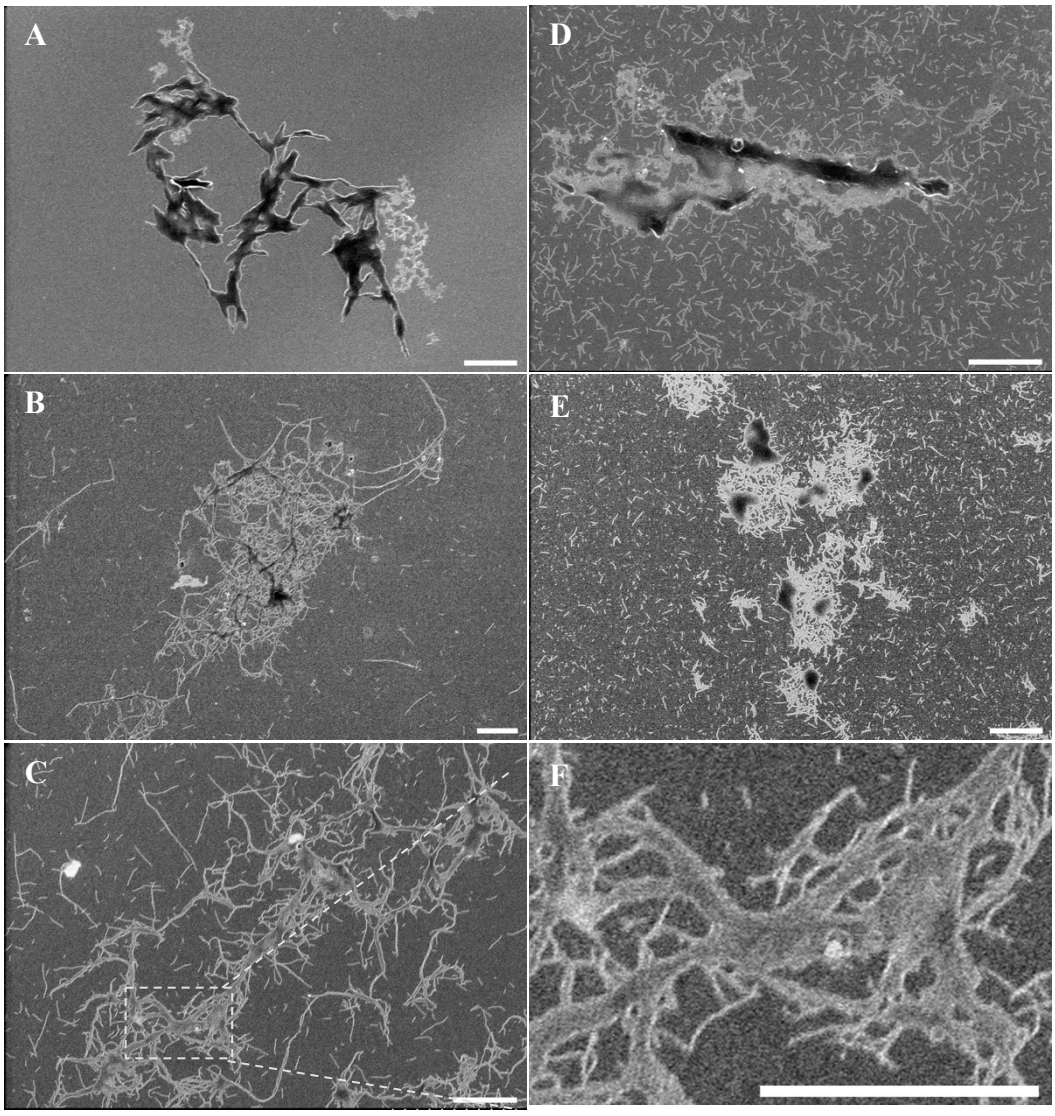

Figure 3-4: SEM images of (A) K1T RNTs, (B) K2T RNTs, (C) K3T RNTs, (D) K4T RNTs and (E) K5T RNTs complexes with siRNA at 30:1 molar ratio in SFM. (F) A magnified region of C showing the coated area of K3T RNTs with siRNA. Scale bar = 500 nm.

Further observation of SEM images (Figure 3-4) showed parts of the complexes acting as "bridges" to connect several small complexes together. For example, complex of K1T RNTs-siRNA (Figure 3-4A) was seen with some RNTs branches bridging between the aggregates, which could be due to the attraction between opposite charges present in the complexes.

The SEM imaging has allowed the visualization of K1T to K5T RNTs-siRNA complexes, indicating that the siRNA were able to interact with the surface of RNTs despite the low number of lysine residues. Thus, increasing molar ratio of KnT RNTs:siRNA would allow more siRNA to be encapsulated by RNTs for the purpose of cellular delivery, which was in agreement with result from Section 3.1.

3.2.2. K3T RNTs and siRNA complexes

3.2.2.1. Scanning Electron Microscopy imaging

The obtained result from gel retardation assay (Section 3.1) suggested that K3T, K4T and K5T were able to fully encapsulate siRNA at 50:1 molar ratio, among which, K3T RNTs had the lowest net charge (Figure 3-3) and hence, was chosen for further study. The size of the complexes at 50:1 molar ratio was observed in micrometer scale (Figure 3-5A), similarly as observed at molar ratio of 30:1 (Figure 3-4C). Hypothetically, smaller complexes could be formed if the solution was diluted to lower concentration in order to decrease the chance of the complexes to aggregate. For consistency with previous work in Chapter II (50 μL complexes solution), further dilution was not done to decrease the concentration,

but 30 seconds sonication was carried out after the 30 minutes of incubation in attempt to break off the large aggregates into smaller ones.

SEM images (Figure 3-5) presented the K3T RNTs- siRNA complexes at 50:1 molar ratio before sonication (A), and after 30 seconds of sonication (B). Sonication was used in attempt to break off big aggregates into smaller ones, however, this was not observed in our experiment. In effect of sonication, only loose parts or branches from the big complexes were broken up, giving smaller complexes that more possible to deliver to the cells (Figure 3-4B). However, big aggregates remained unbroken. Longer sonication time was not used because it could heat up the solution, which then could result in elongation of the RNTs. From this study on, all the incubated mixtures of RNTs and siRNA were being sonicated for 30 seconds before treating the cells in attempt to break off small complexes from the big aggregates.

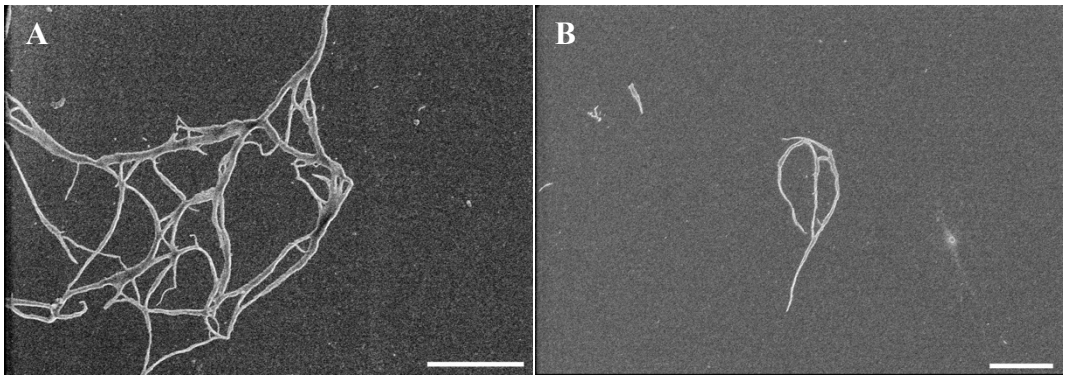

Figure 3-5: SEM images of K3T-siRNA complexes without sonication (A) and with sonication (B). Scale bar = 500 nm

3.2.2.2. Atomic Force Microscopy imaging

AFM technique measures the force on a cantilever tip created by the proximity with the surface atom, thus, creates a 3D detail image of the scanned

surface.[4] There are three operation modes commonly used: contact mode (close contact between the tip and surface), non-contact mode (tip does not contact the sample, attractive forces can be detected) and tapping mode (TM-AFM, alternate between close contact and lifting the tip off the sample).[5]

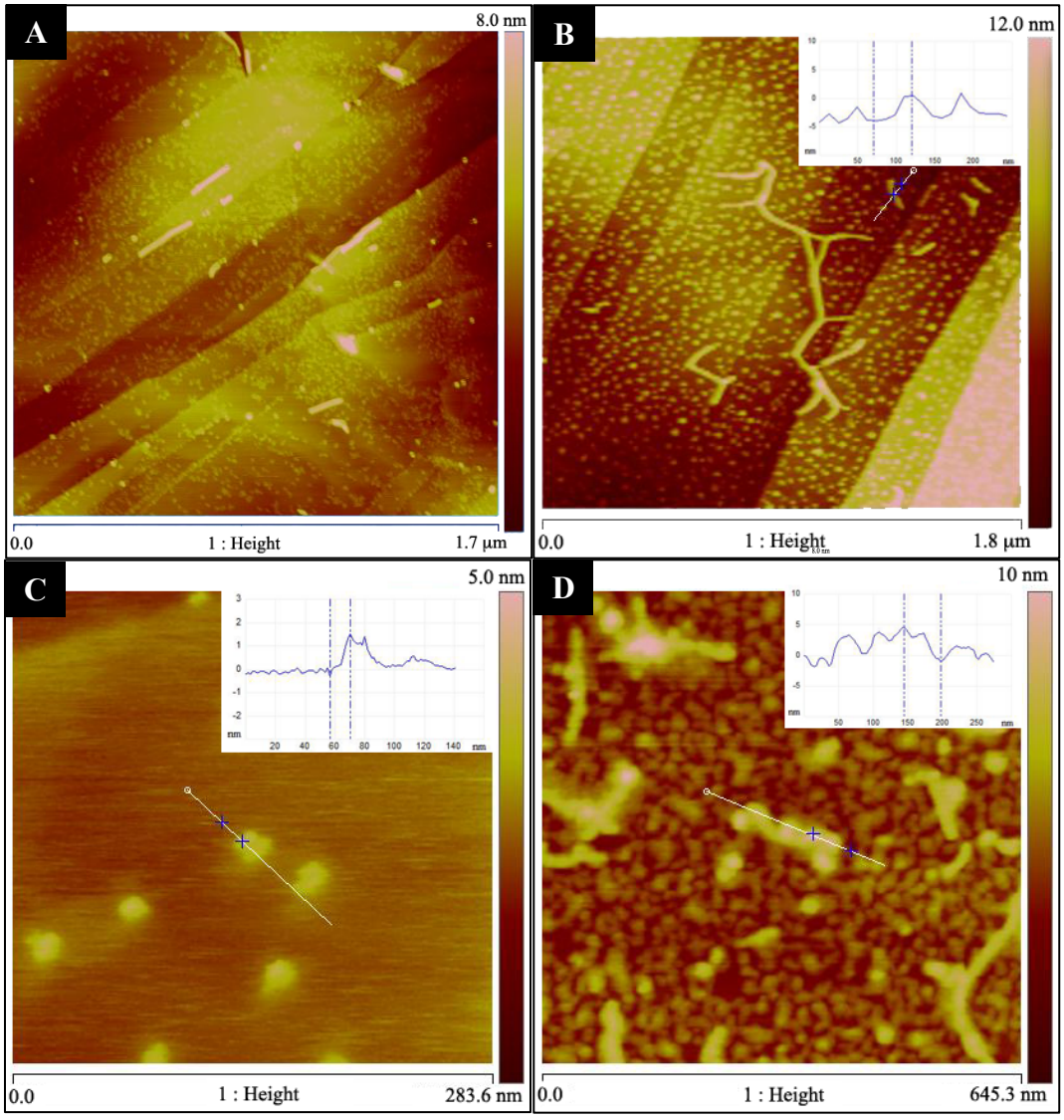

Figure 3-6: AFM images of (A) K3T in water, (B) K3T RNTs-siRNA in SFM, (C) siRNA in water and (D) K3T RNTs-siRNA complexes in SFM (molar ratio of 50:1). Inlets in B, C, D showing the height profile of the cross sections.

In this experiment, TM-AFM method was used to measure the diameter of K3T RNTs in water (Figure 3-6A), K3T RNTs in SFM (Figure 3-6B), siRNA alone (Figure 3-6C) and K3T RNTs-siRNA complexes in SFM (Figure 3-6D). AFM measurement showed the height (diameter) of K3T RNTs in water to be 4.1 ± 0.2 nm[1] whereas, it was 4.3 nm in presence of SFM. This was due to the binding of the salt content in SFM to the charged surface of K3T RNTs. The height profile of siRNA was measured to be 1.8 nm and the length was 7 nm. The complexes of K3T RNTs-siRNA in SFM was measured to be 5.6 ± 0.4 nm in height. The obtained height and observation of the morphology of K3T RNTs compared with K3T RNTs-siRNA complexes clearly showed the difference in morphology between the non-coated and siRNA-coated K3T RNTs. The rather rough surface of K3T RNTs-siRNA complexes (Figure 3-6D) clearly showed that short, negatively charged siRNA were adhering on to the surface of the RNTs.

3.2.2.3. Tramission Electron Microscopy imaging

TEM images are obtained by emitting the electron beam through the samples, the interaction of the electrons transmitted through the specimen is detected by a sensor for high resolution images.[6] TEM images of K3T RNTs-siRNA complexes (molar ratio of 50:1, Figure 3-7A) showed two distinct regions of (1): a highly stained region due to the dense coating of siRNA on the surface of RNTs with diameter of 4.3 ± 0.1 nm, and (2): a less stained region of low-coated K3T RNTs with diameter of 6.8 ± 0.8 nm. A magnified region of a RNT (Figure 3-7B) with black dot on the surface represented the siRNA binding to the surface of RNTs. The diameter values acquired by TEM were relatively bigger compared

to the ones acquired by AFM, since the AFM has a tendency to compress the surface of the materials, resulted in lower values. TEM diameter values were therefore more reliable and strongly supported earlier results by SEM and AFM regarding to the binding interaction between siRNA and the lysine peptides on the surface of K3T RNTs.

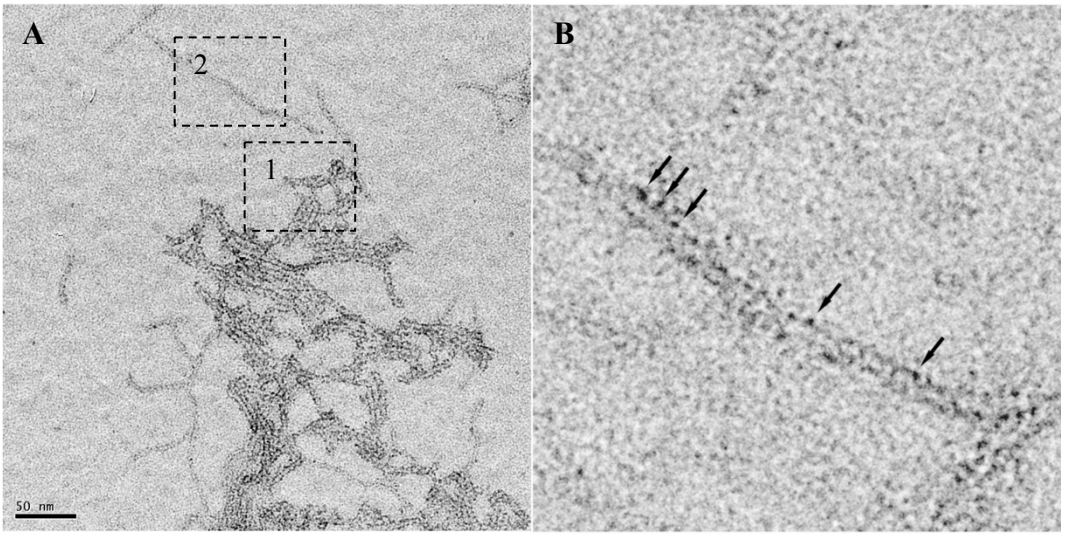

Figure 3-7: (A) TEM images of K3T RNTs-siRNA complexes at molar ratio of 50:1 with region (1) showing the siRNA-coated K3T RNTs and region (2) showing the low-coated K3T RNTs. (B) shows a magnified TEM image of K3T RNTs-siRNA complexes with arrows pointing at the siRNA on the surface of the RNTs.

3.3. Cell Transfection Study by Confocal Microscopy

Confocal microscopy was used to visualize the uptake rate of KnT RNTs-FAM siRNA complexes by HCT116 cells at different time points. The nuclei were stained with DAPI (blue), siRNA was labeled with FAM dye (green) and the acidic compartments of the cells were labeled with DND-99 (red). The delivery of

K1T to K5T RNTs-siRNA complexes (molar ratio of 30:1) were studied at 5 and 10 hours time points.

An obvious increase in signals of FAM-siRNA (higher intensity of green fluorescence) in the cells was observed with increase in time and net charges from K1T to K5T RNTs. Specifically, K1T and K2T RNTs showed low uptake at both 5 and 10 hours time points (Figure 3-8), with low fluorescent signal of FAM-siRNA inside the cells. K3T RNTs-siRNA complexes, on the other hand, showed low cellular uptake within 5 hours (Figure 3-9A), which increased significantly in FAM fluorescent signal within 10 hours (Figure 3-9 B, C). Unlike K1T, K2T and K3T RNTs, K4T and K5T RNTs-siRNA complexes both showed great uptake by the cells within 5 hours (Figure 3-9 D, G respectively) and at 10 hours time point (Figure 3-9 E, F & H, K respectively). The uptakes for K1T and K2T RNTs-siRNA complexes were predicted to increase at later time points when more complexes interact with the cell membrane. However, since K1T and K2T RNTs were not able to fully capture the siRNA, the FAM fluorecent signal would not have been as high as other RNTs. Meanwhile, cells transfected with K3T to K5T RNTs-siRNA complexes showed great fluorescence, which indicated that the RNTs were able to capture and bind well to siRNA. Moreover, the increase in positive charges of these RNTs would assist in the interaction with the anionic cellular membrane.

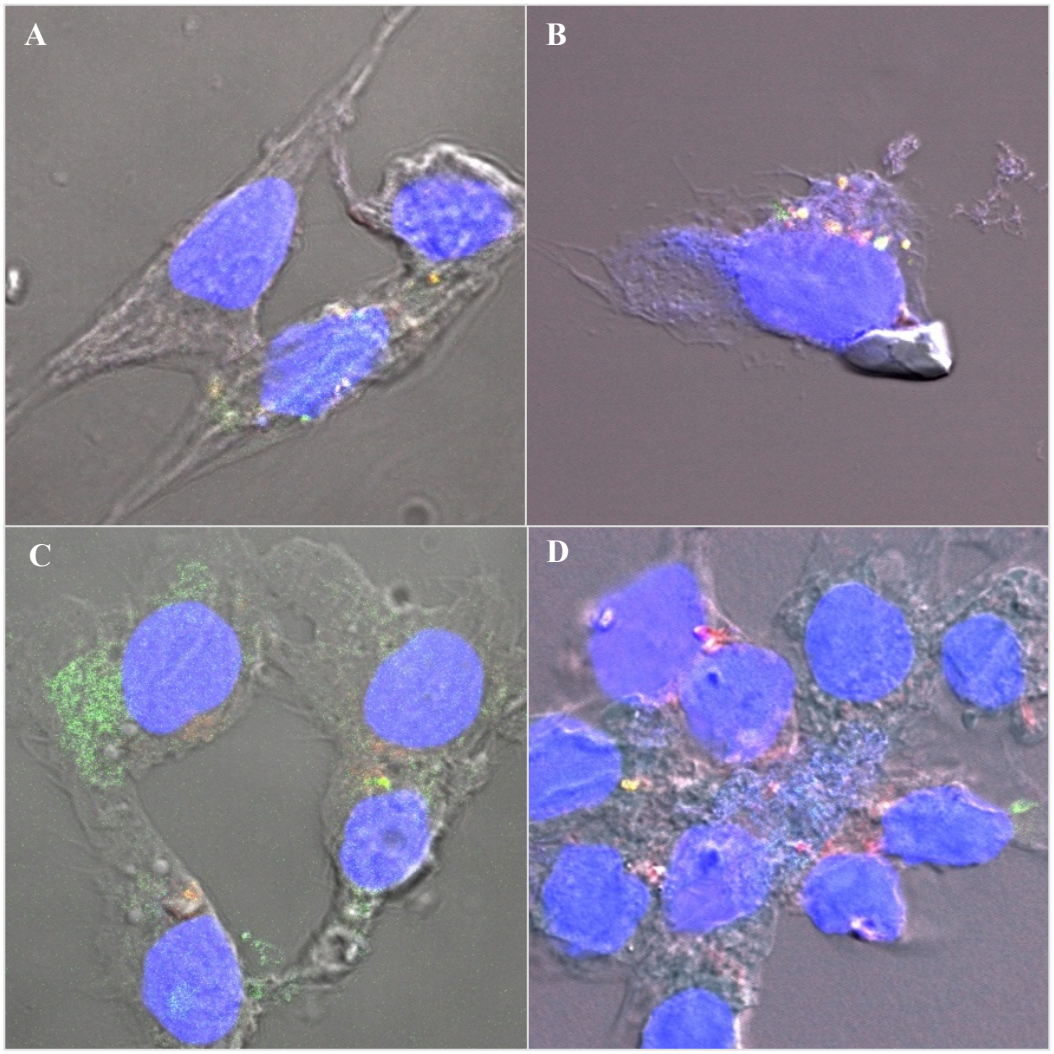

Figure 3-8: Combination of confocal fluorescence and differential interference contrast (DIC) illumination imaging of HCT116 cells after transfection with K1T RNTs (A, B) and K2T RNTs (C,D) with siRNA complexes (molar ratio of 30:1) after 5 hours (A,C) and 10 hours (B,D). siRNA labeled with FAM-dye (green fluorescence), acidic compartments were stained with LysoTrackerRed DND-99 (red fluorescence), and cell nuclei were stained with DAPI-dye (blue fluorescence).

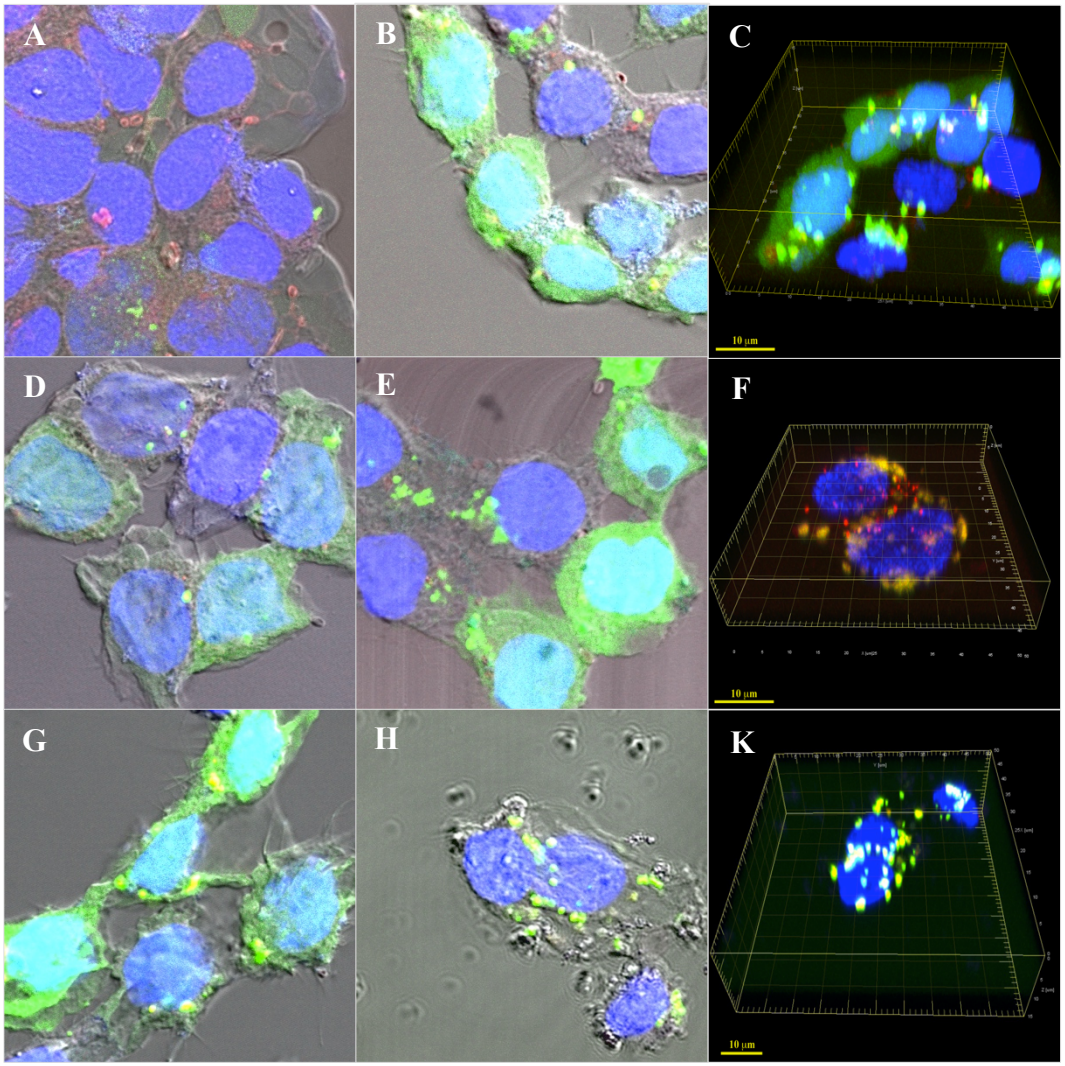

Figure 3-9: Combination of confocal fluorescence and differential interference contrast (DIC) illumination imaging of HCT116 cells after transfection with K3T RNTs (A, B,C), K4T RNTs (D, E, F) and K5T RNTs (G, H, K) and siRNA complexes (molar ratio of 30:1) after 5 hours (A,D,G) and 10 hours (B, C, E, F, H, K)

All the 3D images of K3T, K4T, K5T RNTs-siRNA complexes (Figure 3-9 C, F, K) acquired showed many yellow (or yellowish green) bright dots representing the overlapping between green and red fluorescence of siRNA and

endosome respectively. This supported earlier observation in endocytosis assay (Chapter II, Section 3.5) suggesting the mechanism of uptake of the RNTs-siRNA complexes by the cells was endocytosis. In addition, nearly no green fluorescent signal was shown to overlap with the blue fluorescence from the nucleus, which suggested efficient delivery of siRNA to the cytoplasm, including endosomal escape, by K1T to K5T RNTs.

3.4. Cytotoxicity test of K1T to K5T RNTs

MTT assay was used to assess the toxicity effects of K1T to K5T RNTs to HCT116 cells at increasing dosage from 0.75 μM to 12 μM RNTs for 24 hours (Figure 3-10). The result showed no significant cell death caused by the increase in RNTs concentrations, with the lowest cell viability observed to be 80%. This supported earlier cytoxicity assay (K10T and K15T RNTs, Chapter II, Section 3.7) that RNTs are biocompatible and have negligible lethal effect to the cells. Here, KnT RNTs generally showed low toxic effect to the cells when treated for a short time (~48 hours). However, treating the cells with high dosage of RNTs for a long time would promote intracellular uptake due to continuous interaction between RNTs and the cell membrane over time. Thus, when the cells were unable to remove the RNTs from their system, the accumulation of RNTs inside the cell would eventually impact the cells negatively. As such, dosage of RNTs used should be controlled and future *in vivo* experiment should allow the cells to excrete the RNTs from the cells before transfecting them with more RNTs-siRNA complexes.

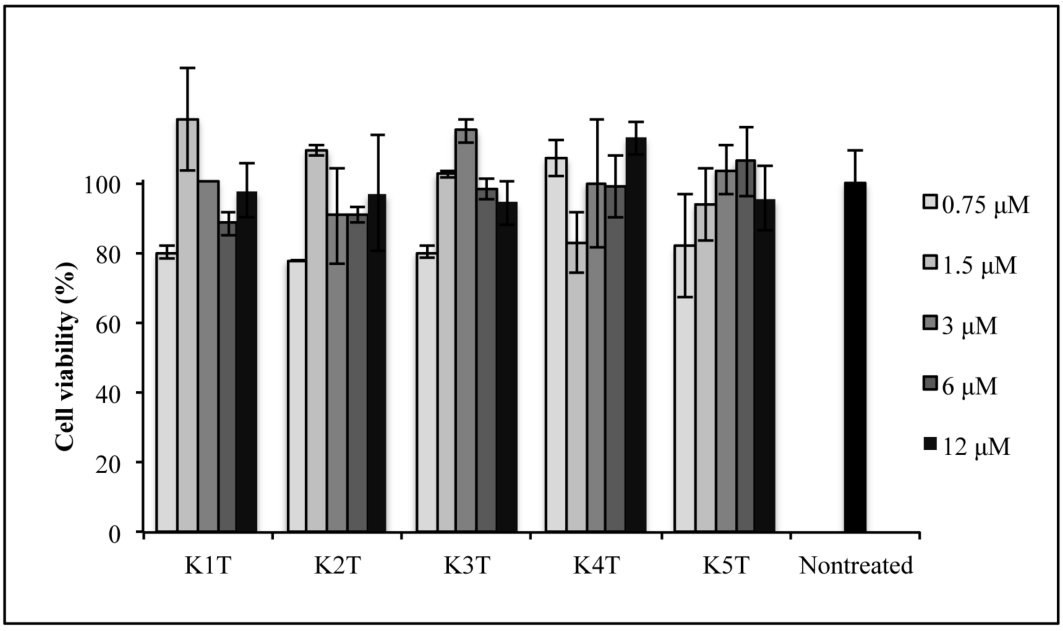

Figure 3-10: MTT assay to measure the cytotoxicity of K1T to K5T from 0.75 μM to 12 μM for 24 hours. Viability of HCT116 cells is shown in percent.

In this chapter, the highest dosage used for cell experiment was 5 μM of K3T RNTs treated for 48 hours (protein silencing experiment), which did not exceed the limit of 12 μM tested. Thus, this was a safe concentration to study without negative impact on the cells and their protein production.

3.5. Proteins Silencing experiments

3.5.1. Luciferase experiments

The ultimate goal for using RNTs as siRNA delivery system is so that the delivered siRNA can enter RNAi pathway and reduce targeted proteins in the cells. The most common method used to assess the effectiveness of siRNA silencing is to measure the targeted protein in the treated sample and compare it to a control. Various bioanalytical methods are known, one of which is luciferase assay, a common technique used for proteins measurement.[7]

Luciferase assay is a bioluminescent assay which measures the light production from an enzyme activity of luciferase when it reacts with its luminescent substrate, luciferin. Here, the assay performed was a dual luciferase assay where firefly and Renilla luciferase vectors were both delivered to the cells. The silencing was calculated by normalizing the activity of the targeted firefly luciferase to the activity of the control Renilla luciferase. By having the Renilla control in the samples, experimental variables such as difference in cell number, delivery efficiency of the luciferase plasmids and protein concentration difference in the samples can be eliminated.

K3T RNTs was chosen to be the candidate for the silencing study, because it has the lowest lysine number that could fully capture siRNA at 50:1 molar ratio as tested in the gel retardation experiment (Section 3.1). Potentially, relatively low net charge of K3T molecule (+4, Table 2-1) could allow for the release of siRNA from the RNTs to the cytoplasm of the cells. Confocal images of HCT116 cells treated with K3T RNTs-siRNA (Figure 3-9 B, C) were evident of the high transfection efficiency and siRNA distribution in the cytoplasm of the cells.

The silencing ability of the firefly pGL3 siRNA (FF siRNA) delivered was tested by transfecting two cell lines (A549 and HCT116) with K3T RNTs - FF siRNA complexes (molar ratio of 50:1) for 24 hours (Figure 3-11). Then, the two plasmids encoding firefly and Renilla luciferase genes were delivered using Lipofectamine to express their corresponding proteins. For both cell lines, FF siRNA delivered was shown to successfully function inside the cells as the signal produced by firefly luciferase was significantly reduced. The silencing effect from

K3T RNTs - FF siRNA treatment compared to the negative control (non-treated) was calculated to be 67 ± 20% for A549 cells and 72 ± 10% for HCT116 cells when using K3T RNTs as siRNA carrier. The positive control of INTERFERin-FF siRNA gave similar results of 74 ± 13% for A549 cells and 61 ± 10% for HCT116 similar to that of K3T RNTs. This showed effective delivery of siRNA by K3T RNTs resulting in excellent silencing ability that was comparable to a commercial siRNA transfecting reagent (INTERFERin). The RNTs had advantage over INTERFERin for their low toxicity effect to the cell even at high dosage (Section 3.4). This is essential for therapeutic application since the carrier system should not affect the viability of non-cancerous cells.

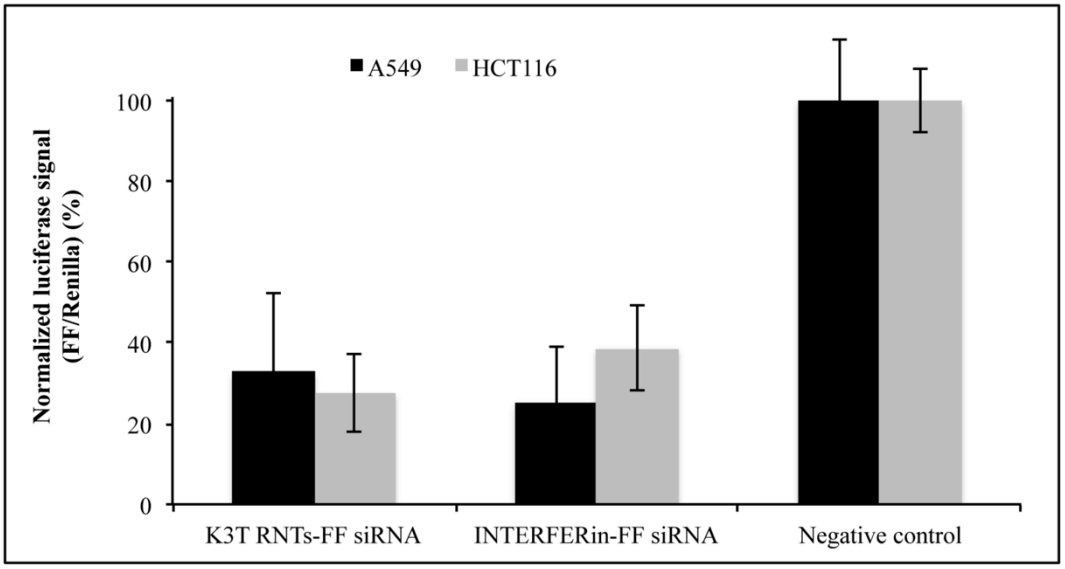

Figure 3-11: Luciferase assay to measure the silencing effect of siRNA (100 nM) delivered by K3T RNTs (molar ratio 50:1) and INTERFERin (positive control) in two cell lines A549 and HCT116.

3.5.2. STAT3 silencing

STAT3 protein regulates gene expression in the cell nucleus and is also found to play an important role in the growth and progression of cancer cells[8]. Thus, inhibition of STAT3 gene is widely considered for cancer therapy, as this protein can upregulate other proteins expression and stimulate tumor angiogenesis[9] and survival[10] (Chapter I, Section 1.2.2). Therefore, targeting endogenous protein such as STAT3 is a preliminary step to examine the silencing efficiency of siRNA delivered by the RNTs.

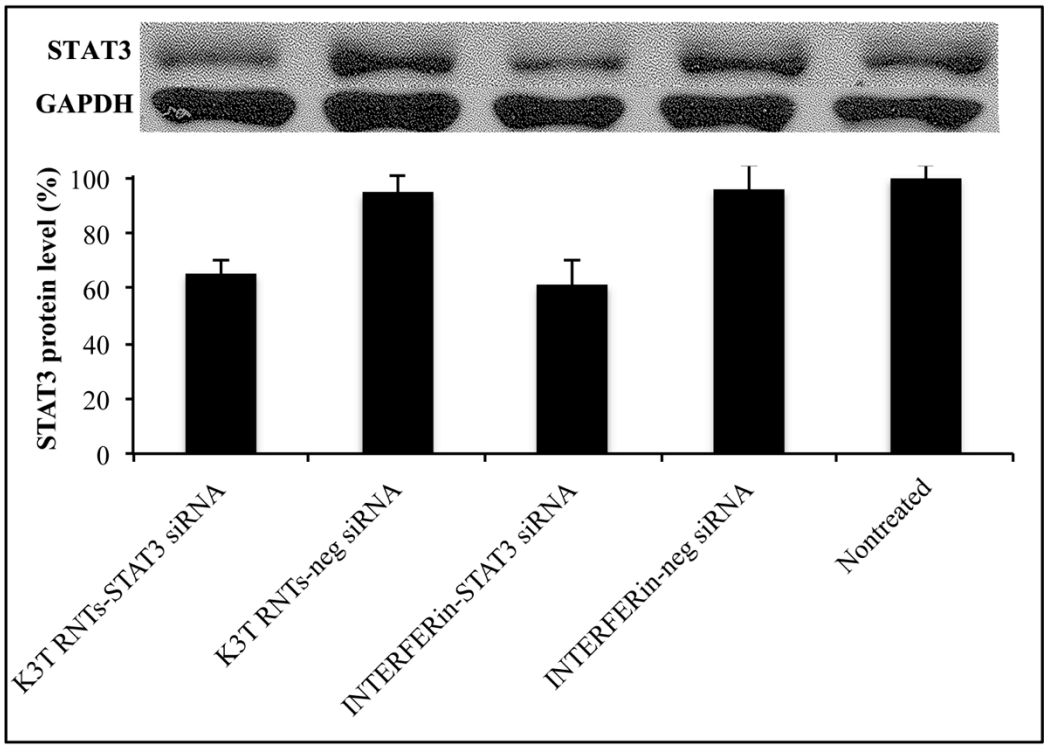

Figure 3-12: Western blot detecting STAT3 proteins in HCT116 cells after transfection with K3T and siRNA (molar ratio 50:1, siRNA = 100nM)

HCT116 cells were treated with K3T RNTs-STAT3 siRNA complexes at molar ratio of 50:1 and INTERFERin-STAT3 siRNA served as positive control.

Here, the silencing from siRNA delivered by K3T RNTs (35%) was almost comparable to the result obtained for the positive control (40%) (Figure 3-12). Similar silencing effect between K3T RNTs and INTERFERin was observed in Section 3.5.1 for firefly luciferase assay, which indicated almost maximum possible silencing effect was achieved in the treatment.

Despite repeating the experiment, it was not successful due to the aging of K3T RNTs solution (four months old), resulting in lower silencing efficiency. In the self-assembly system, RNTs grow longer over time due to the continuous interaction of the K3T molecules in solution to form RNTs, and RNTs can also form bundles due to aging. The rate at which the RNTs grow highly depends on the initial heating step of the solution. For the silencing experiment, the RNTs solution used in this experiment was heated for 15 minutes at 90 ^{o}C. At this high temperature, RNTs most likely grew longer and formed more bundles. The big RNTs bundles and long RNTs would form big complexes with siRNA, which would not be favorable for cellular uptake. This proved that high heating for a long time could affect the properties of the RNTs (elongating the RNTs) and their binding to siRNA negatively, which could lead to low cell transfection efficiency. Therefore, it is preferred to have short RNTs that self-assemble at slow rate, so that they could stay almost at the same length for a long period of time to reduce the formation of big bundles. In the future, the RNTs should be made fresh prior to treatment or the stock solutions used should be stored at 4 ^{o}C, and be within two weeks to one month.

Despite having only one experiment for STAT3 silencing by siRNA delivered by K3T RNTs, data obtained was reliable due to the agreement with the negative and positive controls. Along with the luciferase assay (Section 3.5.1), STAT3 silencing experiment showed strong evidence that siRNA delivered by K3T RNTs was functional such that the proteins targeted was reduced significantly, with similar silencing result compared to the commercial transfecting agent of INTERFERin.

4. Conclusion

This chapter has focused on investigating the low net charged K1T to K5T RNTs. K3T RNTs was studied further for its ability to deliver siRNA for protein silencing purposes. Studies on K1T to K5T RNTs showed their ability to enhance siRNA encapsulation as the molar ratio of RNTs : siRNA was increased, despite having lower charges compared to other KnT RNTs in the library. Here, K3T, K4T and K5T RNTs-siRNA complexes yield complete binding with siRNA in SFM at molar ratio of 50:1. Characterization of K3T RNTs and siRNA was done using SEM, AFM and TEM techniques to observe the binding between K3T RNTs and siRNA. Confocal imaging showed great uptake by the cells of K3T, K4T and K5T RNTs-FAM siRNA complexes (30:1 molar ratio), including great siRNA distribution in the cytoplasm. The cytotoxicity of the five RNTs was also investigated (dosage of 12 μM for 24 hours) and showed no obvious lethal effect (lowest cell viability of 80%) to the cells. Most importantly, the silencing effect of FF siRNA delivered by K3T RNTs performed in two cell lines (HCT116 and A549 cells) showed up to 70% silencing effect, which was comparable to the

positive control of INTERFERin. Lastly, STAT3 siRNA delivered to HCT116 cells by K3T RNTs also showed 35% silencing effect, comparable to the positive control. It was also found that aging of RNTs played an important role in siRNA of siRNA binding and delivery efficiency to the cells. In summary, increase of KnT RNTs : siRNA molar ratio increased the intracellular delivery of siRNA, especially, K3T RNTs were able to successfully deliver siRNA for protein silencing.

References

1. El-Bakkari, M.; Beingessner, R.L.; Alshamsan, A.; Cho, J.-Y.; Fenniri, H. Electrostatic and Steric Effect of Peptides Functionalized on Self-Assembled Rosette Nanotubes. *Mater. Res. Soc. Symp. Proc*. **2011**, 1316, mrs10.1557/opl.2011.436.

2. Santos, T.; Varela, J.; Lynch, I.; Salvati, A.; Dawson, K. Quantitative Assessment of the Comparative Nanoparticle-Uptake Efficiency of a Range of Cell Lines. *Small*. **2011**, 7, 23, 3341-3349.

3. Fenniri, H.; Deng, B.-L.; Ribbe, A.; Hallenga, K.; Jacob, J.; Thiyagarajan, P. Entropically driven self-assembly of multichannel rosette nanotubes. *Proc. Natl. Acad. Sci*. **2002**, 99, 2, 6587-6492.

4. Binnig, G. and Quate, C.F. Atomic Force Microscope. *Phys. Rev. Lett.* **1986**, 56, 930-933.

5. Haugstad, G. *Atomic Force Microscopy: Understanding Basic Modes and Advanced Applications.* John Wiley & Sons, 2012.

6. Williams, J. C. and Paton, N. Transmission Electron Microscopy. In *Systematic Materials Analysis;* Richardson, J. H.; Elsevier, 2012; Vol. 4, p. 408-409.

7. Bruce, A.S. and Navarro, S.L. Dual-Luciferase Reporter Assay: An Advanced Co-Reporter Technology Integrating Firefly and Renilla Luciferase Assays. *Promega Notes Magazine.* **1996**, 2-8.

8. Lassman, S.; Schuster, I.; Walch, A.; Gobel, H.; Jutting, U.; Makowiec, F.; Hopt, U.; Werner, M. STAT3 mRNA and protein expression in colorectal cancer:

effects on STAT3-inducible targets linked to cell survival and proliferation. *J. Clin. Pathol.* **2007**, 60, 173-179.

9. Niu, G. et al. Constitutive Stat3 activity up-regulates VEGF expression and tumor angiogenesis. *Oncogene*. **2002**, 21, 13, 2000-2008.

10. Gritsko, T. et al. Persistent Activation of Stat3 Signaling Induces Survivin Gene Expression and Confers Resistance to Apoptosis in Human Breast Cancer Cells *Clin. Cancer. Res.* **2006**, 12, 11-19

Chapter IV

Delivery of siRNA using K1

Rosette Nanotubes for Protein Silencing

1. Introduction

K1 compound contains a lysine residue covalently attached to the mono-GʌC base (Figure 4-1). The mono-base is different from the twin-GʌC base (Chapter II and III), such that six mono-GʌC bases (Figure 4-2A) each containing a lysine residue, form one rosette (Figure 4-2B), which is maintained by 18 H-bonding.[1] The rosettes then self-assemble into RNTs via π- π stacking[1] (Figure 4-2C). The diameter of K1 RNTs was reported to be approximately 3.5 nm using TEM imaging.[2] K1 RNTs can form under physiological condition and are therefore, stable for biology applications where neutral pH is required.[1]

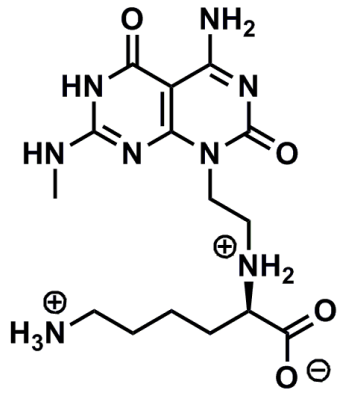

Figure 4-1: Structure of K1 compound showing charges at neutral pH.[1]

K1 RNTs was the first lysine-functionalized RNTs synthesized in Fenniri's group and has since been widely used in many applications, such as tissue engineering,[3,4,5,6] hydrophobic drug delivery [7,8] and nanoparticles syntheses [9,10] (Chapter I, Section 4.2). Successes of K1 RNTs achieved in various biological applications suggested the high biocompatibility of this RNT for cell study. KnT RNTs, especially K3T RNTs demonstrated the competence to deliver siRNA for protein silencing (Chapter III). Similar to KnT RNTs, K1 RNTs also have

positively charged lysine chains present on the nanotubes' surface. As such, K1 RNTs were also considered as a good candidate for siRNA delivery in cancer therapy.

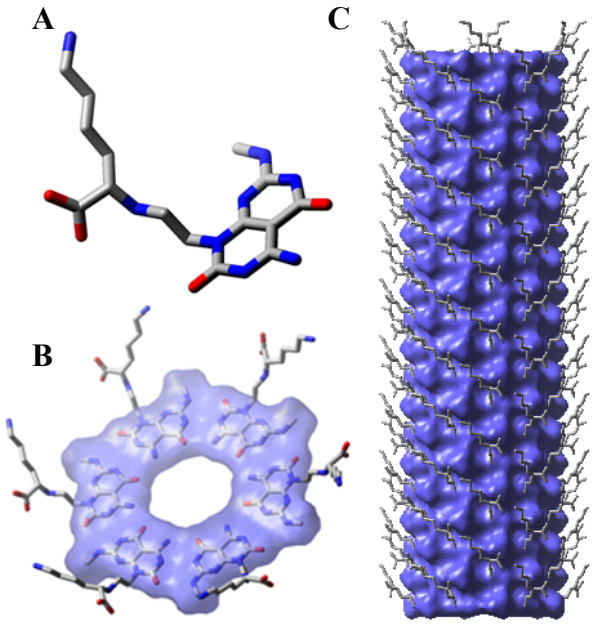

Figure 4-2: Molecular models of (A) K1 compound, (B) a K1 rosette and (C) a K1 RNT.

This chapter will explore the capability for K1 RNTs to deliver siRNA for protein silencing in cancer cells (A549 and HCT116). Firstly, the binding ability of K1 RNTs to siRNA at various molar ratios was examined using gel retardation assay. The size and morphology of the complexes was studied using SEM. The siRNA delivery efficiency by K1 RNTs was inspected using confocal microscopy and flow cytometry techniques. MTT assay was performed to assess the cytotoxicity of K1 RNTs to the cells. Finally, the silencing effect of siRNA delivered by K1 RNTs was evaluated by targeting the production of firefly luciferase and STAT3 proteins.

2. Materials and Methods

2.1. Materials

K1 compound was synthesized in Fenniri's lab (MW = 531.94 g/mol) using previously reported procedure.[1]

2.2. General Methods

K1 RNTs stock solution was prepared by dissolving K1 compound (1 mg/mL) in 1 mL of deionized water, followed by a quick sonication and heating with heat gun for 20 seconds.

K1 RNTs-siRNA complexes were prepared at various molar ratios (50:1, 100:1, 150:1, 200:1, 300:1 and 400:1 K1 RNTs to siRNA respectively, n_{siRNA} = 0.1 nmol) in 60 μL of SFM or water. The complexes were incubated for 30 minutes at rt, followed by 30 seconds of sonication.

2.3. Agarose Gel Electrophoresis

Samples of K1 RNTs-siRNA complexes were prepared as previously described in Section 2.2. Agarose gel shift assay was then carried out to detect unbound siRNA (Chapter II, Section 2.3).

2.4. Characterization by Microscopy

SEM samples were prepared as described earlier (Section 2.2).

2.5. Confocal microscopy for siRNA delivery observation

K1 RNTs-FAM siRNA complexes at various molar ratios (100:1, 150:1, 200:1, 300:1 and 400:1) were prepared (Section 2.2). HCT116 and A549 cells

were transfected with the complexes in 12-well plate for 48 hours at 37 ^{o}C. Microscopy slides were then prepared (Chapter II, Section 2.5.1).

2.6. Flow Cytometry

HCT116 and A549 cells were seeded in 12-well plate for 24 hours (60-70% confluency) prior to the treatment. Cells were transfected with K1 RNTs-FAM siRNA complexes at various molar ratios (50:1, 100:1, 150:1, 200:1, 300:1 and 400:1, in water or SFM). After 48 hours of treatment, the cells were washed with PBS (3 x 30 seconds), detached with Trypsin-EDTA and transferred to conical tubes for centrifugation (5 minutes at 1100 rpm). The supernatant was discarded and the cell pellet was re-suspended with 1% paraformaldehyde for 20 minutes. Cells were then re-centrifuged and the cell pellet was suspended in PBS. The signal of FAM-dye in the fixed cells was measured using FACSCalibur flow cytometer (BD Biosciences).

2.7. Cell Viability study

Cells were transfected with K1 RNTs at various concentrations (5, 10, 20, 30, 40 and 50 μM) for 48 hours. MTT assay was then performed to detect the cell viability (Chapter II, Section 2.6).

2.8. Proteins silencing using K1 RNTs

2.8.1. Luciferase experiment

A549 and HCT116 cells were transfected with complexes of K1 RNTs and firefly luciferase siRNA (FF siRNA) at various molar ratios (50:1, 100:1, 150:1, 200:1, 300:1 and 400:1) for 24 hours. Next, the cells were treated with DNA

plasmids (pGL3 & Renilla) and signals produced by the luciferases were detected (Chapter III, Section 2.7.1).

2.8.2. STAT3 Protein Silencing

A549 and HCT116 cells were transfected with K1 RNTs-STAT3 siRNA complexes at various molar ratios (50:1, 100:1, 150:1, 200:1, 300:1 and 400:1) for 48 hours. Western blot procedure was carried out to detect STAT3 protein level (Chapter III, Section 2.7.2).

3. Results and Discussion

3.1. Properties of K1 RNTs stock solution

From previous chapters (II and III), we learned that the length of the RNTs affects the size of the RNTs-siRNA complexes formed, and that smaller complexes are more susceptible to cellular uptake. K1 molecule (Figure 4-1) has a net charge of +1 and has only one lysine on the side chain hence, the low steric hindrance between K1 molecules allows K1 RNTs to self-assemble easily in aqueous solution. Therefore, heating of the stock solution excessively could result in long RNTs up to micrometer in length[11], which would be challenging for cellular uptake. Thus, K1 RNTs stock solution was heated at low temperature for short time to yield short tubes that are in nanometer range. Time study of K1 RNTs by SEM (Figure 4-3) showed slow growing progress of the RNTs with less than 50 nm observed within 1 hour of aging, comparing to 50-200 nm in length 10 days after. Conclusively, these short RNTs were shown to be more stable for longer time (slower growth) compared to if the stock solution was heated to near-

boiling temperature. The slow growth of the RNTs would keep them fairly consistent in length for the cell study, so that the data were comparable between studies.

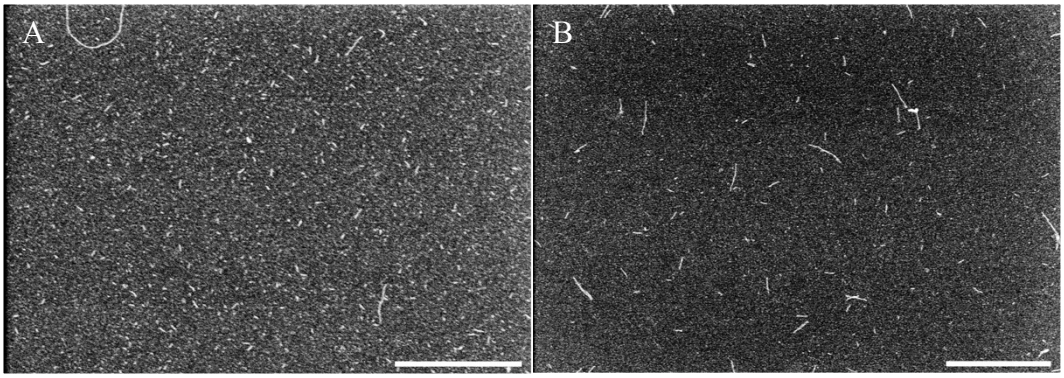

Figure 4-3: SEM images of K1 RNTs at (A) 1 hour and (B) 10 days after the stock solution was made. Scale bar = 500 nm

3.2. Complexation of K1 RNTs and siRNA

Gel shift assay was used to examine the siRNA binding of K1 RNTs at various molar ratios of K1 RNTs to siRNA (50, 100, 150, 200, 300, 400:1). In order to understand the role of the solvent on the interaction of K1 RNTs and siRNA complexes, the complexes were prepared in H_2O (salt-free) and SFM (salt-containing medium).

Full complexation between K1 RNTs and siRNA at molar ratio of 100:1 (Figure 4-4) was observed. In all the ratios, the ability to capture siRNA by K1 RNTs showed no obvious difference when formed in water or the salt-containing SFM. Thus, it was obvious that K1 RNTs could bind to siRNA via electrostatic interaction in salty environment (SFM) or no added salt environment (water).

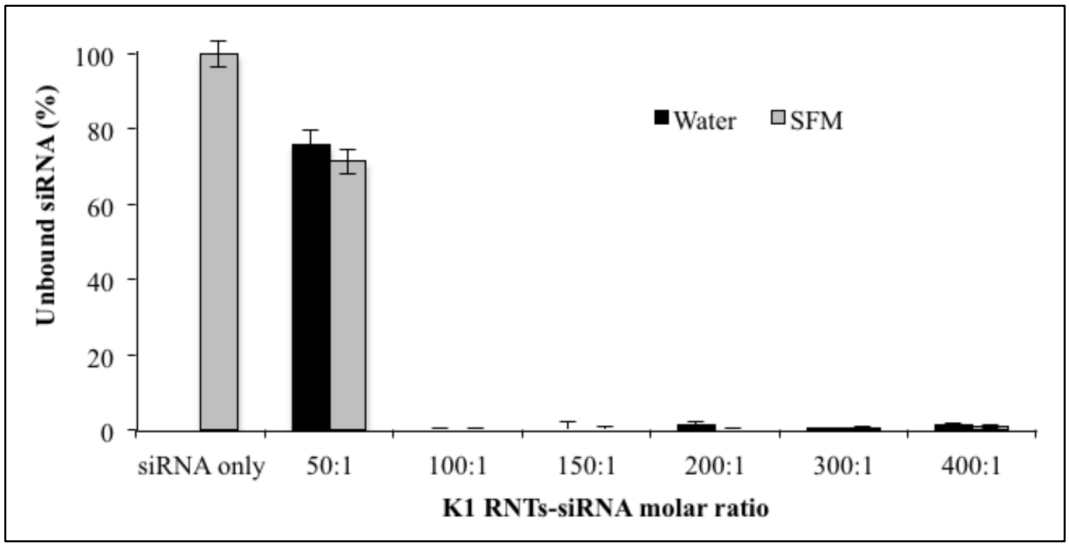

Figure 4-4: Percentage of unbound siRNA in K1 RNTs-siRNA complexes at different molar ratios in SFM and water (n_{siRNA} = 0.1 nmol).

3.3. Characterization of K1 RNTs-siRNA complexes

SEM technique was performed to visualize the size and morphology of K1 RNTs-siRNA complexes at various molar ratios (50, 100, 150, 200, 300, 400:1). Obtained images of the complexes (Figure 4-5, 4-6) generally showed an increase in size (measured using ImageJ) in both media as the molar ratios of RNTs-siRNA increased.

These values (Figure 4-7) suggested that bigger complexes were formed with increasing molar ratio, as more K1 RNTs were available for the complexation with siRNA, which agreed with previous observation for K3T RNTs-siRNA complexes (Chapter III, Section 3.2). In addition, the formation of big complexes could also be due to increasing concentration of K1 RNTs (at constant volume), which led to higher interaction between the K1 RNTs and siRNA, resulting in formation of big complexes.

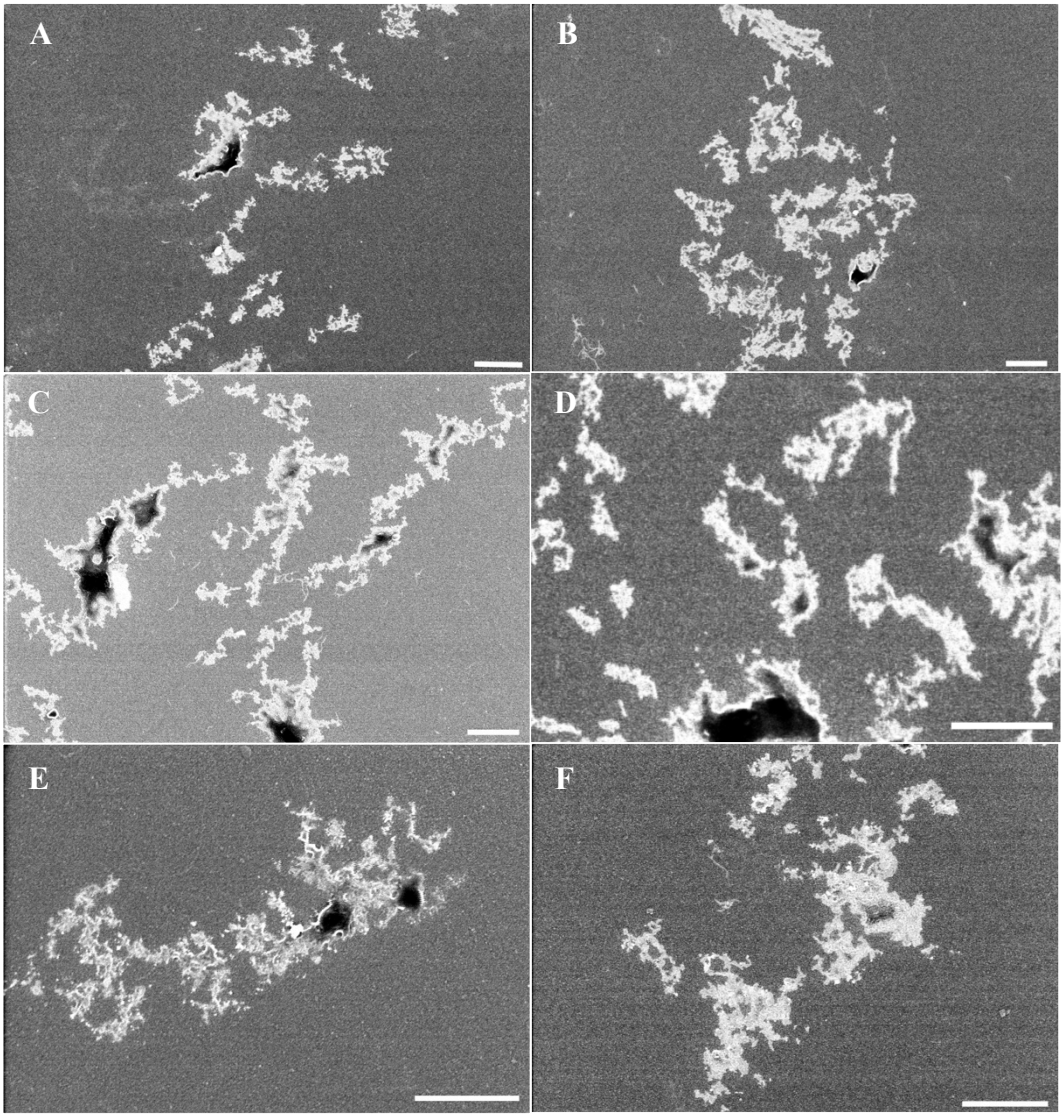

Figure 4-5: SEM images of K1 RNTs-siRNA complexes at molar ratio of (A) 50:1, (B) 100:1, (C) 150:1, (D) 200:1, (E) 300:1, (F) 400:1 in water. Scale bar = 500 nm.

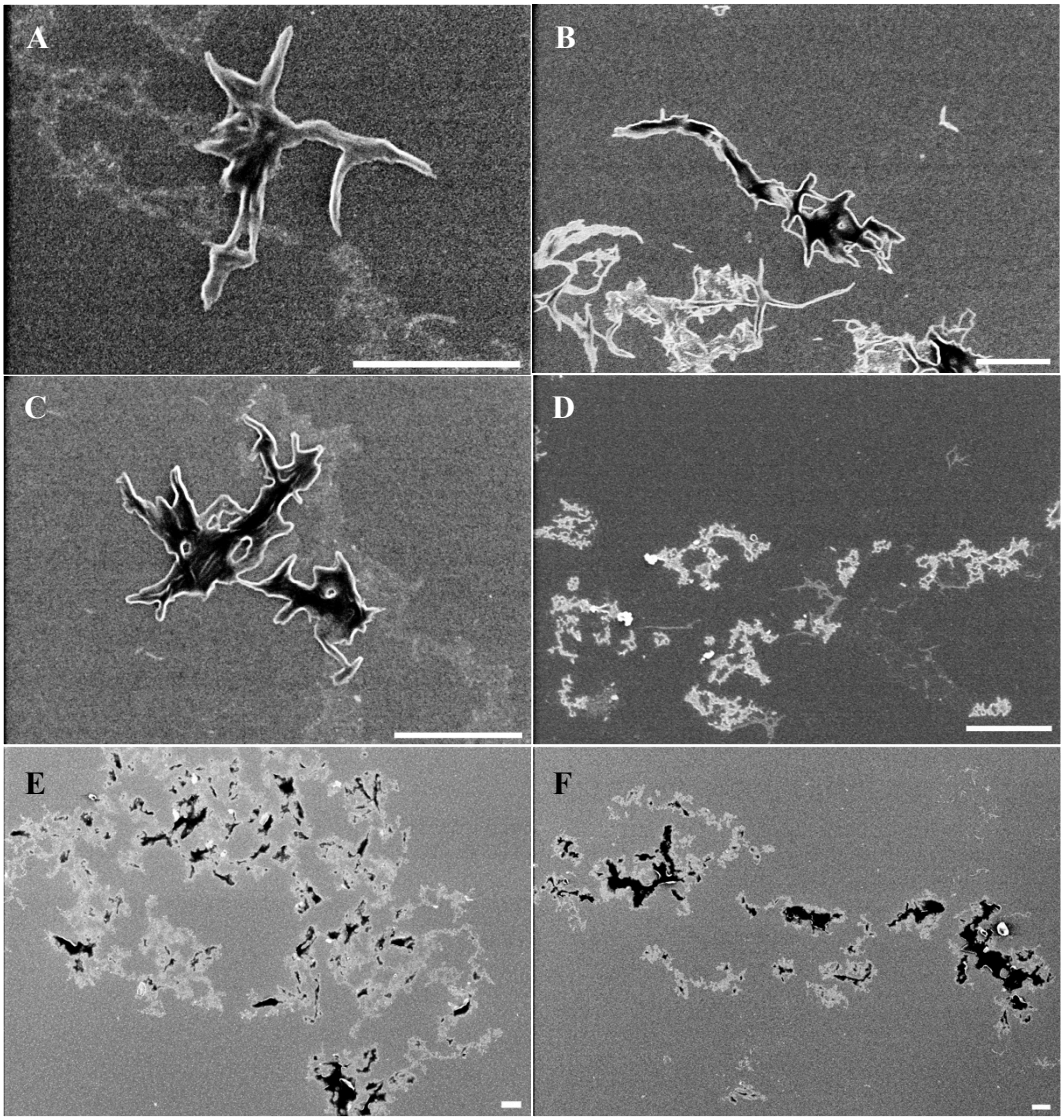

Figure 4-6: SEM images of K1 RNTs-siRNA complexes at molar ratio of (A) 50:1, (B) 100:1, (C) 150:1, (D) 200:1, (E) 300:1, (F) 400:1 in SFM. Scale bar = 500 nm.

Comparison of K1 RNTs-siRNA complexes formation in water (Figure 4-5) and SFM (Figure 4-6) showed that relatively bigger complexes were seen forming in SFM environment (Figure 4-7), which could be explained by the salt content in SFM that increased the binding attraction between RNTs and siRNA.

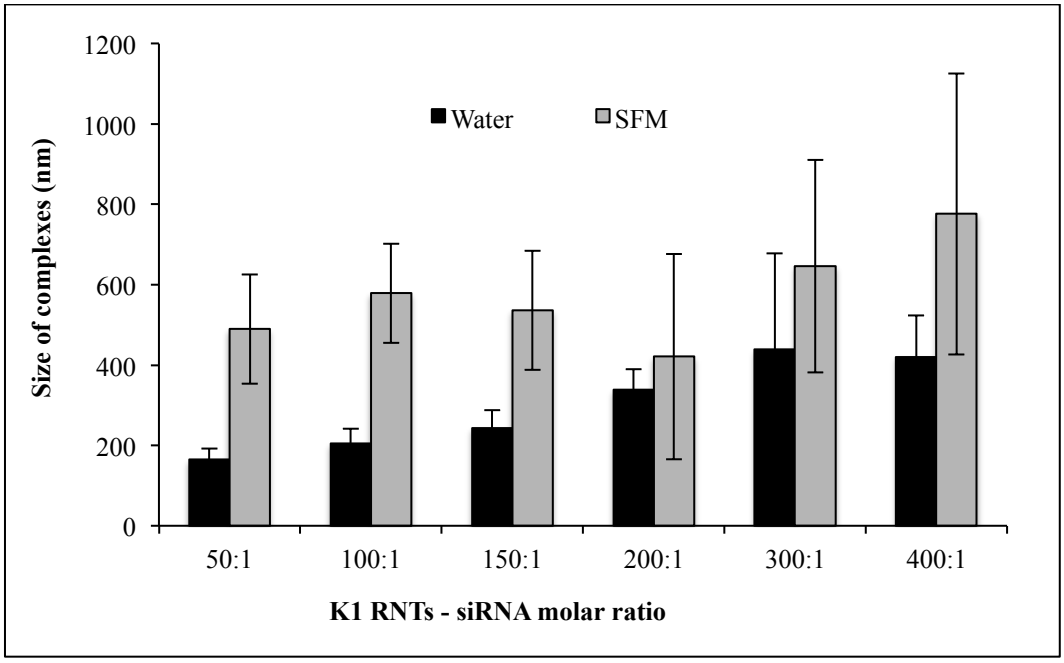

Figure 4-7: Histogram showing the size range of K1 RNTs-siRNA complexes when formed in water (black), and SFM (grey). Size of the complexes were measured using the ImageJ software.

SEM images of K1 RNTs-siRNA complexes showed that the binding of RNTs and siRNA could occur both in water and SFM. However, the salt-containing SFM led to bigger and thicker complexes due to the contribution of ions to neutralize the charges and promote binding attraction between the RNTs and siRNA.

3.4. Transfection Efficiency of siRNA delivered by K1 RNTs

3.4.1. Cellular uptake of siRNA by confocal microscopy

In order to study the uptake efficiency of K1 RNTs-FAM siRNA complexes, A549 (lung carcinoma) and HCT116 (colorectal carcinoma) cells were transfected with the complexes at various molar ratios (100, 150, 200, 300 and 400:1) for 48 hours. Positive control of INTERFERin-siRNA complexes were

transfected to A549 cells showing strong green fluorescent signal of FAM-siRNA, whereas the negative control of siRNA only showed negligible FAM signal (Figure 4-8). Meanwhile, A549 cells (Figure 4-9) and HCT116 cells (Figure 4-10) that were transfected with K1 RNTs-siRNA complexes showed higher signal of FAM-siRNA delivered to the cells, compared to the negative control. This indicated effective delivery of siRNA by K1 RNTs. The green fluorescent signal indicated that A549 cells (Figure 4-9) were uptaking more K1 RNTs-siRNA complexes compared to HCT116 cells (Figure 4-10), with higher green fluorescent signal in the former. This will be further supported in the next section (Section 3.4.2), where flow cytometry method was used to quantify the fluorescent signal of FAM-siRNA in the cells. In both cell lines (A549 and HCT116), FAM fluorescent signal showed the strongest intensity at molar ratios of 150:1 and 200:1 when the RNTs-siRNA complexing in either medium (water or SFM). However, when the molar ratios increased (300:1 and 400:1), big complexes were formed, which led to lower cellular uptake and they were observed to be mainly outside the cells (green fluorescence not overlapping with red fluorescence).

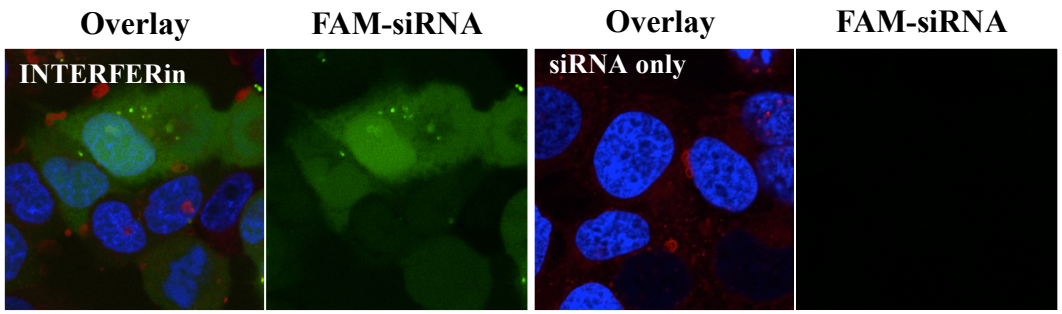

Figure 4-8: Confocal imaging of A549 cells when transfected with INTERFERin-FAM siRNA (positive control) and siRNA only (negative control) for 48 hours.

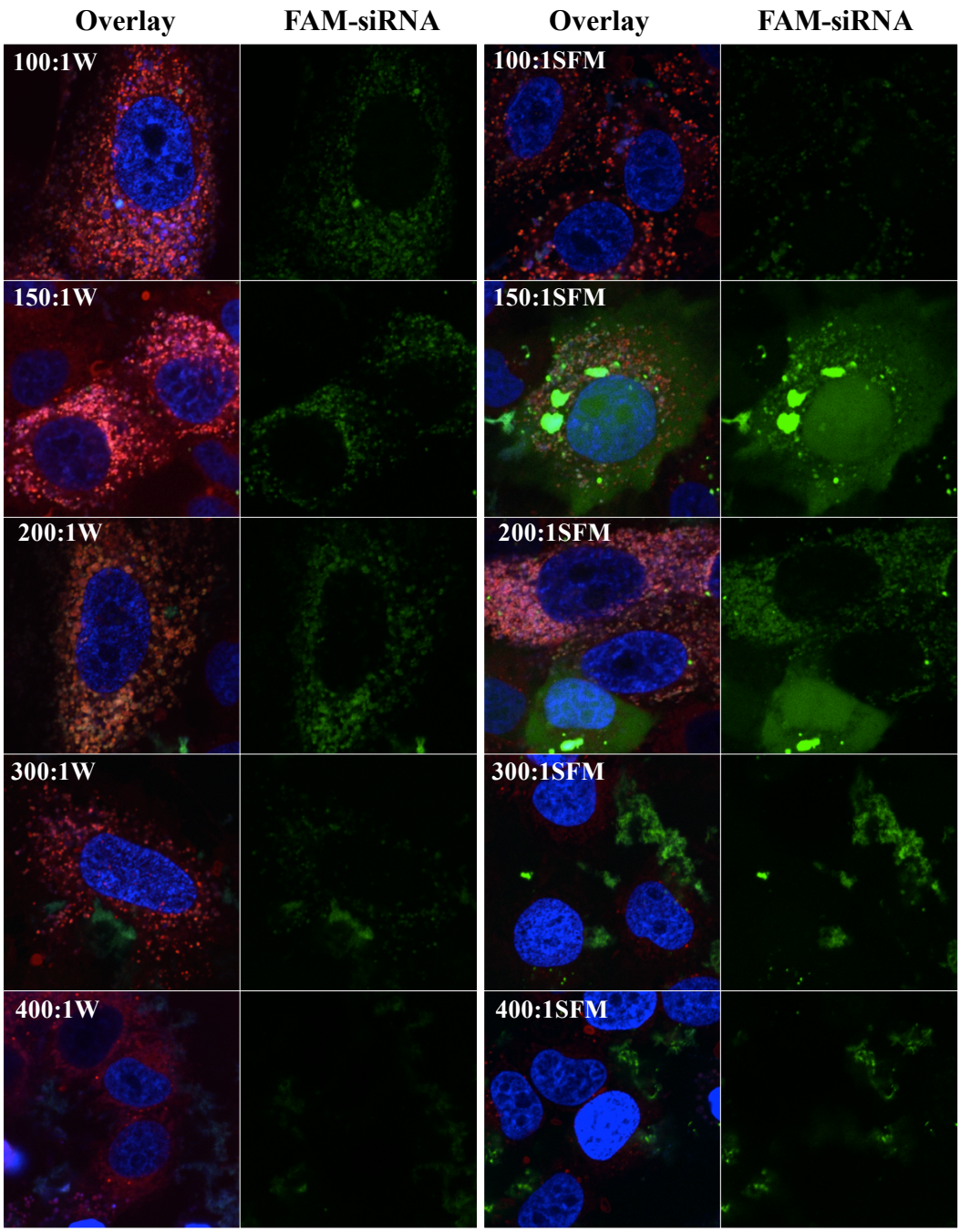

Figure 4-9: Confocal images of A549 cells when transfected for 48 hours with K1 RNTs-siRNA complexes at 100, 150, 200, 300 and 400:1 molar ratios forming in water and SFM. The merged images and their corresponding green channel (right) showing FAM fluorescent signals are shown.

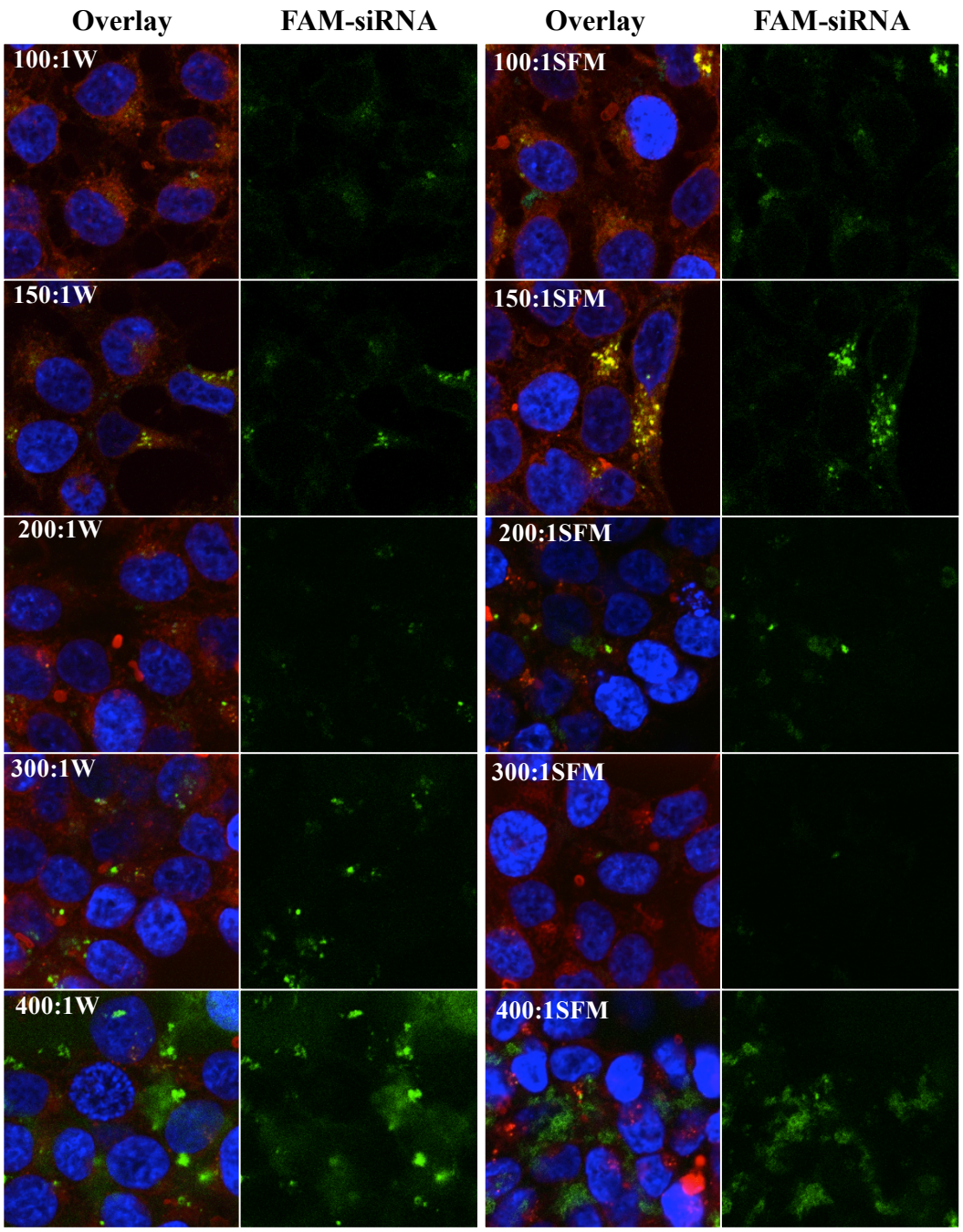

Figure 4-10: Confocal images of HCT116 cells when transfected for 48 hours with K1 RNTs-siRNA complexes at 100, 150, 200, 300 and 400:1 molar ratios forming in water and SFM. The merged images and their corresponding green channel showing FAM fluorescent signals are shown.

Comparison of transfection efficiency between the RNTs-siRNA complexes formed in water and SFM in both cell lines showed that cells might prefer to uptake complexes formed in SFM rather than in water. This could be due to the preference of the cells to uptake complexes of a certain size, or the thicker K1 RNTs-siRNA complexes formed in SFM could protect more siRNA as seen by SEM technique (Section 3.3).

Here, even though both cell lines showed different cellular uptake properties toward K1 RNTs-siRNA complexes, it was evident that K1 RNTs were able to support the delivery of siRNA to the cells. Molar ratio of K1 RNTs to siRNA showed significant impact to the size of the complexes formed and thus, to the transfection efficiency of the complexes to the cells. Specifically, molar ratio of 100:1 and 150:1 of K1 RNTs: siRNA showed to be the best for intracellular delivery, whereas 300:1 and 400:1 complexes were too big to be uptaken by the cells.

3.4.2. Flow cytometry for quantification of FAM-siRNA signal

Flow cytometry is a laser-based technique that can detect fluorescent signal from fixed cells. In this experiment, siRNA was labeled with fluorescent FAM dye, which can be detected using FITC channel. The study was carried out by transfecting A549 and HCT116 cells with K1 RNTs-siRNA complexes at various molar ratios (50:1, 100:1, 150:1, 200:1, 300:1 and 400:1, complexing in water and SFM). Similar to confocal microscopy result (Section 3.4.1), geometric mean of FAM-siRNA signal (inlet charts) demonstrated that A549 cells (Figure 4-11, 4-

12) had higher uptake ability of the complexes compared to HCT116 cells (Figure 4-13, 4-14).

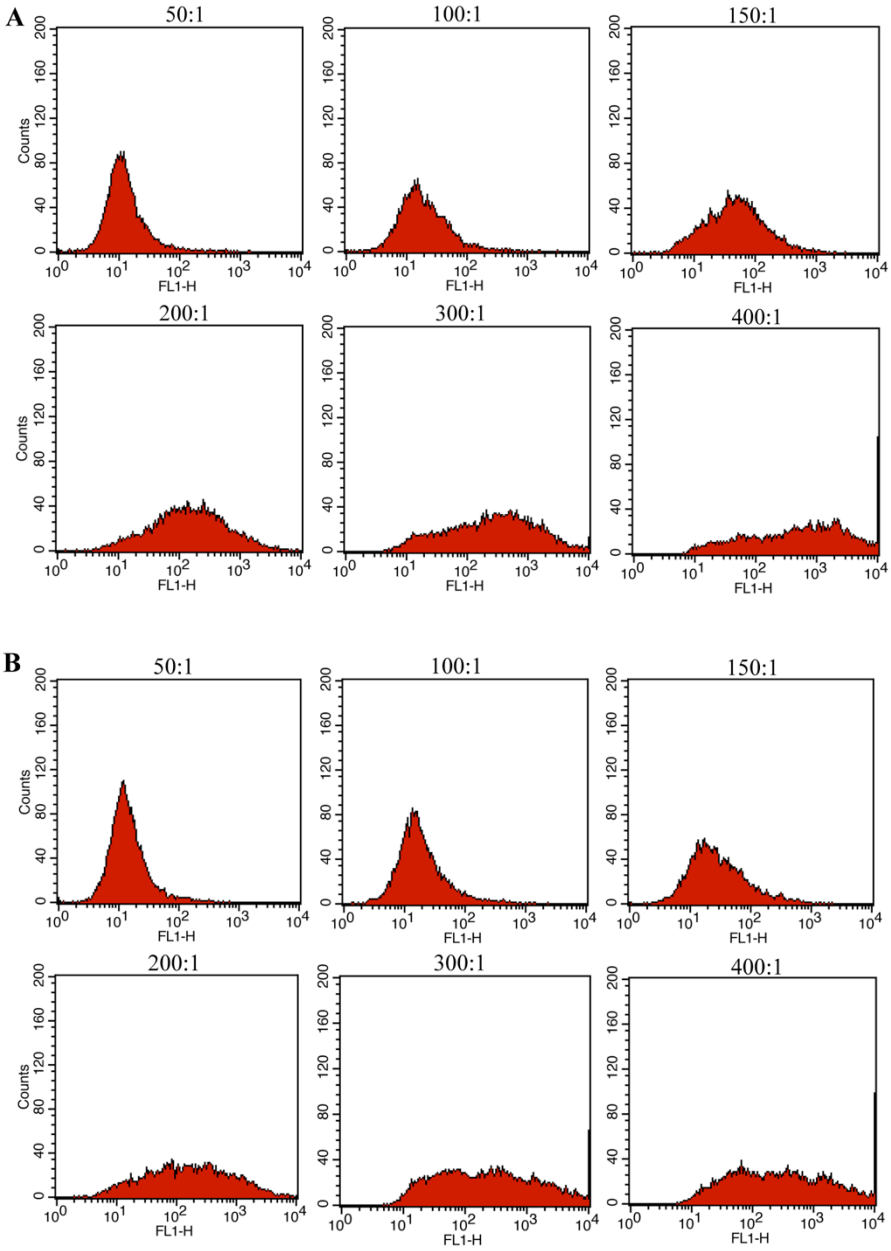

Figure 4-11: Histogram plots measuring the uptake of K1 RNTs-FAM siRNA complexes molar ratios of 50 to 400:1 ratios in (A) water and (B) SFM by A549 cells.

In both cell lines (A549 and HCT116), general trend demonstrated increase in geometric mean of FAM-siRNA signal as the molar ratio of the complexes increased. Enhancement in geometric mean as the molar ratio of K1 RNTs to siRNA increased could be due to the increased binding between RNTs and siRNA, resulting in higher amount of siRNA delivered. Despite the increase in geometric mean of fluorescent intensity, the fluorescent signal count was low, indicating the broad distribution of fluorescent signal among the cells (Figure 4-12, 4-14). Thus, lower number of cells with high uptake of K1 RNTs-siRNA complexes was observed. This supported earlier result from confocal images (Section 3.4.1), which suggested that increasing molar ratio of RNTs to siRNA in the complexes would result in big complexes and lowered the cellular uptake.

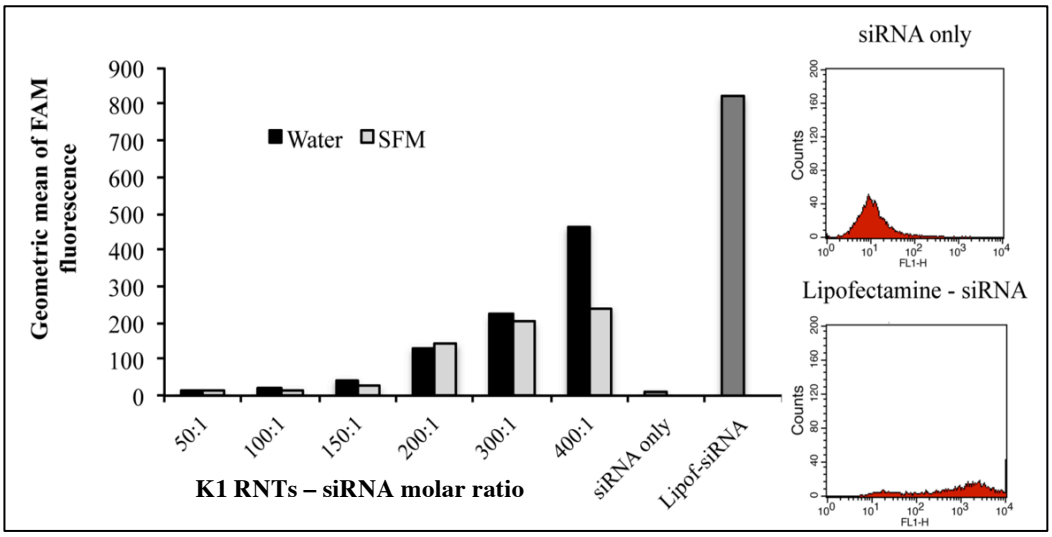

Figure 4-12: Geometric mean of FAM fluorescence showing the uptake of K1 RNTs-FAM siRNA complexes molar ratios of 50 to 400:1 ratios in A549 cells, the negative control (siRNA only) and positive control (Lipofectamine-siRNA).

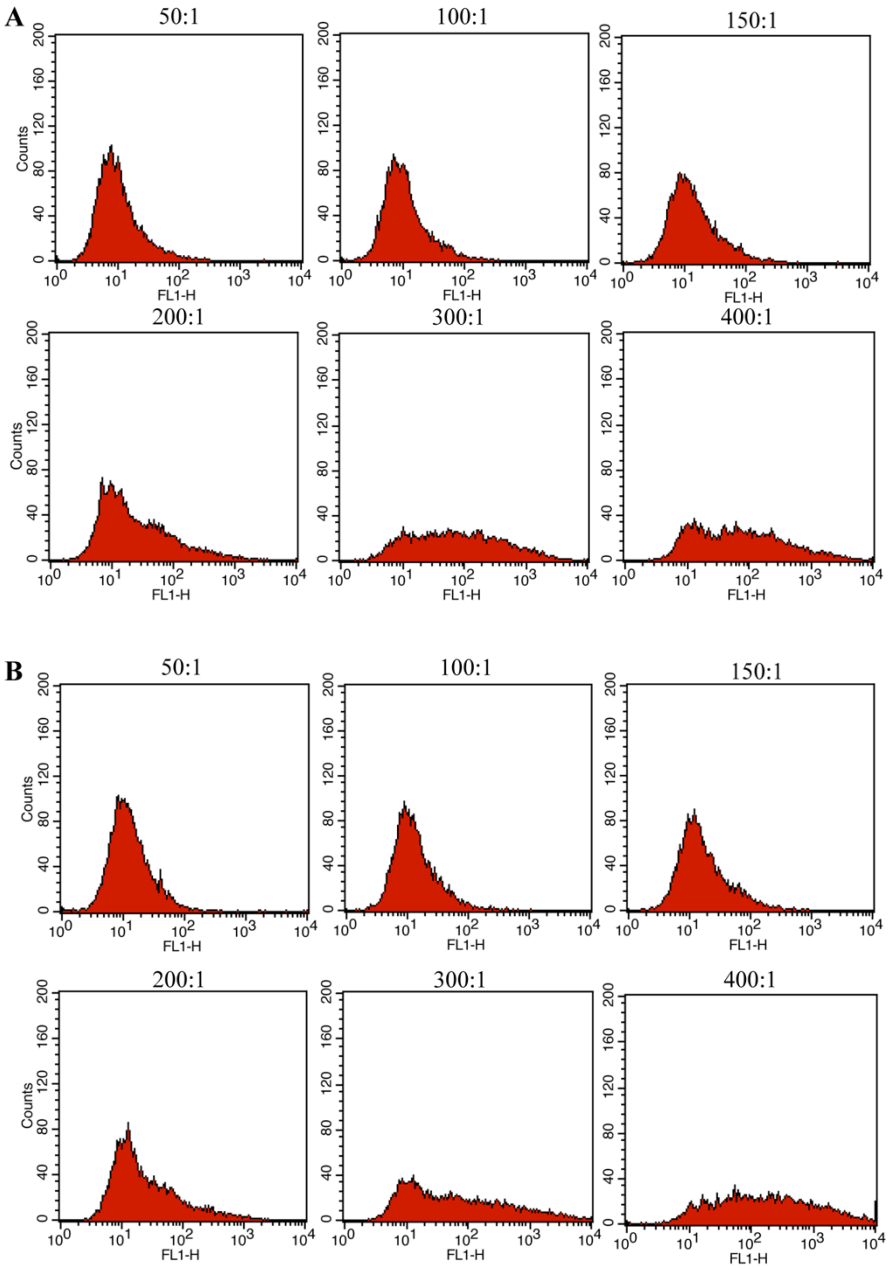

Figure 4-13: Histogram plots measuring the uptake of K1 RNTs-FAM siRNA complexes molar ratios of 50 to 400:1 ratios in (A) water and (B) SFM by HCT116 cells.

Quantification of FAM-siRNA fluorescent signal in the cells by flow cytometry suggested that the cells showed to uptake more siRNA as the molar

ratio of RNTs-siRNA increased. However, the broad distribution of fluorescent signal and the reduction of cell count for the fluorescence indicated that there was a broad distribution of cells with various fluorescent intensities, including some with higher intensity than at lower molar ratios, which resulted in increasing of the geometric mean.

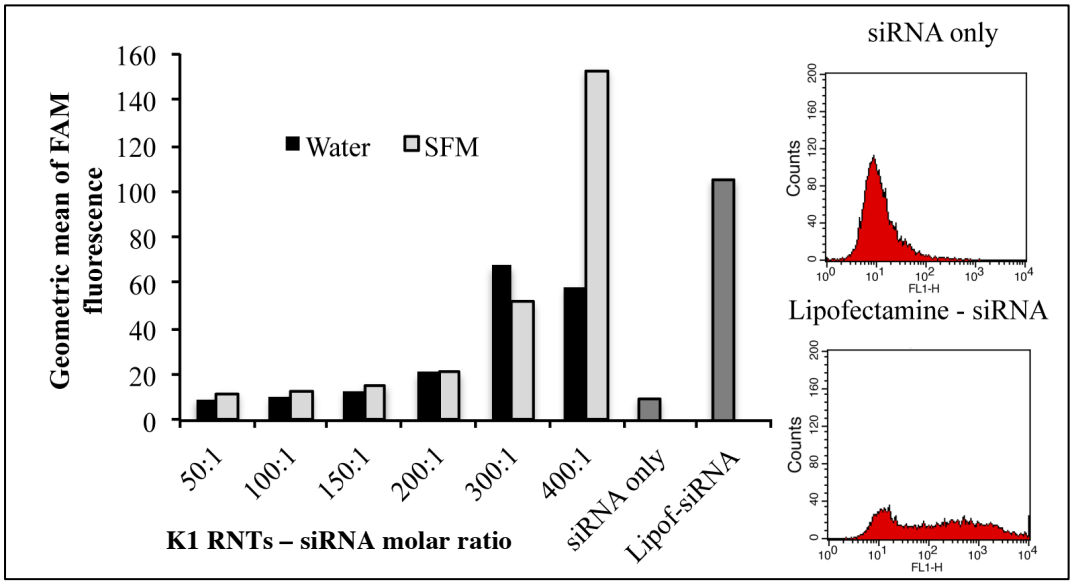

Figure 4-14: Geometric mean of FAM fluorescence showing the uptake of K1 RNTs-FAM siRNA complexes molar ratios of 50 to 400:1 ratios by HCT116 cells, the negative control (siRNA only) and positive control (Lipofectamine-siRNA).

3.5. Cytotoxicity test of K1 RNTs in A549 and HCT116 cells

Cytotoxicity test using MTT assay was done to test the cell viability of A549 and HCT116 when treated with K1 RNTs at concentrations from 0 to 50 μM. In this study, RNTs were observed to be very biocompatible with almost 100% cell viability up to 40 μM (Figure 4-15), and about 80% at 50 μM of K1 in A549 cells and almost 100% cell viability at all dosages in HCT116 cells. As

discussed earlier (Section 3.4), A549 cells was observed to uptake more RNTs-siRNA complexes than HCT116 cells. Thus, the former cells were more susceptible for accumulation of the RNTs-siRNA complexes inside the cells leading to reduction in cell viability. The advantages of using RNTs over the positive controls, such as INTERFERin and Lipofectamine-2000 were due to a more noticeably toxic effect that they had on the cells during the time of treatment.

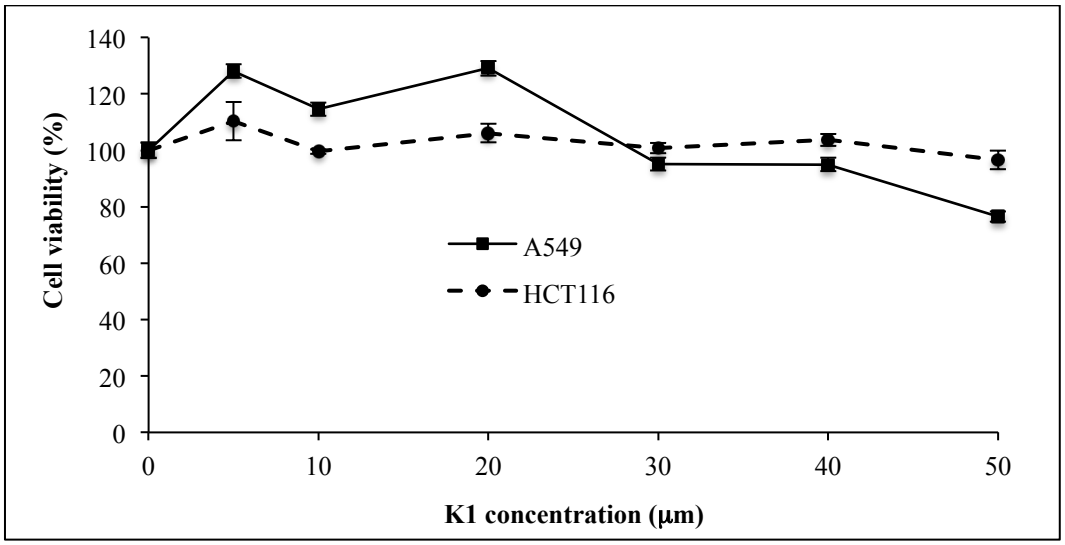

Figure 4-15: Cell viability test using MTT assay to measure the cytotoxicity of K1 RNTs from concentration 0 to 50 μM in A549 and HCT116 cells.

In the cell study, the highest concentration of K1 RNTs used was 40 μM (molar ratio of 400:1, K1 RNTs to siRNA), hence, it is a safe concentration to be used in both A549 and HCT116 cancer cell lines. Conclusively, K1 RNTs have shown to have low cytotoxicity that is suitable for *in vitro* and *in vivo* studies.

3.6. Protein silencing effect of delivered siRNA

3.6.1. Luciferase Assay

Luciferase assay was conducted on A549 and HCT116 cells to study the silencing effect of the siRNA delivered by K1 RNTs. The cells were transfected with firefly luciferase siRNA (FF siRNA) to reduce corresponding proteins, hence, lowered its activity compared to that of the control of Renilla luciferase. The silencing results obtained by transfecting K1 RNTs-FF siRNA complexes at various molar ratios to A549 (molar ratios of 50:1, 100:1, 150:1, 200:1, 300:1 and 400:1, Figure 4-16A) and HCT116 cells (molar ratios of 200:1, 300:1 and 400:1, Figure 4-16B) are summarized in Table 4-1.

A549 cells showed 40-70% lower firefly luciferase activity when transfected with K1 RNTs-siRNA from 50:1 to 300:1 ratios, with negligible difference for media used for complexes formation (water or SFM). Due to the fact that of K1 RNTs solution that tend to stick to the eppendorf tubes, there were variables between experiments, which could explain for the big error bar at 300:1 molar ratio in water. Future work should pay careful attention on the dilution of RNTs and siRNA so that they have relatively equal volume for even mixing. Positive control of lipofectamine was used to deliver siRNA, however, the results were inconclusive due to the strong toxicity to the cells, affecting on the proteins detection and hence, data was not shown here.

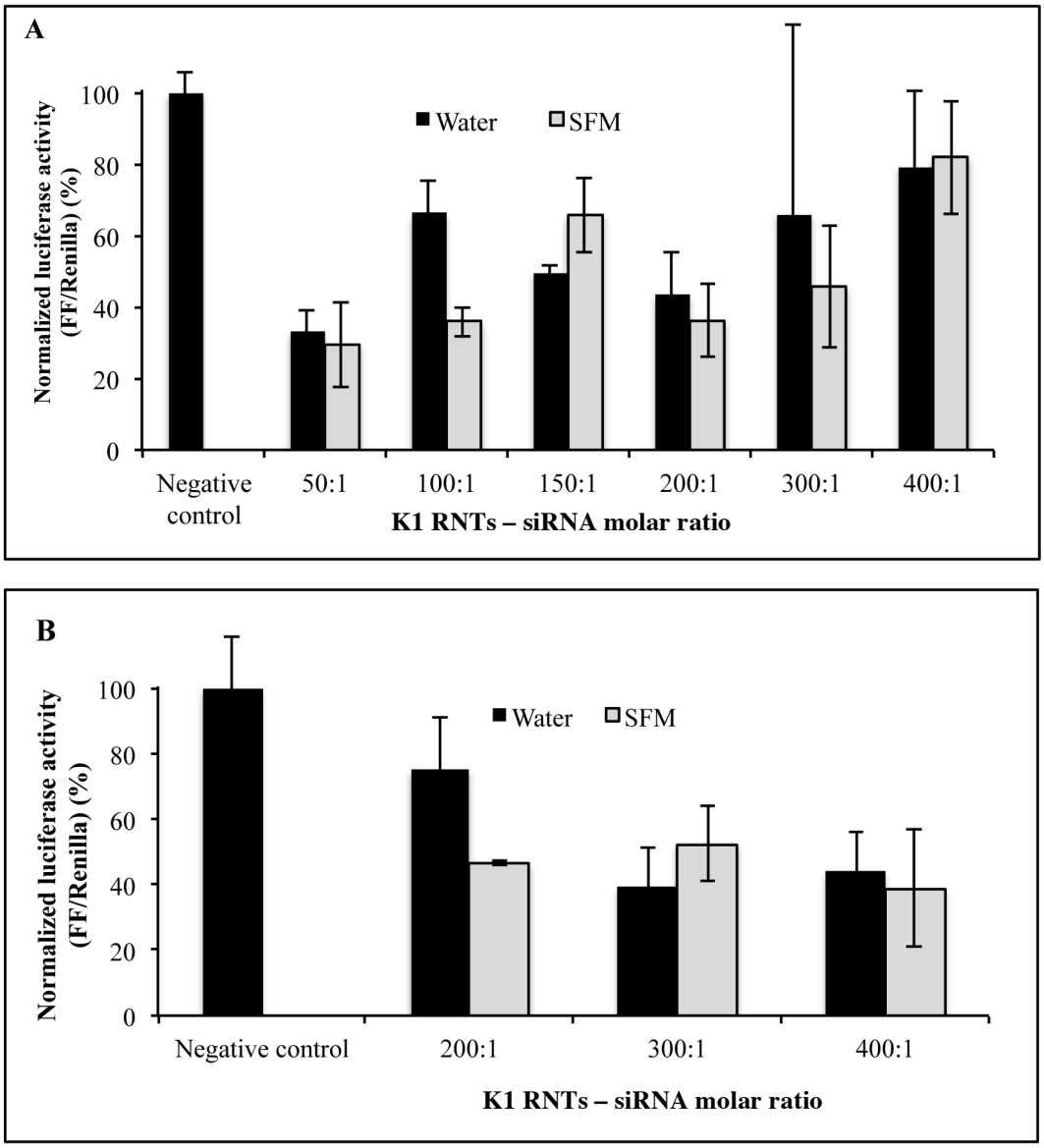

Figure 4-16: Luciferase activity measured in (A) A549 and (B) HCT116 cells when transfected with K1 RNTs-FF siRNA complexes at various molar ratios (complexed in water and SFM). Shown are the normalized values of firefly to the co-transfected Renilla signals.

In A549 cells, general trend showed that increasing molar ratio of K1 RNTs to siRNA led to the decrease in protein silencing. This agreed with confocal imaging result (Section 3.4.1), where bigger complexes were formed that lowered

the transfection efficiency of K1 RNTs-siRNA complexes. It was observed that the molar ratios of 50:1 to 200:1 resulted in similar silencing effects. This proved that the size of the complexes were effective for cellular uptake. Even though molar ratio of 50:1 showed earlier in the agarose gel electrophoresis to not capture siRNA fully, the silencing effect was observed. It is predicted that even small amount of siRNA was enough to yield some protein silencing or K1 RNTs were able to continuously encapsulate siRNA in solution during the treatment.

HCT116 cells were transfected with 200, 300 and 400:1 ratios of K1 RNTs-FF siRNA. For all the molar ratios used, the luciferase activity was reduced ~50-60% showing effective silencing effect even though big complexes were present (Section 3.4.1). This is very similar to results obtained for A549 cells.

K1 RNTs-FF siRNA molar ratio	A549 cells		HCT116 cells	
	Water (%)	SFM (%)	Water (%)	SFM (%)
50:1	62 ± 13	71 ± 12	-	-
100:1	27 ± 9	64 ± 4	-	-
150:1	52 ± 11	34 ± 10	-	-
200:1	63 ± 9	36 ± 10	25 ± 16	53 ± 1
300:1	34 ± 53	46 ± 17	61 ± 12	48 ± 11
400:1	8 ± 10	82 ± 16	56 ± 12	61 ± 18

Table 4-1: Summary of firefly luciferase silencing in luciferase assay in A549 and HCT116 cells when transfected with K1-FFsiRNA complexes at different ratios in water and SFM.

Silencing experiments in A549 and HCT116 cells both showed effective reduction of targeted protein of STAT3. Even though A549 and HCT116 cells

have different characteristics in uptake mechanism and transfection efficiency as seen in confocal and flow cytometry experiments (Section 3.4), similar silencing effects when transfected with K1 RNTs-siRNA complexes were observed. This significantly implies the ability for K1 RNTs to deliver siRNA at various cancer cells. It was evident in both luciferase assay and STAT3 experiments that K1 RNTs were able to deliver siRNA targeting both proteins. These findings are promising for future applications of K1 RNTs as siRNA or DNA carrier.

The results from luciferase assay have strongly suggested that there was effective protein silencing in both cell lines resulting from the FF-siRNA delivered by K1 RNTs. This finding further implies on the ability to use RNTs as an effective siRNA carrier for intracellular delivery.

3.6.2. STAT3 Protein Silencing

In attempt to silence the endogenous protein STAT3 that commonly over-expressed in cancer cells, A549 and HCT116 cells were transfected with K1 RNTs-STAT3 siRNA complexes at different ratios in water. Water was chosen for the complexation between K1 RNTs and siRNA due to the smaller complexes produced (Section 3.3). The result of STAT3 protein level was compared to the protein level of the housekeeping GAPDH. The silencing results in A549 (Figure 4-17) were very promising: up to 57% of STAT3 protein (Table 4-2) was silenced when transfecting the cells with K1 RNTs-STAT3 siRNA complexes at increasing molar ratios from 50:1 to 400:1 respectively. Here, molar ratio of 50, 100:1 and 150:1 were the best candidate, suggesting the complexes created at these ratios were well-uptaken by the cells, which agreed with result from

luciferase assay (Section 3.6.1). Complexes formed at higher molar ratio tend to be bigger, thus not being uptaken so effectively by the cells.

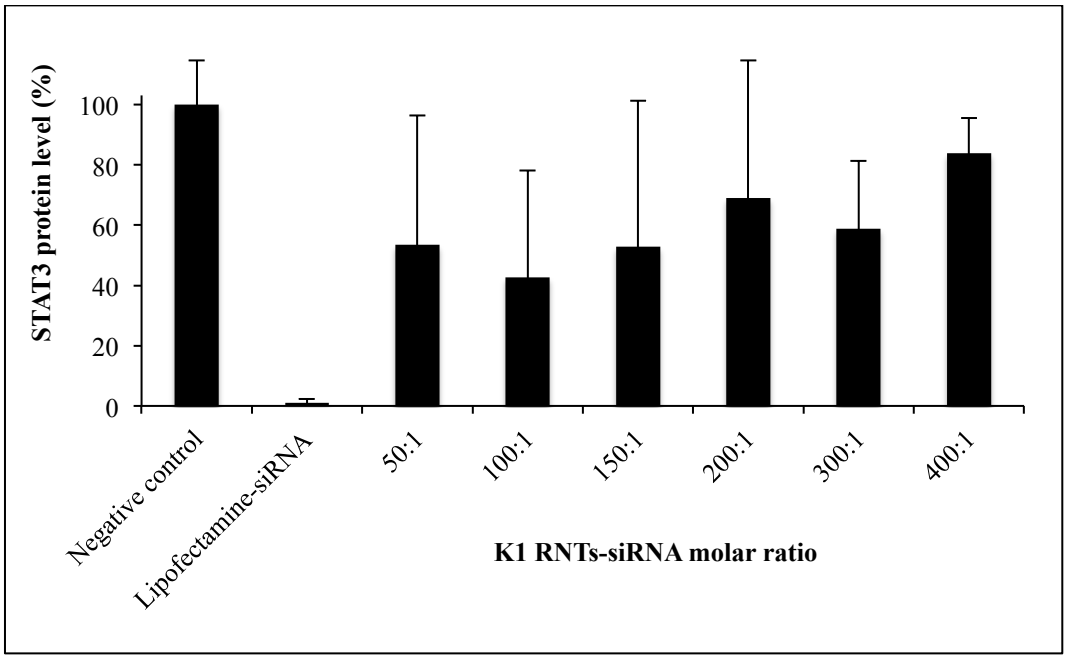

Figure 4-17: STAT3 protein level detected in A549 cells transfected with K1 RNTs-STAT3 siRNA from molar ratios of 50 to 400:1 in water.

K1 RNTs-STAT3 siRNA molar ratio	Trial 1 (%)	Trial 2 (%)	Trial 3 (%)	Average (% silencing)
50:1	3	89	47	47 ± 43
100:1	22	93	57	57 ± 35
150:1	4	38	99	47 ± 48
200:1	2	7	84	31 ± 46
300:1	29	28	67	41 ± 22
400:1	12	7	30	16 ± 12

Table 4-2: Silencing of STAT3 proteins in A549 cells transfecting with K1 RNTs-STAT3 siRNA from molar ratios of 50 to 400:1 in water.

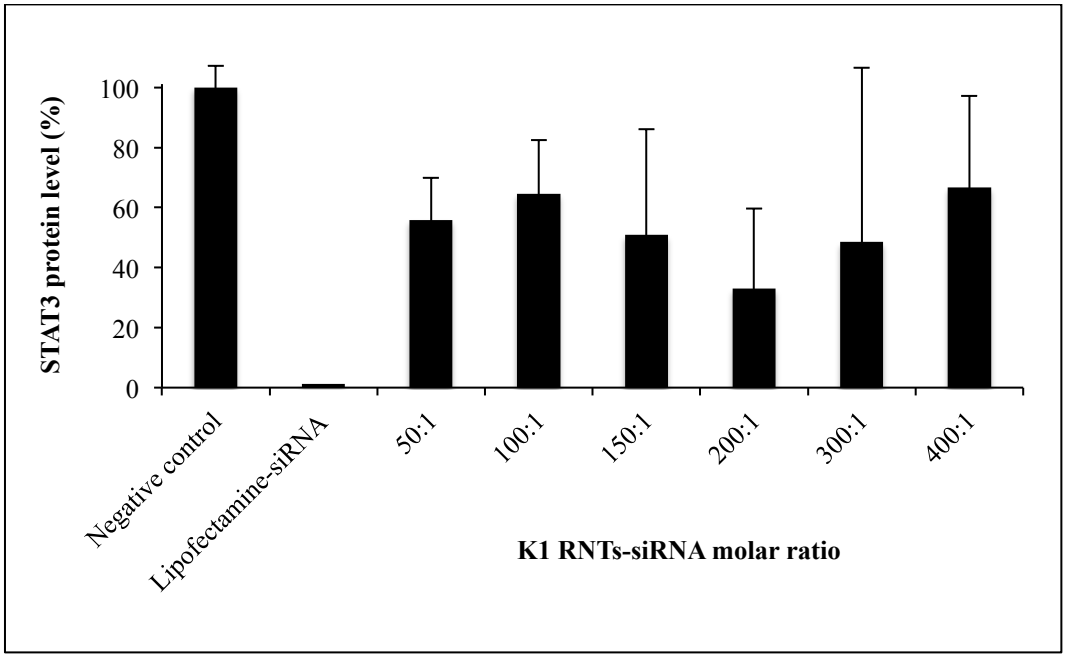

Figure 4-18: STAT3 protein level using WB for HCT116 cells transfected with K1 RNTs-STAT3 siRNA from molar ratios of 50 to 400:1 in water.

K1 RNTs-STAT3 siRNA molar ratio	Trial 1 (%)	Trial 2 (%)	Trial 3 (%)	Average (% silencing)
50:1	32	48	60	46 ± 14
100:1	47	50	18	38 ± 18
150:1	89	47	19	51 ± 35
200:1	69	95	41	68 ± 27
300:1	54	89	0	48 ± 45
400:1	48	59	1	36 ± 31

Table 4-3: Summary of silencing of STAT3 proteins in HCT116 cells when transfected with K1 RNTs-STAT3 siRNA from molar ratios of 50 to 400:1.

HCT116 cells were also transfected with K1 RNTs-STAT3 siRNA complexes at different molar ratios. Results also showed very effective protein silencing by STAT3 siRNA delivered by K1 RNTs (Figure 4-18), with up to 68% STAT3 level was silenced (Table 4-3).

Silencing experiments in A549 and HCT116 cells both showed effective reduction of targeted STAT3 protein. Even though A549 and HCT116 cells have different characteristics in uptake mechanism and transfection efficiency as seen in confocal and flow cytometry experiments (Section 3.4), similar silencing effects when transfected with K1 RNTs-siRNA complexes were observed. This significantly implies the ability for K1 RNTs to deliver siRNA at various cancer cells. It was evident in both luciferase assay and STAT3 experiments that K1 RNTs were able to deliver siRNA targeting both proteins. These findings are promising for future applications of the low toxic K1 RNTs as siRNA or DNA carrier.

4. Conclusion

K1 RNTs were tested on their ability to serve as siRNA carrier in A549 and HCT116 cells. The stock solution was prepared so that short RNTs were obtained in order for smaller complexes being made, which would affect on the cellular uptake. Gel retardation assay showed that starting from molar ratio of 100:1, complete amount of siRNA was captured by K1 RNTs. The size of K1 RNTs-siRNA complexes was observed using SEM, showing the increase in size of the complexes as the molar ratio of K1 RNTs to siRNA increased (both in water and SFM). Confocal and flow cytometry both suggested increasing intracellular uptake of FAM siRNA at increasing molar ratio up to 200:1, and lower uptake at 300 and 400:1 molar ratios as the complexes grew in size. Cytotoxicity of K1 RNTs was evaluated to be very low in both cell lines even when transfected at 50 μM of RNTs (48 hours), with A549 cells being more affected (lowest cell

viability of 80%) by the RNTs compared to HCT116 cells (lowest of 97%), due to the higher uptake ability of the former. Most importantly, both luciferase assay and STAT3-targeting experiment significantly showed effective silencing ability of siRNA delivered by K1 RNTs (40-70% silencing). This has suggested high siRNA-delivery ability of K1 RNTs to the cancer cells, showing promising application for future cancer therapy.

References

1. Fenniri, H.; Mathivanan, P.; Vidale, K.L.; Sherman, D. M.; Hallenga, K.; Wood, K. V.; Stowell, J. G., Helical Rosette Nanotubes: Design, Self–Assembly and Characterization, *J. Am. Chem. Soc.* **2001**, *123*, 3854–3855.

2. Fenniri, H.; Deng, B.L.; Ribbe, A.E.; Hallenga, K.; Jacob, J.; Thiyagarajan, P., Entropically–Driven Self–Assembly of Multi–Channel Rosette Nanotubes, *Proc. Natl. Acad. Sci.*. **2002**, 99, 6487–6492.

3. Zhang, L.; Ramsaywack, S.; Fenniri, H.; Webster, T.J. Helical Rosette Nanotubes as a Biomimetic Tissue Engineering Scaffold Material. *Proc. of AIChE*, *Annual Meeting*, **2006**.

4. Zhang, L.; Chen, Y.; Rodriguez, J.; Fenniri, H.; Webster, T.J. Biomimetic helical rosette nanotubes on nanocrystalline hydroxyapatite coatings on titanium for improving orthopedic implants. *Int. J. Nanomed*. **2008**, 3, 3, 323-333.

5. Chen, Y.; Bilgen, B.; Pareta, R.; Myles, A.; Fenniri, H.; Ciombor, D.; Aaron, R.; Webster, T.J. Self-assembled rosette nanotube/hydrogel composites for cartilage tissue engineering. *Tissue Engineering: Part C*. **2010**, 16, 6, 1233-1244.

6. Fine, E.; Zhang, L.; Fenniri, H.; Webster, T.J. Enhanced endothelial cell functions on rosette nanotube-coated titanium vascular stents. *Int. J. Nanomed*. **2009**, 4, 91-97.

7. Chen, Y.; Song, S.; Zhimin, Y.; Fenniri, H.; Webster, T.J. Self-assembled rosette nanotubes encapsulate and slowly release dexamethasone. *Int. J. Nanomed*. **2011**, 6, 1035-1044.

8. Song, S.; Chen, Y.; Yan, Z.; Fenniri, H.; Webster, T.J. Self-assembled rosette

nanotubes for incorporating hydrophobic drugs in physiological environments. *Int. J. Nanomed*. **2011**, 6, 101-107.

9. Chhabra, R.; Moralez, J.; Raez, J.; Yamazaki, T.; Cho, J.-Y.; Myles, A.J.; Kovalenko, A.; Fenniri, H. One-Pot Nucleation, Growth, Morphogenesis, and Passivation of 1.4 nm Au Nanoparticles on Self-Assembled Rosette Nanotubes. *J. Am. Chem. Soc*. **2010**, 132, 32–33.

10. Chhabra, R. and Fenniri, H. Electroless Synthesis of 1.4 nm Pd and Pt Nanoparticles on Self-Assembled Rosette Nanotubes. *Mater. Res. Soc. Symp. Proc*. **2011**, 1301, 45-50.

11. Fine, E.; Zhang, L.; Fenniri, H.; Webster, T.J. Enhanced endothelial cell functions on rosette nanotube-coated titanium vascular stents. *Int. J. Nanomed.,* **2009**, 4, 91-97.

Significance of this thesis work and outlook

Development of cancer treatment has been advancing over the past few decades. The fast growing field of nanotechnology combined with the discovery of RNAi pathway shows promising results for cancer therapy. The delivery of siRNA is the most common method for cancer treatment due to its specificity to target selected proteins that are essential to the growth and viability of cancer cells. The specificity of this system leads to lower toxicity compared to delivery of drugs that could be harmful to surrounding normal cells. Many efforts have been done to assist the intracellular delivery of siRNA, such as: metal nanoparticles, lipid-like materials, polymers and carbon nanotubes. However, many of the nanocarriers failed to be used in biological systems due to low protection of siRNA against serum degradation and the non-specific toxicity of the nanocarriers themselves. Here, we have assessed lysine functionalized RNTs, which was previously shown to be compatible in biological systems, for their ability for intracellular delivery of siRNA.

Firstly, the series of fifteen lysine-functionalized twin RNTs (KnT RNTs, n = 1 to 15) were examined on their delivery ability of siRNA in chapter II. Results showed increasing binding interaction with siRNA with increasing cationic charges on the RNTs (higher number of lysine residues on the side chains). Due to the strong binding between KnT RNTs and siRNA, the latter were protected from serum degradation. Confocal microscopy study also showed more siRNA was delivered to the cells due to increasing loading ability and increasing interaction

with the cellular surface from K1T to K15T RNTs. Endocytosis was found to be the main pathway for intracellular uptake of KnT RNTs-siRNA. Also, the RNTs (K10T and K15T) were shown to have relatively low toxicity effect to the cells. This work successfully demonstrated the ability of KnT RNTs-siRNA complexes to be uptaken by the cells.

In chapter III, siRNA binding of K1T to K5T RNTs were improved by increasing molar ratios of RNTs to siRNA, which in turn enhanced the cellular delivery of siRNA by these low-charged KnT RNTs. The interaction of K3T RNTs with the siRNA was further studied using various microscopy techniques (SEM, TEM and AFM). The presence of siRNA on the surface of the RNTs strongly indicated binding interactions (mainly electrostatic) of the lysine side chains on the RNTs with the former. Most importantly, K3T RNTs effectively delivered siRNA to the cells for silencing of luciferase and STAT3 proteins.

Finally, chapter IV assessed K1 RNTs (lysine-functionalized mono RNTs) on their ability to serve as siRNA carrier to suppress protein production. Due to the low charges on the RNTs, higher molar ratios of RNTs to siRNA were used to fully capture the siRNA (greater than 100:1). Length of RNTs showed to play an important role for intracellular uptake due to its effect on complexes' size that is favorable for endocytosis. K1 RNTs-siRNA complexes formed in water and serum-free medium showed to have comparable results, with some small effect of the ions on RNTs and siRNA interaction. Silencing of luciferase and STAT3 proteins were achieved in both A549 and HCT116 cell lines showing promising results for future *in vivo* study.

Future work should focus on making uniform complexes of RNTs and siRNA to yield those within hundreds of nanometer in scale, which can be achieved by thorough dilution and sonication of the RNTs and siRNA. In addition, preparation of the RNTs stock solution is important so that the yielded RNTs are short and uniform in size, which would in turn affect the size of RNTs-siRNA complexes. The mixing of RNTs-siRNA complexes could also be done in glass vials because the RNTs tend to stick to the wall of the eppendorf tubes, which could lead to uneven mixing of RNTs with siRNA.

Highly-charged cationic RNTs showed promising ability to bind and protect siRNA from serum degradation with fast intracellular uptake. However, strong binding between RNTs and siRNA may prevent the distribution of the latter in the cytoplasm, and the highly charged RNTs could have higher toxicity effect to the cells. The library of fifteen KnT RNTs allows us to explore on various net charges of the RNTs and find out what best for the binding and cellular delivery and distribution of siRNA for protein silencing. To achieve this, each KnT RNTs need to be assessed carefully according to their optimal molar ratios with siRNA (at which full encapsulation of siRNA is observed).

A strong advantage of using RNTs is the ability to functionalize the side chains with specific antigens, peptides or aptamers. As such, the antigens[1] and peptides can be recognized by receptors that are overexpressed in cancer cells compared to normal cells. Similarly, aptamers can recognize specific antigen or receptors that highly expressed in cancer cells. The modification of RNTs by these molecules can essentially increase the delivery of siRNA to cancer cells via

active targeting instead of passive targeting via EPR effect. The multiple side chains (carrying antigens, peptides or aptamers) express on the surface of RNTs can contribute to multivalent binding effect, which would improve targeting and intracellular uptake of RNTs-siRNA complexes.[2,3]

To further understand siRNA-mediated silencing effect at mRNA level, qRT-PCR (quantitative real time polymerase chain reaction) can be carried out to measure the level of mRNA (encoding the target protein) expressed in the cells.[4, 5] Once optimizing the protein silencing achieved by RNTs-siRNA complexes, various siRNA can be delivered to target proteins that are essential to the viability of the cancer cells.[6,7,8] To determine the efficiency of the delivered siRNA, Western blotting and MTT assay can be used to detect the target proteins and the viability of transfected cells respectively.

Finally, this dissertation strongly demonstrated the ability for RNTs to serve as siRNA carrier due to their biocompatibility, efficient siRNA binding, cellular delivery and protein silencing effect of target proteins. The side chains of the RNTs can be modified to greatly enhance the intracellular delivery of siRNA for active targeting of any cancer cells.

1. Brannon-Peppas, L.; Blanchette, J. Nanoparticle and targeted systems for cancer therapy. *Adv. Drug Deliv. Rev.* **2012**, 64, 206-212.

2. Peer, D.; Karp, J. M.; Hong, S.; Farokhzad, O.; Margalit, R.; Langer, R. Nanocarriers as an emerging platform for cancer therapy. *Nature nanotech*. **2007**, 2, 751-760.

3. Ashley, C. et. al. The targeted delivery of multicomponent cargos to cancer cells by nanoporous particle-supported lipid bilayers. *Nat. Mat.* **2011**, 10, 389-398.

4. Holmes, K.; Williams, C.; Chapman, E.; Cross, M. Detection of siRNA induced mRNA silencing by RT-qPCR: considerations for experimental design.

5. Wang, B.; Tian, S.; Zhou, Q.; Zeng, X. Did your RNAi Experiment Work? Reliably Validating RNA Interferece with qRT-PCR. SABiosciences 6951 Executive Way RNAI

6. Zhu, H.; Yang, K.; Xie, Y.; Lin, Y.; Mao, Q.; Xie, L. Silencing of mutant p53 by siRNA induces cell cycle arrest and apoptosis in human bladder cancer cells. *World J. Surg. Oncol.* **2013**, 11,22.

7. Aliabadi, H.; Landry, B.; Mahdipoor, P.; Uludag, H. Induction of Apoptosis by Survivin silencing through siRNA delivery in a human breast cancer cell line. *Mol. Pharmaceutics*. **2011**, 8, 5, 1821-1830.

8. Chen, A.; Zhang, M.; Dongguang, W.; Stueber, D.; Taratula, O.; Minko, T.; He, H. Co-delivery of Doxorubicin and Bcl-2 siRNA by Mesoporous Silica Nanoparticles Enhances the Efficacy of Chemotherapy in Multidrug-Resistant Cancer Cells. *Small*. **2009**, 5, 23, 2673-2677.